BIO-INSPIRED COOPERATIVE EXPLORATION OF NOISY SCALAR FIELDS

A Thesis
Presented to
The Academic Faculty

by

Wencen Wu

In Partial Fulfillment
of the Requirements for the Degree
Doctor of Philosophy in the
School of Electrical and Computer Engineering

Georgia Institute of Technology
August 2013

BIO-INSPIRED COOPERATIVE EXPLORATION OF NOISY SCALAR FIELDS

Approved by:

Professor Fumin Zhang, Advisor
School of Electrical and Computer Engineering
Georgia Institute of Technology

Professor Magnus Egerstedt
School of Electrical and Computer Engineering
Georgia Institute of Technology

Professor Jeff Shamma
School of Electrical and Computer Engineering
Georgia Institute of Technology

Professor Wassim M. Haddad
School of Aerospace Engineering
Georgia Institute of Technology

Professor Yorai Wardi
School of Electrical and Computer Engineering
Georgia Institute of Technology

Date Approved: 23 April 2013

To my parents,

Deming Wu and Zhijie Miao,

Thanks for your love and support.

ACKNOWLEDGEMENTS

I would like to take this opportunity to express my greatest appreciation to people who have helped and supported me.

I give my deep and special thanks to Dr. Fumin Zhang, my advisor, for his support, guidance, and encouragement during my Ph.D journey. I simply cannot expect a better advisor. He introduced me to the richness and depth of cooperative control and sensing. His sparkling ideas have always inspired me. I am very grateful to Dr. Zhang for sharing his wisdom and breadth of knowledge and for always supporting and encouraging me to aim higher.

I would like to thank my thesis committee members: Prof. Shamma, Prof. Wardi, Prof. Egerstedt, and Prof. Haddad, for their precious time and valuable suggestions for the work done in this dissertation.

I also would like to thank my fellow lab members and my friends who provided great collaboration and assistance during my study. You have also made my long journey much more cheerful.

Finally, from the bottom of my heart, my special appreciations go out to my parents, Deming Wu and Zhijie Miao, for their endless love and support through the years. They are the ones that are always stand by my side and provide me with all the courage and confidence to face every challenge in my life. No word can express my deepest gratitude for what they have done for me. My fiance, Qi Zhou, also deserves my deepest thanks since he is the one who made this journey much more joyful.

TABLE OF CONTENTS

LIST OF FIGURES

SUMMARY

A fundamental problem in mobile robotics is the exploration of unknown fields that might be inaccessible or hostile to humans. Exploration missions of great importance include geological survey, disaster prediction and recovery, and search and rescue. For missions in relatively large regions, mobile sensor networks (MSN) are ideal candidates. The basic idea of MSN is that mobile robots form a sensor network that collects information, meanwhile, the behaviors of the mobile robots adapt to changes in the environment. To design feasible motion patterns and control of MSN, we draw inspiration from biology, where animal groups demonstrate amazingly complex but adaptive collective behaviors to changing environments.

The main contributions of this thesis include platform independent mathematical models for the coupled motion-sensing dynamics of MSN and biologically-inspired provably convergent cooperative control and filtering algorithms for MSN exploring unknown scalar fields in both 2D and 3D spaces. We introduce a novel model of behaviors of mobile agents that leads to fundamental theoretical results for evaluating the feasibility and difficulty of exploring a field using MSN. Under this framework, we propose and implement source-seeking algorithms using MSN inspired by behaviors of fish schools. To balance the cost and performance in exploration tasks, a switching strategy, which allows the mobile sensing agents to switch between individual and cooperative exploration, is developed. Compared to fixed strategies, the switching strategy brings in more flexibility in engineering design. To reveal the geometry of 3D spaces, we propose a control and sensing co-design for MSN to detect and track a line of curvature on a desired level surface.

CHAPTER I

INTRODUCTION

In mobile robotics research, a fundamental problem is the exploration of unknown areas. Serving as mobile sensing agents, robots are deployed to areas that might be inaccessible or hostile to humans with the goal of exploration, that is, collecting information that may help understand physical, chemical or biological environmental processes. A fundamental explorative mission is to measure spatially distributed scalar fields, which include fields such as temperature, salinity, light distribution, and oil concentration. Applications of great interest include geological survey, disaster prediction and recovery, and search and rescue. Various exploration algorithms and strategies have been proposed and successfully demonstrated. For missions in relatively large regions, mobile sensor networks (MSN) are ideal candidates. The basic idea of MSN is that mobile robots form a sensor network that collects information of the environment, meanwhile, the behaviors of the mobile robots adapt to changes in the environment. Compared to exploration using one single robot mounted with sensors, using a group of collaborating robots has its advantages in many aspects. For example, it is more robust to system failures, and it is more efficient in collecting data in a large area. Therefore, MSN becomes one of the emerging research area, which integrates several subtopics including cooperative motion control, swarm motion planning, cooperative sensing, ad-hoc mobile communication, and embedded computing.

In MSN research, most existing work is mission-based that focuses on developing and improving strategies for MSN so that desired explorative performance can be achieved in certain scalar fields. Instead of proposing new designs, we aim to develop an abstract theoretical foundation to rigorously define explorative behaviors of mobile sensing agents, and analyze the movements of agents that lead to higher probability of successful exploration.

For this purpose, we develop fundamental theoretical results that describe exploration behaviors of mobile sensing agents in a noisy scalar field by introducing notions of coherent and incoherent steps, and propose criteria for evaluating the feasibility and difficulty of exploring the field by establishing the notion of local explorability, which analyzes the tendency that such field would induce false-walks for a sensing agent. We are able to connect the variance of Gaussian noise with the success rate of coherent steps of mobile sensing agents, and explain why gradient following and level curve tracking desirable strategies in exploration. We are also able to theoretically justify the minimum number of agents required to achieve a certain level of success rate.

Under the proposed framework, we investigate biologically inspired co-design of cooperative control and sensing for MSN exploring unknown scalar fields in both 2D and 3D spaces, with the focus on source-seeking and level curve tracking. To design feasible motion patterns and control of MSN, we draw inspiration from biology, where animal groups survive even in the most challenging environments. Collective behaviors, which are observed in various species such as fish schools, bird flocks, and ant colonies, are proved to be beneficial to other members in the group and profitable for the survival of the entire group. The collective behaviors of animal groups are amazingly complex but adaptive to changing environments, which provide novel aspects for designing engineering systems. Therefore, it is interesting to study the collective behaviors of animal groups and gain insights for the control and sensing of MSN in exploring unknown scalar fields.

Autonomous sensing agents that are capable of localizing sources in a scalar field are of great importance in various scenarios such as locating chemical spills, detecting fire in its early stage, and monitoring algae blooms. Inspired by behaviors of fish schools seeking darker (shaded) regions in environments with complex lighting variations, we develop a distributed source-seeking algorithm for MSN that seek for a local minimum of a field with no explicit gradient estimation. We decompose the velocity of each agent so that the speed of the agent group is proportional to the measured field values while the group remaining

in a constant formation, and prove the convergence of the trajectory of the agent group to a local minimum. The algorithm is well suited for source-seeking problems when gradient information is hard to obtain and the communication among agents is constrained. Thus, it has the potential to be applied to various exploration scenarios.

To balance the cost and performance in exploration tasks, we propose and implement a switching strategy, which allows the mobile sensing agents to switch between individual and cooperative exploration when searching a local minimum of an unknown field. The switching strategy is inspired by the observation that certain species of fish tend to move in a group only when an individual fish is not confident with the information it senses (e.g., food concentration). Compared to fixed strategies, the switching strategy strikes a balance between exploration complexity and exploration performance in terms of convergence rate and exploration cost, which brings in more flexibility in engineering design. Other than source-seeking problem, the switching strategy can also be applied to other exploration tasks such as target tracking as long as a cost function related to convergence rate is defined.

The structure of 3D scalar fields is of great importance to exploration tasks in the air by unmanned aerial vehicles (UAV) and underwater by autonomous underwater vehicles (AUV). The development of MSN that are able to track small scale features in three dimensional space takes the research to a new direction. To this end, we develop control and filtering algorithms for MSN to cooperatively detect and track a desired curve on a desired level surface in an unknown 3D scalar field while moving in a formation. We construct a cooperative Kalman filter to combine sensor readings from all sensing agents and design steering control laws to control the motion of the MSN using differential geometry-based methods. In this way, the local structure of the field can be estimated from the measurements taken by all the agents. We propose an algorithm that allows the MSN to estimate principal curvatures and principal directions of lines of curvature using the measurements of the agents. In addition, we theoretically justify the minimum number of agents that can be utilized to accomplish the exploration task.

The rest of the dissertation is organized as follows. Chapter II introduces background information of biologically inspired cooperative exploration using MSN. Chapter III proposes the discretized models of mobile sensing agents exploring noisy scalar fields, which serves as the theoretical framework. Chapter IV presents information dynamics of coordinating agents, cooperative filters, and formation control of MSN. Chapter V develops bio-inspired gradient-based and gradient-free source-seeking algorithms, and demonstrates the implementation in a multi-robot test-bed. Chapter VI introduces a switching strategy that allows mobile agents to switching between individual exploration and cooperative exploration, and presents the application of the switching strategy in tracking tracking. Chapter VII discusses exploration in 3D spaces by introducing the motion and sensing design for MSN detecting and tracking a line of curvature on a desired level surface. Chapter VIII provides concluding remarks and the contributions of the thesis. Finally, in Chapter IX, publications related to the thesis work are listed.

CHAPTER II

BACKGROUND

This chapter provides the background of biologically inspired cooperative exploration using MSN. In particular, the first part of the chapter presents the state of the art techniques and applications of cooperative exploration of noisy scalar fields. The second part of the chapter provides a literature review of bio-inspired approaches for exploration using MSN.

2.1 Cooperative Exploration of Scalar fields

In robotics research, the exploration problem arises when robots are deployed to provide information of an unknown area that might be unreachable or hostile to humans [6, 107, 125]. On the one hand, human activities may be harmful to the natural environment, resulting in poisonous oil spills, gas leakage, and fire. On the other hand, in ecology, the propagation of plants and the dynamics of biological variables have direct impact on the environment such as marine ecosystems and global climate. To understand, model, and estimate the dynamics of physical and biological quantities of the environment, researchers have paid great attention to the exploration of spatially distributed scalar fields, in which each location in the field is associated with a coordinate-independent scalar value. The gradient at each location of the field can be represented as $\nabla z(\mathbf{r}) = \begin{pmatrix} \frac{\partial z(\mathbf{r})}{\partial \mathbf{r}_1} & \frac{\partial z(\mathbf{r})}{\partial \mathbf{r}_2} & \dots & \frac{\partial z(\mathbf{r})}{\partial \mathbf{r}_n} \end{pmatrix}$, with $z(\mathbf{r})$ and $\mathbf{r} \in \mathbb{R}^n$ representing the scalar field and a location in the field, respectively. Examples of scalar fields can be physical fields in terms of temperature, pressure, and light distribution and chemical fields in terms of salinity, oil, and gas concentration. Different exploration missions of great interest are encountered such as monitoring the dynamics of algae blooms, locating chemical spills, and tracking boundaries of fire propagation.

To efficiently and successfully explore an unknown field, the exploration system is required to be reliable and adaptive. Though exploration algorithms and strategies for

a single robot mounted with sensors have been intensively developed and improved in the literature [18, 38, 80], recent attention has been paid to cooperative exploration using MSN [84, 90, 98, 126] that mobile robots form a sensor network to collect information of the environments. A collaborating group of sensing agents outperforms a single sensing agent in many aspects [19,31,34]. For example, in some scenarios, a group of mobile sensing agents can accomplish a task in less time than a single agent [17, 45]. In addition, the information gathered from multiple agents can be merged and filtered so that more accurate knowledge of the field can be obtained [83, 92]. Furthermore, the multi-agent system is adaptive to system failure, i.e., algorithms can be designed to ensure the functioning of the system when one agent fails [137]. Because of the advantages of cooperative exploration over individual exploration, various cooperative exploration algorithms have been developed in the literature. The rest of this section provides a brief review of exploration algorithms of scalar fields using MSN based on different exploration missions.

2.1.1 Environmental Sampling

One important area of the exploration problem is the environmental sampling, which deals with providing a sample coverage of the environment so that the dynamics of physical and biological quantities such as temperature, salinity, and chemical concentration can be monitored. To collect information of a field, sensing agents that have the ability of measuring the values of the field at their locations are deployed in the field. The sensing agents can be in the form of a static sensor network, a mobile sensor network, or the mix of both. To reconstruct a scalar field, the typical goal is to optimize the trajectories of sensor networks so that the errors in the estimate of the field of interest are minimized over the region in space and time. To this end, references [41, 69, 70] introduce ocean sampling field experiments, in which a mobile ocean sampling sensor network is designed to sample the temperature distribution in the ocean so that the "best" data set that minimizes a sampling metric, which is based on objective analysis, can be collected. The sampling metric evaluates the errors

in the collected data set that will be assimilated in ocean models. The cooperative control of multiple sensors is based on virtual bodies and artificial potentials, and the mobile sensors are controlled to move along optimal trajectories, which are specified as ellipses. Reference [129] presents analytical and experimental results so that the gliders deployed in the experiments can be controlled to achieve desired patterns on closed curves. Reference [88] describes the implementation of a cooperative control system for underwater gliders in these experiments. To tackle the coverage problem, reference [28] presents control and coordination algorithms for mobile sensing networks to achieve optimal coverage of a scalar area by using gradient descent algorithms for a class of utility functions. Other work related to sampling and coverage can be found in [22, 42, 136].

2.1.2 Source Seeking

Besides the sampling problem, source seeking with a cooperative group of sensing agents has also been widely investigated in the literature. Exploration tasks that require vehicles or robots to localize and identify a feature of interest are of great concern to researchers and are important in many scenarios such as locating the position of oil spills and identifying the origin of a fire. References [5, 69, 87] present a control strategy for groups of vehicles to move in a formation to seek for local maxima or minima in a noisy, unknown, and distributed environmental field. The underlying coordination framework uses virtual bodies and artificial potentials. The gradient estimation and optimal formation geometry design and adaptation are developed using the least square method. Reference [27] designs a distributed Kriging algorithm that estimates the distribution of a random field and of its gradient. The networked agents use the information gained on the spatial field to implement a gradient ascent coordination algorithm. Based on gradient estimations from noisy measurements, reference [23] presents a recursive spatial-estimation-based distributed learning algorithm and a cooperative control for multiple agents moving towards peaks of an unknown field. The approach introduced in reference [74], which characterizes swarm

cohesiveness as a stability property, uses a Lyapunov approach to develop conditions under which the local actions of agents will lead to cohesive foraging even in the presence of noises. The method assumes each agent can sense the gradient of the field at its current location with some errors. Reference [82] presents a source-seeking algorithm that produces an outer-loop control law which only depends on direct measurements of the signal from a group of agents in a circular formation. The circular formation is designed to estimate approximations of gradient directions. In [77], an integrated acoustic navigation system and a coordination control maneuver for a formation of three AUVs and one surface craft to search for gradients is proposed. Reference [4] develops source seeking controllers for randomly switching signal field. The key idea is to find a stochastic trajectory (i) converging to the unknown source with probability 1 and (ii) followed by the robot without a position sensor. In [102–104], the continuous time and discrete time extremum seeking algorithms with sinusoidal perturbation have been modified and extended to assume time varying gains and incorporate stochastic perturbations. The proposed algorithms can be applied to mobile sensors as a tool for achieving optimal observation positions. The method in [99] samples the field so that a map of the field can be estimated. The location of the maximum or minimum position can be determined through the map.

2.1.3 Boundary Tracking

In addition to the sampling and source seeking problems, boundary tracking or perimeter surveillance, which aims to estimate the boundary of a possibly time-varying region of interest and track it as it propagates, has also received great attention from researchers. Applications can be monitoring the fire propagation and algae blooms. Based on the "snake algorithm" from the computer vision literature, references [10, 76] develop collective motion algorithms for a swarm of sensing agents that detect and track the boundary of harmful algae blooms. The algorithm requires the sensing agents to estimate the gradients of the

concentration in the field while moving. Reference [62] proposes the gradient-free"UUV-gas" algorithm, in which the agents turn clockwise or counterclockwise with a constant angular velocity depending on the concentration measurements. This algorithm is tested on the Caltech's multi-vehicle wireless test-bed [51]. Reference [56] also introduces a gradient-free algorithm, which considers the boundary as a hidden Markov model (HMM) with separated observations obtained by sensing agents. The method formulates the estimation of the boundary as an optimization problem. Reference [57] validates the algorithm through experiments with on-board sensors. In [128, 131, 132], a group of sensing agents move in a formation to estimate gradients of a field at the formation center and curvatures of level curves passing through the formation center. By adopting geometric methods, the group of agents are able to track a desired level curve. Our previous work [116] extends the work into three dimensional space, in which steering control laws and curvature estimation algorithms are designed for a group of agents to detect and track lines of curvature on a desired level surface. Reference [105] presents an algorithm that distributes interpolation points along a time-varying boundary so that an optimal approximated polygon can be obtained. The algorithm collects estimates of the tangent and curvature of the boundary from the concentration measurements instead of concentration gradients. In [20, 25, 26], a group of nonholonomic robots with collision avoidance controllers and bang-bang angular velocity controllers are used to detect and surround a dynamic perimeter of oil spill. References [21, 64] develop a cooperative forest fire surveillance algorithm. The vehicles use infrared sensors to capture the temperature propagation and exchange information with other vehicles and a base station. Other work that investigates the boundary tracking problem can be found in [2, 53, 79, 97, 134].

2.2 Biologically Inspired Approaches for Exploration Using MSN

After thousands of years evolution, animal species have developed amazingly complex but adaptive motion patterns so that they can survive even in the most challenging environments. Great effort has been made by behavioral biologists to observe and explain various motion patterns of animal species. The observations from biology inspire researchers in engineering to design novel strategies for robots in exploration missions. For example, [8, 9] study the collective transport strategies in ants and translate them to swarm robotic systems. References [47, 67, 68] present bio-inspired foraging strategies for static environments based on behaviors of species such as insects, blue crabs, and lobsters. In [48], coalition formation in multi-agent systems is introduced based on bottlenose dolphin alliances.

Among all exploration mission, source-seeking is of great importance in various scenarios such as finding the leaks of poisonous chemicals and detecting fire in its early stage. The fluid flow environment, in which a chemical source is present, varies depending on different Reynolds numbers. Low values of Reynolds numbers indicate smooth variations in chemical concentration, which implies that the gradients of the chemical concentration is well defined. At medium to high Reynolds values, chemical dispersion is dominated by turbulent mixing, which produces poorly defined and time-varying gradients [65]. We have reviewed the source-seeking in smooth fields in the previous section. In this section, we provide a review of source-seeking in turbulent fields, which is also referred to as "odor localization" or "plume tracking". Various algorithms have been developed inspired by animal behaviors such as moths [35, 71], blue crabs [112], and bees [68].

In general, the source-seeking problem can be viewed as a three-stage process [65]: (1) search for the presence of a source, (2) search for the source based on sensing, and (3) identify the source. Most of the algorithms are distinguished by the second step, which is localizing the source. We can achieve the source localization by either (1) producing a map or model of the chemical concentration based on the history of measurements of the agents

so that the source location can be determined from the map or (2) controlling the sensing agents to actively track a chemical plume until they identify a source. For the map-based approaches, [37,89] introduce a plume mapping method, which is based on hidden Markov methods (HMMs), that provides a probability map of the source location. In [39, 40], Bayesian occupancy grid mapping is adapted to produce a map that shows the probability of each discrete cell in the map containing an active plume source. Reference [72] maps the structure of a gas distribution by creating concentration grid maps using a Gaussian weighting function.

For the second approach that directs sensing agents to trace a chemical plume, researchers have developed both gradient-based and gradient-free algorithms. For gradient-based tracking, [94, 95] present a search algorithm named Hex-Path algorithm, which defines a path using the edges of closely packed hexagons. Another family of gradient-based algorithms originates from Braitenberg style vehicles [16]. In the developed algorithms [60, 73], chemical sensors can be connected to the wheels of vehicles through cross-coupling or "same side" connection so that the vehicles can be directed to the location with higher concentration. A third type of gradient-based methods is called E. coli algorithm, which controls the robot to move in a random direction for randomly generated units every time a new measurement arrives. The turning angle depends on the difference between the current measurement and the previous measurement. The algorithm is implemented in [96] and [75], but in [75], the algorithm is referred to as the "biased random walk". In addition to the aforementioned algorithms, the zigzag/dung beetle method inspired by beetles is implemented in [38,96]. The algorithm uses an odor probe with four sensors to estimate the gradients and provide bearing offset for the robot. Besides gradient-based algorithms, various gradient-free algorithms have been investigated. One type of the gradient-free algorithms is recognized as plume-centered upwind search, which is inspired by blue crabs [61, 111]. The algorithm involves estimating the center of the plume and controlling the robot to move to the center position. Then the robot traces the plume by modifying its moving direction

based on bilateral measurements. Another gradient-free approach is inspired by silkworm moth, which is divided into four actions: surge, cast, circle, and circle to finish. Various versions of this approach have been achieved [91, 96].

Most of the bio-inspired source-seeking algorithms introduced previously focus on using one single robot. However, collective behaviors of animal groups also provide inspirations for researchers in designing collective source-seeking algorithms. In biology, collective behaviors are observed in different species such as fish, birds and ants [29, 43, 66]. Collective behaviors are proved to be beneficial to other members in the group of a species and profitable for the survival of the entire group [24]. Therefore, researchers in engineering have been studying the collective behaviors of animal groups and gaining inspirations for the control of multi-robot systems. Various collective behaviors of animal groups such as collective transportation in ants [8, 9] and coalition formation in dolphin alliances [48] have been adopted in designing exploration strategies.

For the source-seeking problem, collective behaviors of animal groups also provide inspirations for researchers in designing algorithms using MSN. References [49, 52, 54] present algorithms of odor localization by groups of autonomous mobile robots. Specifically, reference [49] uses the Spiral Surge Algorithm to locate the source and find that elementary communication among a group of agents can increase the efficiency of the odor localization system performance. Reference [54] utilizes the modified particle swarm optimization method to address the problem of odor source localization in a dynamic environment that the odor distribution is changing over time. References [77, 93, 127] describe plume tracing algorithms that manage a distributed sensor network of autonomous vehicles to search for plumes in an unknown field. These plumes characterize the environment by creating a gradient field of some measurable physical quantity. To collaboratively search and locate an indeterminate number of emission sources in an unknown large-scale area, reference [30] provides a biasing expansion swarm approach (BESA) for multiple simple mobile agents with limited sensing and communication capabilities.

CHAPTER III

COHERENT STEPS OF SENSING AGENTS IN EXPLORABLE FIELDS

A common challenge in the MSN research is how to effectively handle the significant level of noise in the measurements. In the existing work on exploration, the main contribution is on developing and improving strategies for MSN so that desired explorative performance can be achieved in certain scalar fields. Instead of proposing new designs, we aim to develop an abstract theoretical foundation to rigorously define explorative behaviors of mobile sensing agents, and to analyze the movements of agents that lead to higher probability of successful exploration. For example, there exist several designs to achieve gradient climbing [4, 13, 27, 82, 87] and level curve tracking [116, 132]. However, our results explain why gradient following and level curve tracking desirable strategies in exploration.

For this purpose, we first propose a very simple but general discrete time model that captures two types of explorative behaviors [118–120]. We say an agent performs a seeking step if it intends to increase or decrease its measurements by making a move. We say an agent performs a strolling step if it intends to maintain a constant measurement. Due to the noise in measurements, the intended change in the measurements can only be achieved with certain probability. Those moves that achieve a success rate higher than a pre-selected threshold (usually greater than 50%) will be called coherent steps. For certain fields, coherent steps are easier to achieve than other fields. We will rigorously define a notion of explorability that is associated with a noisy scalar field to indicate whether agents will be able to achieve coherent steps with a certain level of success rate. Under the proposed framework, we are able to connect the variance of Gaussian noise with the success rate for coherent steps of mobile sensing agents. We will show that among all possible coherent

steps, gradient following achieves the highest success rate among all seeking steps, and level curve tracking achieves the highest success rate among all strolling steps.

3.1 Modeling Mobile Sensing Agents

Consider a deterministic smooth function $z(\mathbf{r}) : \mathbb{R}^n \to \mathbb{R}$, in which $\mathbf{r} \in \mathbb{R}^n$. $z(\mathbf{r})$ can be considered as a scalar field. Suppose mobile sensing agents are deployed in the field. The measurement process of an agent taken at a location $\mathbf{r}$ is modeled as a random variable $Y(\mathbf{r}) = z(\mathbf{r}) + W(\mathbf{r})$, where the term $W(\mathbf{r})$ represents the total noise. A realization of the random variable $W(\mathbf{r})$ is denoted by $w(\mathbf{r})$, representing the instant noise value at location $\mathbf{r}$ at the time of measurement. Then, the instant measurement taken at $\mathbf{r}$ can be written as

$$y(\mathbf{r}) = z(\mathbf{r}) + w(\mathbf{r}). \tag{1}$$

We first propose a general model to describe explorative behaviors of an agent. We assume that each agent starts from a starting location $\mathbf{r}_0$. It will take only one measurement at $\mathbf{r}_0$, denoted by $y(\mathbf{r}_0)$, as one realization of the random variable $Y(\mathbf{r}_0)$. Afterwards it moves to another location $\mathbf{r}$. Then it sets the new location $\mathbf{r}$ as its starting location, takes only one measurement at $\mathbf{r}$, denoted by $y(\mathbf{r})$, as one realization of the random variable $Y(\mathbf{r})$, and then moves to another location. This process will be repeated until a mission is finished. This simple model is very general that captures most of the explorative behaviors including identifying and tracking level curves and seeking extremums.

3.1.1 Steps and false-walks

Based on the relative displacement between $\mathbf{r}$ and $\mathbf{r}_0$, the field value $z(\mathbf{r})$ may increase, decrease, or remain unchanged compared to $z(\mathbf{r}_0)$. Let $\varepsilon^+ > 0$ and $\varepsilon^0 > 0$ be given. Define the sets $U^+(\varepsilon^+) = \{\mathbf{r}|z(\mathbf{r}) - z(\mathbf{r}_0) > \varepsilon^+\}, U^-(\varepsilon^+) = \{\mathbf{r}|z(\mathbf{r}) - z(\mathbf{r}_0) < -\varepsilon^+\}, U^0(\varepsilon^0) = \{\mathbf{r}||z(\mathbf{r}) - z(\mathbf{r}_0)| \leq \varepsilon^0\}$, and $B(\delta_1) = \{\mathbf{r}| \parallel \mathbf{r} - \mathbf{r}_0 \parallel \leq \delta_1\}$.

We define a *seeking step* of a mobile agent to be as follows.

Definition 3.1.1 *An* $(\varepsilon^+, \delta_1)$ *seeking step is a movement performed by a sensing agent starting from* $\mathbf{r}_0$ *and ending at* $\mathbf{r}$ *such that* $\mathbf{r} \in (U^+(\varepsilon^+) \cup U^-(\varepsilon^+)) \cap B(\delta_1) \neq \emptyset$.

The definition for the seeking step requires the step size δ_1 to be large enough so that there exist locations $\mathbf{r}$ from $\mathbf{r}_0$ so that the field values $z(\mathbf{r})$ and $z(\mathbf{r}_0)$ are differed at least by ε^+. An example of the seeking step will be to climb the local gradient of the field $z(\mathbf{r})$. We define a *strolling step* of a mobile agent to be as follows:

Definition 3.1.2 *An* $(\varepsilon^0, \delta_1)$ *strolling step is a movement performed by a sensing agent starting from* $\mathbf{r}_0$ *and ending at* $\mathbf{r}$ *so that* $\mathbf{r} \in U^0(\varepsilon^0) \cap B(\delta_1) \neq \emptyset$.

We see that a strolling step aims to track a level surface of the field $z(\mathbf{r})$. The constant δ_1 will be called the step size, and the constants ε^+ and ε^0 will be called the resolutions. Figure 1 illustrates the seeking steps and strolling steps of mobile sensing agents in a scalar field. The colored lines are level curves of the field, along which the field values are constant. Therefore, one example of strolling step is moving along one level curve, as illustrated by the step of the robot in the middle of the field. Since the gradient directions are perpendicular to tangent vectors of level curves, one example of seeking step is moving along the gradient direction at the current position of the agent, as illustrated by the steps of the robots in the right and left of the field.

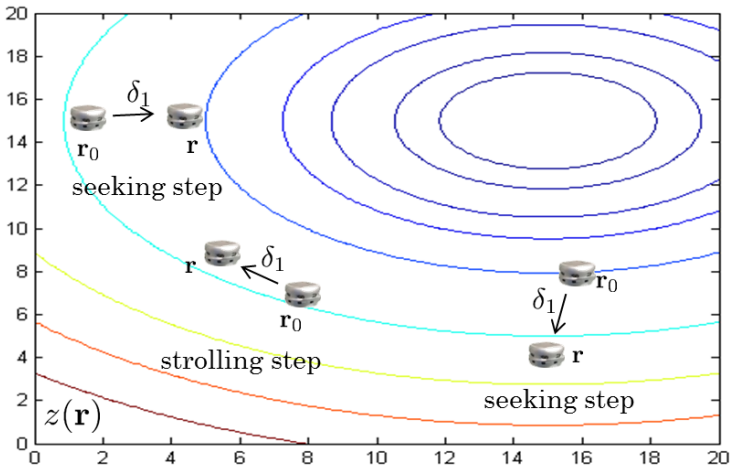

Figure 1: Seeking steps and strolling steps of mobile sensing agents in a scalar field.

With the presence of noises, when an agent moves one step in the field, the measurement $y(\mathbf{r})$ may not always be consistent with the field value $z(\mathbf{r})$. For example, $z(\mathbf{r})$ decreases compared to $z(\mathbf{r}_0)$ while the sensor readings $y(\mathbf{r})$ may increase compared to $y(\mathbf{r}_0)$. To describe such inconsistency, we introduce the concept of a *false-walk* as follows [118].

Definition 3.1.3 *Given $\delta_1 > 0$, $\varepsilon > 0$, $\varepsilon^+ > \varepsilon$, and $0 < \varepsilon^0 < \varepsilon$. A false-walk is an $(\varepsilon^+, \delta_1)$ seeking or $(\varepsilon^0, \delta_1)$ strolling step performed by a sensing agent such that one of the following conditions is satisfied:*

1. *If $\mathbf{r} \in U^+(\varepsilon^+)$, then, $y(\mathbf{r}) \leq y(\mathbf{r}_0) + \varepsilon$.*
2. *If $\mathbf{r} \in U^-(\varepsilon^+)$, then, $y(\mathbf{r}) \geq y(\mathbf{r}_0) - \varepsilon$.*
3. *If $\mathbf{r} \in U^0(\varepsilon^0)$, then, $|y(\mathbf{r}) - y(\mathbf{r}_0)| > \varepsilon$.*

The inconsistency between measurements and field values in a false-walk causes inaccurate extraction of information from sensor readings. Thus, in desirable exploration tasks, we want to reduce the probability of false-walks.

3.1.2 Coherent Steps and Local Explorability

The measurement equation $Y(\mathbf{r}) = z(\mathbf{r}) + W(\mathbf{r})$ can be interpreted as defining a noisy scalar field over any location $\mathbf{r} \in \mathbb{R}^n$. We found it convenient to take this view to categorize the steps of agents into *coherent* and *incoherent* steps.

Definition 3.1.4 *Consider two given constants (p, ε) where $0 < p < 1$, $\varepsilon^0 < \varepsilon < \varepsilon^+$, and steps from $\mathbf{r}_0$ to $\mathbf{r}$. We say an $(\varepsilon^+, \delta_1)$ seeking step is coherent if $\Pr(Y(\mathbf{r}) - Y(\mathbf{r}_0) > \varepsilon) > \frac{1+p}{2}$ for $\mathbf{r} \in U^+(\varepsilon^+)$ and $\Pr(Y(\mathbf{r}) - Y(\mathbf{r}_0) < -\varepsilon) > \frac{1+p}{2}$ for $\mathbf{r} \in U^-(\varepsilon^+)$. We say an $(\varepsilon^0, \delta_1)$ strolling step is coherent if $\Pr(|Y(\mathbf{r}) - Y(\mathbf{r}_0)| \leq \varepsilon) > \frac{1+p}{2}$. Otherwise, the seeking and strolling steps are incoherent.*

Note that since the values of $\varepsilon^+, \varepsilon^0$, and δ_1 can be arbitrarily selected, not all steps can be coherent. We see from the following proposition, which is easily proved from Definition 3.1.4, that a coherent step results in a relatively low probability of false-walks.

Proposition 3.1.5 *The probability for a an agent to make a false-walk from* $\mathbf{r}_0$ *to* $\mathbf{r}$ *satisfies* $\Pr(FW) \leq \frac{1-p}{2}$ *if and only if the step made is coherent.*

Proposition 3.1.5 indicates that a coherent step will give a success rate $\frac{1+p}{2}$ for the agent to achieve the desired seeking step or strolling step.

A natural question to ask is: how difficult is it for an agent to generate a coherent step in the noisy field $Y(\mathbf{r})$? Intuitively, if most of the steps of an agent are coherent, then we can say the noise term $W(\mathbf{r})$ does not have much effect on corrupting $z(\mathbf{r})$. We found it convenient to introduce a concept as *explorability* to describe the difficulty to explore the field $Y(\mathbf{r})$.

Definition 3.1.6 *Given* $\varepsilon > 0$ *and* $0 < p < 1$*, the field* $Y(\mathbf{r})$ *is locally* (p, ε) *explorable at* $\mathbf{r}_0$ *if there exist* $\varepsilon^+ > \varepsilon$ *and* $0 < \varepsilon^0 < \varepsilon$*, such that for all* $\delta_1 > 0$ *satisfying that* $(U^+(\varepsilon^+) \cup U^-(\varepsilon^+) \cup U^0(\varepsilon^0)) \cap B(\delta_1)$ *has a non-zero Lebesgue measure, the following conditions are satisfied:*

1. *If* $\mathbf{r} \in U^+(\varepsilon^+) \cap B(\delta_1)$*, then* $\Pr(Y(\mathbf{r}) > Y(\mathbf{r}_0) + \varepsilon) > \frac{1+p}{2}$.
2. *If* $\mathbf{r} \in U^-(\varepsilon^+) \cap B(\delta_1)$*, then* $\Pr(Y(\mathbf{r}) < Y(\mathbf{r}_0) - \varepsilon) > \frac{1+p}{2}$.
3. *If* $\mathbf{r} \in U^0(\varepsilon^0) \cap B(\delta_1)$*, then* $\Pr(|Y(\mathbf{r}) - Y(\mathbf{r}_0)| \leq \varepsilon) > \frac{1+p}{2}$.

Moreover, $Y(\mathbf{r})$ is (p, ε) explorable on an open set $C(\mathbf{r})$ if for every $\mathbf{r}_0 \in C(\mathbf{r})$, $Y(\mathbf{r})$ is locally (p, ε) explorable at $\mathbf{r}_0$. We refer to p as the *explorable probability* and ε as the *resolution*. We see δ_1 as the step size if an agent moves from $\mathbf{r}_0$ to $\mathbf{r}$. It is then straightforward to prove the following proposition from Definitions 3.1.4 and 3.1.6.

Proposition 3.1.7 Given $\varepsilon > 0$ and $0 < p < 1$, the field $Y(\mathbf{r})$ is locally (p, ε) explorable at location $\mathbf{r}_0$ if and only if there exist $\varepsilon^+ > \varepsilon$ and $0 < \varepsilon^0 < \varepsilon$, such that any $(\varepsilon^+, \delta_1)$ seeking step and any $(\varepsilon^0, \delta_1)$ strolling step from $\mathbf{r}_0$ to $\mathbf{r}$ are coherent.

In an explorable field, the difference between the noisy measurements $Y(\mathbf{r}_0)$ and $Y(\mathbf{r})$ is consistent with the difference between the mean field values $z(\mathbf{r}_0)$ and $z(\mathbf{r})$ with a probability greater than $\frac{1+p}{2}$. This connects the false-walks made by mobile agents with explorability. We have the following proposition.

Proposition 3.1.8 *Given $\varepsilon > 0$ and $0 < p < 1$, the field $Y(\mathbf{r})$ is locally (p, ε) explorable at location $\mathbf{r}_0$ if and only if there exist $\varepsilon^+ > \varepsilon$ and $0 < \varepsilon^0 < \varepsilon$, such that the probability of false-walks for $(\varepsilon^+, \delta_1)$ seeking steps and $(\varepsilon^0, \delta_1)$ strolling steps is less than $\frac{1-p}{2}$, that is,* $\Pr(FW) \leq \frac{1-p}{2}$.

The proof of the proposition is straightforward from the definition of the local explorability and false-walk. The proposition implies that the explorable probability p is an indictor of the probability of a false-walk. Hence the explorable probability p can be used as one criterion for the difficulty of exploring the noisy field $Y(\mathbf{r})$.

3.2 Agents in Gaussian Fields

In the rest of the chapter, we assume that the noise term $W(\mathbf{r})$ is Gaussian distributed with variance σ^2 and mean zero, i.e., $W(\mathbf{r}) \sim \mathcal{N}(0, \sigma^2)$. This assumption allows us to obtain more in-depth theoretical results to characterize the explorative behaviors of mobile sensing agents.

3.2.1 Explorability and Variance

Consider a step made by an agent from $\mathbf{r}_0$ to $\mathbf{r}$. Define a new random variable $Z(\mathbf{r}) = W(\mathbf{r}) - W(\mathbf{r}_0)$. Then, we obtain $Y(\mathbf{r}) - Y(\mathbf{r}_0) = z(\mathbf{r}) - z(\mathbf{r}_0) + Z(\mathbf{r})$. Since $W(\mathbf{r}) \sim \mathcal{N}(0, \sigma^2)$, according to the properties of Gaussian distribution, we have $Z(\mathbf{r}) \sim \mathcal{N}(0, 2\sigma^2)$. We then derive the relationship between noise variance σ and explorable probability p.

When $\mathbf{r}\in U^{-}(\varepsilon^{+})\cap B(\delta_1)$, $z(\mathbf{r})-z(\mathbf{r}_0)<-\varepsilon^{+}$. We derive

$$\begin{aligned}\Pr(Y(\mathbf{r})<Y(\mathbf{r}_0)-\varepsilon) &= \Pr(z(\mathbf{r})-z(\mathbf{r}_0)+W(\mathbf{r})-W(\mathbf{r}_0)<-\varepsilon)\\ &= \Pr(Z(\mathbf{r})<-\varepsilon-(z(\mathbf{r})-z(\mathbf{r}_0)))\\ &= \frac{1}{\sqrt{4\pi\sigma^2}}\int_{-\infty}^{-\varepsilon-(z(\mathbf{r})-z(\mathbf{r}_0))} e^{-\frac{z^2}{4\sigma^2}}dz\\ &= \frac{1}{2}(1+\mathrm{erf}(\frac{-\varepsilon-(z(\mathbf{r})-z(\mathbf{r}_0))}{2\sigma})),\end{aligned} \tag{2}$$

where erf represents the Gauss error function [1]. Similarly, when $\mathbf{r}\in U^{+}(\varepsilon^{+})\cap B(\delta_1)$,

$$\Pr(Y(\mathbf{r})>Y(\mathbf{r}_0)+\varepsilon) = 1-\frac{1}{2}(1+\mathrm{erf}(\frac{\varepsilon-(z(\mathbf{r})-z(\mathbf{r}_0))}{2\sigma})). \tag{3}$$

And when $\mathbf{r}\in U^{0}(\varepsilon^{0})\cap B(\delta_1)$, which indicates $|z(\mathbf{r})-z(\mathbf{r}_0)|\leq\varepsilon^{0}$, we obtain

$$\Pr(|Y(\mathbf{r})-Y(\mathbf{r}_0)|\leq\varepsilon) = \frac{1}{2}(\mathrm{erf}(\frac{\varepsilon-(z(\mathbf{r})-z(\mathbf{r}_0))}{2\sigma})+\mathrm{erf}(\frac{\varepsilon+(z(\mathbf{r})-z(\mathbf{r}_0))}{2\sigma})). \tag{4}$$

According to the definition of local explorability (Definition 3.1.6), if field $Y(\mathbf{r})$ is locally explorable, Equations (2), (3), and (4) should be greater than $\frac{1+p}{2}$. For Equations (2) and (3) to be greater than $\frac{1+p}{2}$, we obtain

$$\sigma<\frac{|z(\mathbf{r})-z(\mathbf{r}_0)|-\varepsilon}{2\mathrm{erf}^{-1}(p)}. \tag{5}$$

For Equation (4) to be greater than $\frac{1+p}{2}$, we have

$$\mathrm{erf}(\frac{\varepsilon-(z(\mathbf{r})-z(\mathbf{r}_0))}{2\sigma})+\mathrm{erf}(\frac{\varepsilon+(z(\mathbf{r})-z(\mathbf{r}_0))}{2\sigma})>1+p. \tag{6}$$

The results indicate that as long as noise variance σ satisfies Equations (5) and (6), field $Y(\mathbf{r})$ is locally (p,ε) explorable at $\mathbf{r}_0$. The results also verify the intuition that when the noise strength gets lower, a higher explorable probability can be achieved.

3.2.2 Coherent/Incoherent Steps in Gaussian Scalar Fields

The following corollary holds for agents in Gaussian scalar fields.

Corollary 3.2.1 Given a noisy Gaussian scalar field $Y(\mathbf{r}) = z(\mathbf{r}) + W(\mathbf{r})$, in which $W(\mathbf{r}) \sim \mathcal{N}(0, \sigma^2)$, and constants $\varepsilon > 0$, $0 < p < 1$, $\varepsilon^+ > \varepsilon$, and $0 < \varepsilon^0 < \varepsilon$. An $(\varepsilon^+, \delta_1)$ seeking step, if exists, is coherent with $\Pr(FW) \leq \frac{1-p}{2}$, if $\sigma < \frac{\varepsilon^+ - \varepsilon}{2\text{erf}^{-1}(p)}$. An $(\varepsilon^0, \delta_1)$ strolling step, if exists, is coherent with $\Pr(FW) \leq \frac{1-p}{2}$, if $\text{erf}(\frac{\varepsilon - \varepsilon^0}{2\sigma}) + \text{erf}(\frac{\varepsilon + \varepsilon^0}{2\sigma}) > 1 + p$.

Proof From Equation (5), we derive $\sigma < \frac{\varepsilon^+ - \varepsilon}{2\text{erf}^{-1}(p)}$. From Equation (6), we derive $\text{erf}(\frac{\varepsilon - \varepsilon^0}{2\sigma}) + \text{erf}(\frac{\varepsilon + \varepsilon^0}{2\sigma}) > 1 + p$. The rest of proof follows from Propositions 3.1.7 and 3.1.8. ■

Proposition 3.1.5 indicates that coherent steps are needed to ensure the probability of false-walks to be less than $\frac{1-p}{2}$. Corollary 3.2.1 provides an approach to check if a step is coherent or not through examining the noise variance. However, in practical scenarios, the values of ε^+ or ε^0 may be unknown to the agents. Therefore, for any strategy that wishes to achieve coherent steps, we need to determine whether coherent steps are performed based on the measurements taken. The following theorem provides a method to do so.

Theorem 3.2.2 Given $\varepsilon > 0$ and $0 < p < 1$, for a step from $\mathbf{r}_0$ to $\mathbf{r}$ with step size δ_1 in a locally (p, ε) Gaussian explorable field, if $\Pr(Y(\mathbf{r}) - Y(\mathbf{r}_0) > \varepsilon) > \frac{1+p}{2}$, then, there exists $\varepsilon^+ > \varepsilon$ such that $\mathbf{r} \in U^+(\varepsilon^+)$. If $\Pr(Y(\mathbf{r}) - Y(\mathbf{r}_0) < -\varepsilon) > \frac{1+p}{2}$, then, there exists $\varepsilon^+ > \varepsilon$ such that $\mathbf{r} \in U^-(\varepsilon^+)$.

Proof If the step satisfies $\Pr(Y(\mathbf{r}) - Y(\mathbf{r}_0) > \varepsilon) > \frac{1+p}{2}$, according to Equation (3), we obtain $1 - \frac{1}{2}(1 + \text{erf}(\frac{\varepsilon - (z(\mathbf{r}) - z(\mathbf{r}_0))}{2\sigma})) > \frac{1+p}{2}$, which yields $\text{erf}(\frac{\varepsilon - (z(\mathbf{r}) - z(\mathbf{r}_0))}{2\sigma}) < -p$. Since the error function $\text{erf}(\cdot)$ is monotonically increasing, we have $\frac{\varepsilon - (z(\mathbf{r}) - z(\mathbf{r}_0))}{2\sigma} < -\text{erf}(p)$, which produces $z(\mathbf{r}) - z(\mathbf{r}_0) > \varepsilon + 2\sigma\text{erf}(p)$. Since $\sigma > 0$ and $0 < p < 1$, therefore, there exists $\varepsilon^+ = \varepsilon + 2\sigma\text{erf}(p) > \varepsilon$ such that if $\Pr(Y(\mathbf{r}) - Y(\mathbf{r}_0) > \varepsilon) > \frac{1+p}{2}$, $z(\mathbf{r}) - z(\mathbf{r}_0) > \varepsilon^+$, which indicates that $\mathbf{r} \in U^+(\varepsilon^+)$. Similarly, we can prove that if $\Pr(Y(\mathbf{r}) - Y(\mathbf{r}_0) < -\varepsilon) > \frac{1+p}{2}$, there exists $\varepsilon^+ = \varepsilon + 2\sigma\text{erf}(p) > \varepsilon$ such that $z(\mathbf{r}) - z(\mathbf{r}_0) < -\varepsilon^+$, which indicates that $\mathbf{r} \in U^-(\varepsilon^+)$. Therefore, the step is an $(\varepsilon^+, \delta_1)$ coherent seeking step. ■

Similar to Theorem 3.2.2, we have the following theorem for coherent strolling steps.

Theorem 3.2.3 Given $\varepsilon > 0$ and $0 < p < 1$, for a step from $\mathbf{r}_0$ to $\mathbf{r}$ with step size δ_1 in a locally (p, ε) Gaussian explorable field, if $\Pr(|Y(\mathbf{r}) - Y(\mathbf{r}_0)| \leq \varepsilon) > \frac{1+p}{2}$ and $2\text{erf}(\frac{\varepsilon}{2\sigma}) > 1 + p$, then, there exists $\varepsilon^0 < \varepsilon$ such that $\mathbf{r} \in U^0(\varepsilon^0)$.

Proof Suppose $0 \leq |Y(\mathbf{r}) - Y(\mathbf{r}_0)| \leq y_{\max}$. If $\Pr(|Y(\mathbf{r}) - Y(\mathbf{r}_0)| \leq \varepsilon) > \frac{1+p}{2}$, Equation (6) holds. Since the error function $\text{erf}(\cdot)$ is monotonically increasing, as $|Y(\mathbf{r}) - Y(\mathbf{r}_0)|$ decreases from $y_{\max}$ to 0, the left side of Equation (6) increases from $\text{erf}(\frac{\varepsilon - y_{\max}}{2\sigma}) + \text{erf}(\frac{\varepsilon + y_{\max}}{2\sigma})$ to $2\text{erf}(\frac{\varepsilon}{2\sigma})$. If $y_{\max} \geq \varepsilon$, $\text{erf}(\frac{\varepsilon - y_{\max}}{2\sigma}) + \text{erf}(\frac{\varepsilon + y_{\max}}{2\sigma}) \leq \text{erf}(\frac{\varepsilon}{\sigma}) \leq 1$, which contradicts Equation (6). Thus, $y_{\max} < \varepsilon$. Therefore, if $\Pr(|Y(\mathbf{r}) - Y(\mathbf{r}_0)| \leq \varepsilon) > \frac{1+p}{2}$ and $2\text{erf}(\frac{\varepsilon}{2\sigma}) > 1 + p$, then, there exists $\varepsilon^0 < \varepsilon$, which satisfies $\text{erf}(\frac{\varepsilon - \varepsilon^0)}{2\sigma}) + \text{erf}(\frac{\varepsilon + \varepsilon^0}{2\sigma}) = 1 + p$, such that $|z(\mathbf{r}) - z(\mathbf{r}_0)| \leq \varepsilon^0$, which means $\mathbf{r} \in U^0(\varepsilon^0)$. Therefore, the step is an $(\varepsilon^0, \delta_1)$ strolling step. ■

Theorems 3.2.2 and 3.2.3 indicate that in an explorable Gaussian field, if we are able to observe from the measurements of the agents taken along their trajectories a consistent pattern, then, we will be confident that the steps they are taking are coherent. For example, suppose a Gaussian exploable field is smooth with a single extremum, e.g., maximum or minimum point. $\{\mathbf{r}_k\}, k = 1, \cdots, \ldots$ in a (p, ε) is a trajectory in the field with step size δ_1. If we are able to estimate statistically that $\Pr(Y(\mathbf{r}_k) - Y(\mathbf{r}_{k-1}) > \varepsilon) > \frac{1+p}{2}$, then, we can say that the trajectory will converge to a neighborhood of the maximum point. If for every k, $\Pr(Y(\mathbf{r}_k) - Y(\mathbf{r}_{k-1}) < -\varepsilon) > \frac{1+p}{2}$, then, the trajectory will converge to a neighborhood of the minimum point. If $\Pr(|Y(\mathbf{r}_k) - Y(\mathbf{r}_{k-1})| \leq \varepsilon) > \frac{1+p}{2}$, then, the trajectory will stay in the neighborhood of a level curve with value $z(\mathbf{r}_0)$.

We have seen from Proposition 3.1.7 that, a field being locally (p, ε) explorable at $\mathbf{r}_0$ is the sufficient and necessary condition for every $(\varepsilon^+, \delta_1)$ seeking step and every $(\varepsilon^0, \delta_1)$ strolling step from $\mathbf{r}_0$ to $\mathbf{r}$ being coherent. In real-world applications, the step size or the speed of a robot and the resolution of a sensor are usually pre-determined and fixed. Therefore, given any fixed step size δ_1 and resolution ε, we aim at finding the steps that can achieve maximum p. To examine this problem, we first define gradient climbing/descent and level curve tracking as follows.

Definition 3.2.4 *Given a scalar field $z(\mathbf{r})$ and an agent that moves one step from $\mathbf{r}_0$ to $\mathbf{r}$ with step size δ_1 in the field, if $\mathbf{r}-\mathbf{r}_0 = \pm\delta_1 \frac{\nabla z(\mathbf{r}_0)}{|\nabla z(\mathbf{r}_0)|}$, where $\nabla z(\mathbf{r}_0)$ is the gradient of the field at location $\mathbf{r}_0$, then, the agent is performing gradient climbing/desecent. If $z(\mathbf{r})-z(\mathbf{r}_0)=0$, then, the agent is performing level curve tracking.*

Based on Definition 3.2.4, we introduce the following Proposition, which explains why gradient following and level curve tracking are desirable strategies in exploration.

Proposition 3.2.5 *For an agent that moves one step from $\mathbf{r}_0$ to $\mathbf{r}$ with step size δ_1 in field $Y(\mathbf{r})$, among all possible coherent steps, gradient following achieves the highest success rate among all seeking steps, and level curve tracking achieves the highest success rate among all strolling steps.*

Proof We discuss seeking steps and strolling steps separately.

(1) For $(\varepsilon^+, \delta_1)$ seeking steps, $|z(\mathbf{r})-z(\mathbf{r}_0)| > \varepsilon^+$ and Equation (5) should be satisfied. Since the error function erf$(\cdot)$ is increasing, we obtain $p < \text{erf}(\frac{|z(\mathbf{r})-z(\mathbf{r}_0)|-\varepsilon}{2\sigma})$. Since p can be arbitrarily close to erf$(\frac{|z(\mathbf{r})-z(\mathbf{r}_0)|-\varepsilon}{2\sigma})$, then, when $\frac{|z(\mathbf{r})-z(\mathbf{r}_0)|-\varepsilon}{\sigma}$ increases, the upper bound of p increases as well. Thus, for every fixed ε, when $\mathbf{r}-\mathbf{r}_0$ is aligned with the gradient direction, e.g., in linear cases, $\mathbf{r}-\mathbf{r}_0 = \pm\delta_1 \frac{\nabla z(\mathbf{r}_0)}{\|\nabla z(\mathbf{r}_0)\|}$ and $|z(\mathbf{r})-z(\mathbf{r}_0)| = \delta_1 \parallel \nabla z(\mathbf{r}_0) \parallel$, we can obtain the supremum of p as $p_{\text{sup}} = \text{erf}(\frac{\delta_1\|\nabla z(\mathbf{r}_0)\|-\varepsilon}{2\sigma})$.

(2) For $(\varepsilon^0, \delta_1)$ strolling steps, $|z(\mathbf{r})-z(\mathbf{r}_0)| \le \varepsilon^0$, and Equation (6) needs to be satisfied. We derive three special cases from Equation (6).

1. $z(\mathbf{r})-z(\mathbf{r}_0) = \pm\varepsilon^0$. In this case, Equation (6) becomes erf$(\frac{\varepsilon-\varepsilon^0}{2\sigma})+\text{erf}(\frac{\varepsilon+\varepsilon^0}{2\sigma}) > 1+p$,

2. $z(\mathbf{r})-z(\mathbf{r}_0) = 0$. In this case, Equation (6) becomes $2\text{erf}(\frac{\varepsilon}{2\sigma}) > 1+p$.

3. When $|z(\mathbf{r})-z(\mathbf{r}_0)|$ goes from ε^0 to 0, the left side of Equation (6) increases from erf$(\frac{\varepsilon-\varepsilon^0}{2\sigma})+\text{erf}(\frac{\varepsilon+\varepsilon^0}{2\sigma})$ to $2\text{erf}(\frac{\varepsilon}{2\sigma})$. p can also be arbitrarily close to $2\text{erf}(\frac{\varepsilon}{2\sigma})-1$. Therefore, the local supremum of p is $p_{\text{sup}} = 2\text{erf}(\frac{\varepsilon}{2\sigma})-1$.

From the above discussion, when the moving direction of a step is aligned with the gradient direction or the tangent directions of a level curve, the explorable probability assumes local supremums. ■

3.3 Conclusion

This chapter provides simple discretized behavior models for mobile sensing agents exploring noisy scalar fields. We conclude that the steps taken by agents can be categorized into coherent steps and incoherent steps. Coherent steps are desired since the variation in the measurements of the agents and the variation in the underlying field along the trajectories of the agents tend to be consistent with each other. We argue that gradient seeking or level curve tracking strategies often lead to higher probability of producing coherent steps, which explains why these two strategies are widely studied and implemented in exploration missions.

CHAPTER IV

COORDINATING AGENTS

In exploration missions, a collaborating group of sensing agents outperforms a single sensing agent in many aspects [19, 31, 34] such as accuracy, adaptiveness, and efficiency. It has been shown that cooperative filtering using measurements from multiple agents can reduce the noise level, thus providing more accurate information for exploration. Under the framework of coherent steps of sensing agents and explorability, we investigate the cooperative filtering and cooperative control among multiple agents.

In this chapter, we first introduce the information dynamics of cooperative exploration by defining the state equation and measurement equation for a group of collaborating agents. The state is defined to be a vector consisting of the field value and gradient at the group center. To produce estimated field values and gradients, we construct a cooperative H_∞ filter and prove the sufficient conditions for the convergence and feasibility of the cooperative H_∞ filter. The use of the cooperative filters will reduce the noise level, hence will increase the success rate for coherent steps. We then present the formation control for the group of agents. In the last part of this chapter, we theoretically justify the minimum number of agents required to achieve a certain level of success rate.

4.1 Information Dynamics of Cooperative Exploration

Consider N mobile sensing agents in field $Y(\mathbf{r}) = z(\mathbf{r}) + W(\mathbf{r})$. $z(\mathbf{r}) : \mathbb{R}^n \to \mathbb{R}$, in which $\mathbf{r} \in \mathbb{R}^n$ and $n = 2$ or 3. Denote the position of the ith agent at kth time step as $\mathbf{r}_{i,k}, i = 1 \cdots, N$, the measurement taken by the ith agent as $y(\mathbf{r}_{i,k})$ and the true field value at location $\mathbf{r}_{i,k}$ as $z(\mathbf{r}_{i,k})$.

In the cooperative exploration phase, the sensing agents are required to move in a formation or cluster to estimate local structures of a field. Formation control is achieved by

using the Jacobi transform [132] [133], which decouples the dynamics of the formation and the dynamics of the motion of the center of the formation so that separate control laws can be designed for formation control and motion control. Therefore, when considering the motion of the agents in cooperative exploration, we treat the agents as an entire group and refer to it as a "super-agent", the position of which is denoted by $\mathbf{r}_{c,k} = \frac{1}{N}\sum \mathbf{r}_{i,k}$. Figure 2 illustrates a symmetric arrangement of a formation of three sensing agents.

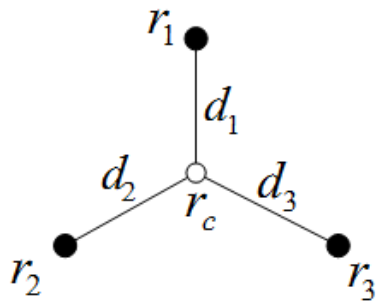

Figure 2: Symmetric arrangement of a formation of three sensing agents in 2D space.

Denote the field value at the formation center as $z(\mathbf{r}_{c,k})$. If $\mathbf{r}_{i,k}$ is close to $\mathbf{r}_{c,k}$, then, we can use Taylor's expansion to approximate $z(\mathbf{r}_{i,k})$. That is,

$$z(\mathbf{r}_{i,k}) \approx z(\mathbf{r}_{c,k}) + (\mathbf{r}_{i,k} - \mathbf{r}_{c,k})^T \nabla z(\mathbf{r}_{c,k}) + \frac{1}{2}(\mathbf{r}_{i,k} - \mathbf{r}_{c,k})^T \nabla^2 z(\mathbf{r}_{c,k})(\mathbf{r}_{i,k} - \mathbf{r}_{c,k}), \qquad (7)$$

in which $\nabla z(\mathbf{r}_{c,k})$ is the gradient of the field and $\nabla^2 z(\mathbf{r}_{c,k})$ is the Hessian of the field at $\mathbf{r}_{c,k}$. Choose the state to be $\mathbf{s}_k = (z(\mathbf{r}_{c,k}), \nabla z(\mathbf{r}_{c,k})^T)^T$. When the center of the super-agent moves, the state evolves according to

$$\begin{aligned} z(\mathbf{r}_{c,k}) &= z(\mathbf{r}_{c,k-1}) + (\mathbf{r}_{c,k} - \mathbf{r}_{c,k-1})^T \nabla z(\mathbf{r}_{c,k-1}), \\ \nabla z(\mathbf{r}_{c,k}) &= \nabla z(\mathbf{r}_{c,k-1}) + H_{c,k-1}(\mathbf{r}_{c,k} - \mathbf{r}_{c,k-1}), \end{aligned} \qquad (8)$$

where $H_{c,k-1}$ is the estimate of the field Hessian $\nabla^2 z(\mathbf{r}_{c,k-1})$. Define $\mathbf{h}_{k-1} = (0, \mathrm{E}[H_{c,k-1}(\mathbf{r}_{c,k} - \mathbf{r}_{c,k-1})]^T)^T$ and $A_{k-1} = \begin{pmatrix} 1 & (\mathbf{r}_{c,k} - \mathbf{r}_{c,k-1})^T \\ 0 & \mathbf{I}_{n\times n} \end{pmatrix}$, in which E denotes the expectation with

respect to the measurement noise in the process of estimating the field Hessian. We can see that A_{k-1} is nonsingular. Then the state equation can be expressed as

$$\mathbf{s}_k = A_{k-1}\mathbf{s}_{k-1} + \mathbf{h}_{k-1} + \mathbf{v}_{k-1}, \tag{9}$$

where $\mathbf{v}_{k-1}$ is the $N \times 1$ modeling noise vector, which accounts for positioning errors, estimation errors for the Hessians, and errors caused by higher-order terms omitted from the Taylor expansion. Let C_k be a $N \times (n+1)$ matrix with its ith row defined by $[1, (\mathbf{r}_{i,k} - \mathbf{r}_{c,k})^T]$ and D_k be a $N \times n^2$ matrix with its ith row vector defined by the Kronecker product $\frac{1}{2}((\mathbf{r}_{i,k} - \mathbf{r}_{c,k}) \otimes (\mathbf{r}_{i,k} - \mathbf{r}_{c,k}))^T$. Define a $N \times 1$ measurement vector $\mathbf{y}_k = [y(\mathbf{r}_{i,k})]$ and a noise vector $\mathbf{w}_k = [w_{i,k}]$ for $i = 1, \cdots, N$. We can write down the measurement equation as

$$\mathbf{y}_k = C_k\mathbf{s}_k + D_k\vec{H}_{c,k} + \mathbf{w}_k, \tag{10}$$

where $\vec{H}_{c,k}$ is the estimate of $H_{c,k}$ in a vector form, i.e., $\vec{H}_{c,k} = [H_{c,k(11)}\, H_{c,k(12)}\, H_{c,k(21)}\, H_{c,k(22)}]^T$, in two dimension. The estimation of the Hessian matrix $H_{c,k}$ in 2D is discussed in [132], and we will introduce the estimation in 3D in Chapter VII.

4.2 Cooperative H_∞ Filter

Based on the state Equation (9) and measurement Equation (10), a cooperative filter can be constructed to produce estimates of field value and gradient at the center of the multi-agent group. Reference [132] proposes a cooperative Kalman filter and proves the convergence of the cooperative Kalman filter. Typically, the optimality of the Kalman filter requires the noise to be zero-mean Gaussian. However, in real-world exploration tasks, the noise properties might be unknown. For possibly non-Gaussian noise, we construct a cooperative H_∞ filter, which does not require the knowledge of noise properties except that the noises are assumed to have bounded power [85, 100, 108, 123, 124]. An important constraint of the H_∞ filter is that the existence of the filter requires the fulfillment of a set of feasibility conditions, which further creates constraints on the exploration behaviors for the

cooperative agent formation. Convergence analysis of H_∞ filters has been performed in literature [14, 15]. Based on these work, we develop sufficient conditions for the cooperative H_∞ filter to admit feasible solutions and convergence.

4.2.1 Construction of the Cooperative H_∞ Filter

Define a cost function J as the ratio between the energy of the estimation error and the energy of the disturbances

$$J = \frac{\sum_{k=0}^{M-1} \|\mathbf{s}_k - \hat{\mathbf{s}}_k\|_{Q_k}^2}{\|\mathbf{s}_0 - \hat{\mathbf{s}}_0\|_{P_0^{-1}}^2 + \sum_{k=0}^{M-1} (\|w_k\|_{W_k^{-1}}^2 + \|v_k\|_{V_k^{-1}}^2)}, \tag{11}$$

where $\hat{\mathbf{s}}_0$ is the initial estimate of $\mathbf{s}_0$, $P_0 > 0, Q_k \geq 0, W_k > 0$ and $V_k > 0$ are the weighting matrices chosen by design, which depend on the noise strengths. For example, we choose $V_k > W_k$ if we know that the sensor noise is stronger than the state noise. The goal of the H_∞ filter is to guarantee that the cost J is less than a prescribed noise attenuation level γ that can be expressed as $J < \gamma^2$.

Given the state Equation (9) and the measurement Equation (10), a cooperative H_∞ filter can be designed. Following the general steps of constructing the H_∞ filter [100], the equations of the cooperative H_∞ filter are as follows.

$$S_k = P_k^{-1} - \frac{1}{\gamma^2} Q_k + C_k^T W_k^{-1} C_k, \tag{12}$$

$$K_k = S_k^{-1} C_k^T W_k^{-1}, \tag{13}$$

$$\hat{s}_{k+1} = A_k \hat{s}_k + \mathbf{h}_k + A_k K_k (\mathbf{y}_k - C_k \hat{s}_k - D_k \vec{H}_{c,k}), \tag{14}$$

$$P_{k+1} = A_k S_k^{-1} A_k^T + V_k. \tag{15}$$

Note that the cooperative H_∞ filter can only be computed when the agents are in a formation and the performance of the cooperative H_∞ filter depends on the configurations of the formation.

4.2.2 Convergence and Feasibility of the Cooperative H_∞ Filter

The convergence of H_∞ filtering has been investigated for both continuous-time and discrete-time systems. Readers can refer to [85, 108, 123, 124] and the references therein. The main feasibility results for discrete-time filtering are summarized in Theorem 4.2.1.

Theorem 4.2.1 *Consider the system (9), (10) and the cost function (11). Under the condition that A_k is nonsingular for each k, an H_∞ filter guaranteeing an attenuation level γ exists between time $k = 0$ and $k = M$ if and only if there exist two sequences of positive definite matrices $\{S_k\}_{k=0}^{M-1}$ and $\{P_k\}_{k=0}^{M-1}$ such that*

$$P_{k+1} = A_k S_k^{-1} A_k^T + V_k, \tag{16}$$

$$S_k = P_k^{-1} - \frac{1}{\gamma^2} Q_k + C_k^T W_k^{-1} C_k, \tag{17}$$

$$S_0 = P_0^{-1}, \tag{18}$$

$$S_k > 0, k = 0, 1, \cdots, M-1. \tag{19}$$

A feasible solution is defined as a positive definite solution P_k of the equation (16) that satisfies the equation (17).

The difference Riccati equation (DRE) (16) can also be written as

$$\begin{aligned} P_{k+1} &= A_k (P_k^{-1} - \frac{1}{\gamma^2} Q_k + C_k^T W_k^{-1} C_k)^{-1} A_k^T + V_k \\ &= A_k P_k A_k^T - A_k P_k [(C_k^T W_k^{-1} C_k - \frac{1}{\gamma^2} Q_k)^{-1} + P_k]^{-1} P_k A_k^T + V_k. \end{aligned} \tag{20}$$

As $k \to \infty$, if we drop the subscript ∞ for simplicity, then the Riccati equation (20) becomes

$$P = APA^T - AP[(C^T W^{-1} C - \gamma^{-2} Q)^{-1} + P]^{-1} PA^T + V. \tag{21}$$

The finite-horizon H_∞ problem becomes an infinite-horizon problem. If the solution to the infinite-horizon H_∞ filter exists, then the equation (21) admits a positive definite stabilizing solution P^s. In our case, since the noise properties of the field are unknown, we select

$Q_k \to \sigma_1^2 I, V_k \to \sigma_2^2 I$, and $W_k \to \sigma_3^2 I$, where I is the identity matrix. When $k \to \infty$, the formation is stabilized, then C goes to a constant matrix

$$C = \begin{pmatrix} 1 & (\mathbf{r}_1 - \mathbf{r}_c)^T \\ \vdots & \vdots \\ 1 & (\mathbf{r}_N - \mathbf{r}_c)^T \end{pmatrix} = \begin{pmatrix} 1 & \mathbf{d}_1^T \\ \vdots & \vdots \\ 1 & \mathbf{d}_N^T \end{pmatrix}, \tag{22}$$

where in 2D, $\mathbf{d}_i = [d_{i1}\ d_{i2}]^T$.

We now apply the feasibility and convergence conditions to the cooperative H_∞ filter and derive the sufficient conditions for the attenuation level and initial uncertainty that guarantee the convergence and feasibility of the cooperative H_∞ filter, which can give us a guidance in choosing γ and P_0 when implementing the filter. We have the following proposition.

Proposition 4.2.2 *Assume that equation (21) admits a positive definite solution P^s. Starting from initial condition $0 < P_0 < P^s$, the solution P_k of the Riccati equation (20) at every step k exists and converges when $k \to \infty$. Moreover, if*

(1) $\mathbf{r}_{c,k+1} - \mathbf{r}_{c,k} \to 0$ as $k \to \infty$, and

(2) the attenuation level γ satisfies

$$\gamma^2 > \max(0, \frac{\sigma_1^2\sigma_3^2}{N - |\sum_{i=1}^N d_{i1}| - |\sum_{i=1}^N d_{i2}|}, \frac{\sigma_1^2\sigma_3^2}{\sum_{i=1}^N d_{i1}^2 - |\sum_{i=1}^N d_{i1}| - |\sum_{i=1}^N d_{i1}d_{i2}|}, \frac{\sigma_1^2\sigma_3^2}{\sum_{i=1}^N d_{i2}^2 - |\sum_{i=1}^N d_{i2}| - |\sum_{i=1}^N d_{i1}d_{i2}|}), \tag{23}$$

we obtain the solution that $P^s = \frac{1}{2}(\sigma_2^2 I + (\sigma_2^4 I + 4\sigma_2^2 X)^{\frac{1}{2}})$ where $X = (\sigma_3^{-2} C^T C - \sigma_1^2 \gamma^{-2} I)^{-1}$.

Proof Let's first consider the solution P^s of the Riccati equation (21). Given the condition (1), we can approximate A_k by the identity matrix I. If we substitute $A = I$ into equation (21), then after rearranging terms, we can obtain

$$P^2 - \sigma_2^2 P - \sigma_2^2 (\sigma_3^{-2} C^T C - \sigma_1^2 \gamma^{-2} I)^{-1} = 0. \tag{24}$$

Define $X = (\sigma_3^{-2} C^T C - \sigma_1^2 \gamma^{-2} I)^{-1}$. Then the above equation can be written as $P^2 - \sigma_2^2 P - \sigma_2^2 X = 0$. For a quadratic matrix equation of the form

$$Q(Z) = A'Z^2 + B'Z + C' = 0, A', B', C' \in R^{n \times n}, \tag{25}$$

only when (1) $A' = I$, (2) B' and C' commute, and (3) the square root of $B'^2 - 4C'$ exists, we can apply the formula for the roots of a scalar quadratic equation and find a closed-form solution to the equation (25) [50]. The solution is $Z = \frac{1}{2}(-B' \pm (B'^2 - 4C')^{\frac{1}{2}})$. By comparison, $A' = I, B' = -\sigma_2^2 I$, and $C' = -\sigma_2^2 X$ satisfy the first two conditions. If the square root of $\sigma_2^4 I + 4\sigma_2^2 X$ exists, then we can get the solution as $P^s = \frac{1}{2}(\sigma_2^2 I + (\sigma_2^4 I + 4\sigma_2^2 X)^{\frac{1}{2}})$.

To check whether the square root of $\sigma_2^4 I + 4\sigma_2^2 X$ exists or not is equivalent to check whether $\sigma_2^4 I + 4\sigma_2^2 X$ is positive definite or not. From the facts that the identity matrix is positive definite and the sum of two positive definite matrices is positive definite, it is suffice to check the definiteness of $X^{-1} = \sigma_3^{-2} C^T C - \sigma_1^2 \gamma^{-2} I$. We can compute that $C^T C = \begin{pmatrix} N & \sum_i^N \mathbf{d}_i^T \\ \sum_i^N \mathbf{d}_i & \sum_i^N \mathbf{d}_i \mathbf{d}_i^T \end{pmatrix}$. Plug $C^T C$ into X^{-1}, we have

$$X^{-1} = \begin{pmatrix} \sigma_3^{-2} N - \sigma_1^2 \gamma^{-2} & \sigma_3^{-2} \sum_i^N \mathbf{d}_i^T \\ \sigma_3^{-2} \sum_i^N \mathbf{d}_i & \sigma_3^{-2} \sum_{i=1}^N \mathbf{d}_i \mathbf{d}_i^T - \sigma_1^2 \gamma^{-2} I \end{pmatrix}. \tag{26}$$

We know that a symmetric matrix is positive definite if (1) all the diagonal entries are positive and (2) each diagonal entry is greater than the sum of the absolute values of all other entries in the same row. Therefore, we should have

$$\sigma_3^{-2} \sum_{i=1}^N d_{ij}^2 - \sigma_1^2 \gamma^{-2} > \sigma_3^{-2} |\sum_{i=1}^N d_{ij}| + \sigma_3^{-2} |\sum_{i=1}^N d_{i1} d_{i2}|, j = 1, 2. \tag{27}$$

and

$$\sigma_3^{-2} N - \sigma_1^2 \gamma^{-2} > \sigma_3^{-2} |\sum_{i=1}^N d_{i1}| + \sigma_3^{-2} |\sum_{i=1}^N d_{i2}|. \tag{28}$$

which yield

$$\gamma^2 > \frac{\sigma_1^2 \sigma_3^2}{N - |\sum_{i=1}^N d_{i1}| - |\sum_{i=1}^N d_{i2}|} > 0, \tag{29}$$

and

$$\gamma^2 > \frac{\sigma_1^2\sigma_3^2}{\sum_{i=1}^N d_{ij}^2 - |\sum_{i=1}^N d_{ij}| - |\sum_{i=1}^N d_{i1}d_{i2}|} > 0, j = 1,2. \tag{30}$$

Therefore, the matrix X^{-1} is positive if equation (138) is satisfied. This is the sufficient condition for our case so that we can get the solution P^s.

From Theorem 2 in [14], for some constant $\varepsilon > 0$ and the solution Y of a Lyapunov equation defined in [14], if $0 < P_0 < P^s + (Y + \varepsilon I)^{-1}$, then the solution P_k of equation (16) is feasible for all $k > 0$ and converges to the stabilizing solution P^s as $k \to \infty$. Since the matrix Y is positive definite, we can consider a stricter condition, which is $0 < P_0 < P^s$. Therefore, if $0 < P_0 < P^s$, the solution P_k to the Riccati equation (20) is feasible for all k and converges to the stabilizing solution P^s as $k \to \infty$. ■

Now let's consider a symmetric formation. Suppose the N agents are arranged so that $|\mathbf{d}_{i,k}| = a, i = 1, \cdots, N$, where a is a constant. Denote the phase angle of the vector $\mathbf{d}_{1,k}$ in the inertial frame by θ, and the angle between $\mathbf{d}_{i,k}$ and $\mathbf{d}_{1,k}$ by $\theta_i = \frac{2\pi}{N}(i-1)$. Then we can obtain $\mathbf{d}_{i,k} = a(\cos(\theta_i + \theta), \sin(\theta_i + \theta))^T$. We have the following corollary for the symmetric formation.

Corollary 4.2.3 *Assume that equation (21) admits a positive definite solution P^s. For a symmetric formation, starting from initial condition $0 < P_0 < P^s$, the solution P_k of the Riccati equation (20) at every step k exists and converges when $k \to \infty$. Moreover, if*

(1) $\mathbf{r}_{c,k+1} - \mathbf{r}_{c,k} \to 0$ as $k \to \infty$, and

(2) the attenuation level γ satisfies

$$\gamma^2 > \max\left(\frac{\sigma_1^2\sigma_3^2}{N}, \frac{2\sigma_1^2\sigma_3^2}{aN}\right), \tag{31}$$

then,

$$P^s = \frac{1}{2} diag\Big(\sigma_2\Big(\sigma_2^2 + \frac{4\gamma^2}{\sigma_3^{-2}\gamma^2 N - \sigma_1^2}\Big)^{\frac{1}{2}} + \sigma_2^2, \sigma_2\Big(\sigma_2^2 + \frac{8\gamma^2}{a\sigma_3^{-2}\gamma^2 N - 2\sigma_1^2}\Big)^{\frac{1}{2}} + \sigma_2^2,$$
$$\sigma_2\Big(\sigma_2^2 + \frac{8\gamma^2}{a\sigma_3^{-2}\gamma^2 N - 2\sigma_1^2}\Big)^{\frac{1}{2}} + \sigma_2^2\Big). \tag{32}$$

Proof When the formation is symmetric, we use the following relationships,

$$\sum_{i=1}^{N} \mathbf{d}_i = a \sum_{i=1}^{N} (\cos(\theta_i + \theta), \sin(\theta_i + \theta))^T = \mathbf{0}, \tag{33}$$

$$\sum_{i=1}^{N} d_{i1}^2 = a^2 \sum_{i=1}^{N} \cos^2(\theta_i + \theta) = \frac{1}{2} a^2 N, \tag{34}$$

$$\sum_{i=1}^{N} d_{i2}^2 = a^2 \sum_{i=1}^{N} \sin^2(\theta_i + \theta) = \frac{1}{2} a^2 N, \tag{35}$$

$$\sum_{i=1}^{N} d_{i1}^2 d_{i2}^2 = a^2 \sum_{i=1}^{N} \cos(\theta_i + \theta) \sin(\theta_i + \theta) = 0. \tag{36}$$

Therefore, we can obtain that $X = diag(\sigma_3^{-2}N - \sigma_1^2\gamma^{-2}, \frac{1}{2}a\sigma_3^{-2}N - \sigma_1^2\gamma^{-2}, \frac{1}{2}a\sigma_3^{-2}N - \sigma_1^2\gamma^{-2})^{-1}$. In order to obtain $X > 0$, we should have $\gamma^2 > \max(\frac{\sigma_1^2\sigma_3^2}{N}, \frac{2\sigma_1^2\sigma_3^2}{aN})$. If we plug X into $P^s = \frac{1}{2}(\sigma_2^2 I + (\sigma_2^4 I + 4\sigma_2^2 X)^{\frac{1}{2}})$ obtained in Proposition 4.2.2, we can obtain the equation (32). The rest of the proof is similar to the proof of Proposition 4.2.2. ■

Remark: The condition (1) in Proposition 4.2.2 and Corollary 4.2.3 is satisfied if the formation center eventually stops moving. If the source seeking strategy is successful, then this condition will be satisfied since the formation center will stay near a local minimum of the field.

Proposition 4.2.2 and Corollary 4.2.3 imply that a lower noise attenuation level γ and a smaller error bound P^s can be achieved as the number of agents increases and the formation gets larger. The choices of γ and P_0 also depend on the noise strength, which requires users to have some preliminary knowledge of the field before running the filter.

4.3 Formation Shape Control

The collaborating agents are controlled to maintain a desirable formation. The formation shape is described using Jacobi vectors $\mathbf{q}_{j,k}, j = 1, \cdots, N-1$ that satisfy

$$[\mathbf{r}_{c,k}, \mathbf{q}_{1,k}, \cdots, \mathbf{q}_{N-1,k}] = [\mathbf{r}_{1,k}, \mathbf{r}_{2,k}, \cdots, \mathbf{r}_{N,k}]\Psi, \tag{37}$$

where Ψ is the Jacobi transform. For example, if we deploy three agents, the Jacobi vectors are

$$\begin{aligned}\mathbf{q}_{1,k} &= \frac{\sqrt{2}}{2}(\mathbf{r}_{2,k} - \mathbf{r}_{3,k}),\\ \mathbf{q}_{2,k} &= \frac{\sqrt{6}}{6}(2\mathbf{r}_{1,k} - \mathbf{r}_{2,k} - \mathbf{r}_{3,k}),\end{aligned} \tag{38}$$

and the Jacobi transform is

$$\Psi = \begin{pmatrix} \frac{1}{3} & \frac{1}{3} & \frac{1}{3} \\ 0 & \frac{\sqrt{2}}{2} & -\frac{\sqrt{2}}{2} \\ \frac{\sqrt{6}}{3} & -\frac{\sqrt{6}}{6} & -\frac{\sqrt{6}}{6} \end{pmatrix}. \tag{39}$$

The Jacobi transform decouples the kinetic energy of the entire system [132] [133], which enables us to design separate control laws for the formation center motion and the formation shape.

At step k, we apply the control laws

$$\mathbf{u}_{j,k} = -K_1(\mathbf{q}_{j,k} - \mathbf{q}_j^0) - K_2\dot{\mathbf{q}}_{j,k}, \quad j = 1, \cdots, N-1 \tag{40}$$

to $\ddot{\mathbf{q}}_{j,k} = \mathbf{u}_{j,k}$, where K_1 and K_2 are positive constant gains and $\mathbf{q}_j^0$ are designed vectors that define a desired formation. The control laws have an exponential rate of convergence. If we take the inverse Jacobi transform, then the new positions of the agents $\mathbf{r}_{i,k+1}, i = 1, \cdots, N$ can be obtained by

$$[\mathbf{r}_{1,k+1}, \mathbf{r}_{2,k+1}, \cdots, \mathbf{r}_{N,k+1}] = [\mathbf{r}_{c,k+1}, \mathbf{q}_{1,k+1}, \cdots, \mathbf{q}_{N-1,k+1}]\Psi^{-T}. \tag{41}$$

By applying the formation controller (40), the agents converge to a desired formation so that the cooperative exploration is achieved.

4.4 Estimating Minimum Number of Agents

We have discussed the coherent steps of sensing agents in Gaussian fields in Chapter III. In this section, we theoretically justify that using cooperative filters can reduce noise levels,

thus, can increase the probability of coherent steps. We make the following assumption for the properties of $\mathbf{v}_k$ and $\mathbf{w}_k$ in state equation (9) and measurement equation (10).

Assumption 4.4.1 *$\mathbf{v}_k$ and $\mathbf{w}_k$ are zero mean Gaussian with covariance matrices $V_k = E[\mathbf{v}_k\mathbf{v}_k^T] = \sigma_2^2 I_{3\times 3}$ and $W_k = E[\mathbf{w}_k\mathbf{w}_k^T] = \sigma_3^2 I_{3\times 3}$.*

4.4.1 Cooperative Kalman Filter

A cooperative Kalman filter can be computed to provide estimates of field value and gradient at the formation center [132]. The cooperative Kalman filter equations are as follows

$$\begin{aligned}
\mathbf{s}_{k(-)} &= \mathbf{A}_{k-1}\mathbf{s}_{k-1(+)} + \mathbf{h}_{k-1},\\
P_{k(-)} &= \mathbf{A}_{k-1}P_{k-1(+)}\mathbf{A}_{k-1}^T + V_{k-1},\\
K_k &= P_{k(-)}C_k^T[C_kP_{k(-)}C_k^T + W_k]^{-1},\\
\mathbf{s}_{k(+)} &= \mathbf{s}_{k(-)} + K_k(\mathbf{y}_k - C_k\mathbf{s}_{k(-)} - D_k\vec{H}_{c,k}),\\
P_{k(+)}^- &= P_{k(-)}^{-1} + C_k^TW_k^{-1}C_k. \qquad (42)
\end{aligned}$$

The subscript $(-)$ and $(+)$ indicate the predictions and the updated estimates, respectively. The convergence of the cooperative Kalman filter can be proved in a similar way as the proof in [132].

Suppose we control the agents in the group to form a formation that is symmetric with respect to the formation center. The distance from each agent to the center of the formation is a, which means $\| \mathbf{r}_{i,k} - \mathbf{r}_{c,k} \| = a$. As $k \to \infty$, A_∞ goes to $I_{3\times 3}$ since $(\mathbf{r}_{c,k} - \mathbf{r}_{c,k-1}) \to 0$. Similar to the proof in H_∞ filter case, we can calculate that, as $k \to \infty$, $C^TW^{-1}C = \frac{1}{\sigma_2^2}\mathrm{diag}(N, \frac{1}{2}a^2N, \frac{1}{2}a^2N)$ holds. Hence, we obtain the closed form of the error covariance of the cooperative Kalman filter P as

$$\begin{aligned}
P &= \mathrm{diag}(-\frac{1}{2}\sigma_2^2 + \frac{\sigma_2}{2}\sqrt{\sigma_3^2 + \frac{4\sigma_3^2}{N}}, -\frac{1}{2}\sigma_2^2 + \frac{\sigma_2}{2}\sqrt{\sigma_2^2 + \frac{8\sigma_3^2}{a^2N}}, -\frac{1}{2}\sigma_2^2 + \frac{\sigma_2}{2}\sqrt{\sigma_2^2 + \frac{8\sigma_3^2}{a^2N}})\\
&= \mathrm{diag}(P(1), P(2), P(3)), \qquad (43)
\end{aligned}$$

where $P(1)$ is the error covariance of the filtered measurements, and $P(2)$ and $P(3)$ correspond to the error covariance of the field gradient estimation at the center of the formation. To evaluate the noise reduction ability, we need to compare $P(1)$ with σ_3^2. We provide the following lemma to address this comparison.

Lemma 4.4.2 *Consider that N sensing agents move in field $Y(\mathbf{r})$ in a symmetric formation. Suppose the cooperative Kalman filter is computed. If $\sigma_2 = \frac{1}{m}\sigma_3$, where $m > 1$ is a constant, then under Assumption 4.4.1, the error covariance of the filtered measurements $P(1)$ is less than the variance of noise σ_3 if $N \geq 2$.*

Proof According to Assumption 4.4.1, $\sigma_2 = \frac{1}{m}\sigma_3$. Substituting σ_1 into $P(1)$ yields $P(1) = \frac{1}{2m^2}\sqrt{1+\frac{4}{N}}\sigma_3^2$. If we set $P(1) < \sigma_3^2$, then $N > \frac{4}{4m^4-1}$. Since $m > 1$, which indicates $\frac{4}{4m^4-1} < \frac{4}{3}$, then, as long as $N > \frac{4}{3}$, $P(1) < \sigma_3^2$ holds. Therefore, since N should be an integer, $N \geq 2$ guarantees that cooperative exploration reduces the noise. ■

In Lemma 4.4.2, we assume $\sigma_2 = \frac{1}{m}\sigma_3$, where $m > 1$. Remember that σ_2 represents the variance of the modeling noise, which accounts for positioning errors, estimation errors for the Hessian, and errors caused by higher-order terms omitted from the Taylor expansion. The assumption $m > 1$ indicates that if the modeling noise strength is less than the noise strength in the measurements taking by agents, then by increasing the number of agents, the errors in the output of the cooperative Kalman filter will be reduced. Otherwise, the errors induced by the construction of the filter might compensate for the noise reduction ability by the filter.

4.4.2 Estimating the Minimum Number of Agents by Cooperative Exploration in Gaussian Fields

The expression of $P(1)$ in of the cooperative Kalman filter indicates that as the number of agents N increases, $P(1)$ decreases. Therefore, by comparing $P(1)$ with σ_3^2, we can evaluate the lower bound of the required number of agents that guarantees coherent steps of the super-agent.

Proposition 4.4.3 *Under Assumption 4.4.1, suppose a super-agent formed by N collaborating agents in a symmetric formation moves from* $\mathbf{r}_{c,0}$ *to* $\mathbf{r}_c$ *in field* $Y(\mathbf{r}) = z(\mathbf{r}) + W(\mathbf{r})$. *Given constants* $\varepsilon > 0$, $0 < p < 1$, $\varepsilon^+ > \varepsilon$, *and* $0 < \varepsilon^0 < \varepsilon$. *An* $(\varepsilon^+, \delta_1)$ *seeking step of the super-agent is coherent if N satisfies*

$$N > \frac{16\sigma_3^4}{m^2(\frac{|z(\mathbf{r}_c)-z(\mathbf{r}_{c,0})|-\varepsilon}{\text{erf}^{-1}(p)})^4 - 4\sigma_3^4}. \tag{44}$$

An $(\varepsilon^0, \delta_1)$ *strolling step of the super-agent is coherent if N satisfies*

$$\begin{aligned} &\text{erf}(\frac{\sqrt{2}m(\varepsilon-(z(\mathbf{r}_c)-z(\mathbf{r}_{c,0})))}{2(1+\frac{4}{N})^{\frac{1}{4}}\sigma_3}) + \text{erf}(\frac{\sqrt{2}m(\varepsilon+(z(\mathbf{r}_c)-z(\mathbf{r}_{c,0})))}{2(1+\frac{4}{N})^{\frac{1}{4}}\sigma_3}) \\ &\qquad > 1 + p, \end{aligned} \tag{45}$$

Proof Substituting $P(1)^{\frac{1}{2}} = \frac{1}{\sqrt{2}m}(1+\frac{4}{N})^{\frac{1}{4}}\sigma_3$ for σ in Equations (5) and (6) yields Equations (44) and (45). According to the definition of coherent steps, if N satisfies Equations (44) and (45), the step is coherent. ■

Based on Proposition 4.4.3, if a step of an agent from any location $\mathbf{r}_0$ is incoherent, then, we can increase the number of agents in the field and let them perform cooperative exploration. If the number of agents N satisfies Equations (44) and (45), then the step of the super-agent in cooperative exploration is coherent, which indicates that the probability of false-walks of the super-agent can be guaranteed to be less than $\frac{1-p}{2}$.

Although the number of agents N can be increased to decrease the probability of false-walks, in real-world applications, we need to balance the tradeoffs between accuracy and cost. Therefore, we propose the following algorithm, which allows the agents to self-organize into groups with an estimated minimum number of agents that grantees coherent steps along their trajectories. After the agents form a group with estimated minimum number of agents, they start cooperative exploration. The rest of the agents can be assigned to other exploration tasks.

Algorithm 4.4.4 *Given the field* $Y(\mathbf{r}) = z(\mathbf{r}) + W(\mathbf{r})$ *and* $\varepsilon > 0$ *and* $0 < p < 1$, *suppose N agents are deployed in the field.*

S.1 From time instant $k = 1$, the agents individually perform exploration tasks with step size δ_1 according to any strategy.

S.2 At $k = M$, the ith agent estimates the field noise variance by

$$\hat{\sigma}_3^2 = \frac{1}{M}\sum_{j=1}^{M}(y(\mathbf{r}_{i,j}) - \frac{1}{M}\sum_{l=1}^{M} y(\mathbf{r}_{i,l}))^2, \tag{46}$$

and estimates the number of the agents required to guarantee coherent steps by

$$N_{\min} > \frac{16\hat{\sigma}_3{}^4}{m^2(\frac{(|z(\mathbf{r}_{i,M}) - z(\mathbf{r}_{i,M-1})| - \varepsilon)}{\mathrm{erf}^{-1}(p)})^4 - 4\hat{\sigma}_3^4}, \tag{47}$$

Then the ith agent forms a group of $N_{\min}$ with the $N_{\min} - 1$ agents closest to it. The distance between the ith and jth agents is measured by $d_{i,j} = |\mathbf{r}_{i,k} - \mathbf{r}_{j,k}|$. If $N < N_{\min}$, all the agents form a group with N agents.

S.3 From $k = M + 1$, the group performs cooperative exploration. A cooperative Kalman filter can be constructed to produce estimates of the field value and gradient at the formation center. The remaining agents continue individual exploration.

Note that the cooperative exploration uses the model we introduced in this chapter. However, the cooperative exploration tasks are not fixed. Given the estimated state (field value and gradient at the formation center), various exploration tasks can be achieved such as source seeking and level curve tracking, which will be introduced in the following chapters.

CHAPTER V

BIO-INSPIRED SOURCE SEEKING

As noted in the introduction, autonomous sensing agents that are capable of localizing sources in a scalar field are of great importance in various scenarios such as locating chemical spills, detecting fire in its early stage, and monitoring the algae bloom. Researchers have developed various source-seeking algorithms, many of which are inspired by behaviors of different animal species [49, 52, 54, 61, 96].

The existing algorithms can be categorized into two directions: gradient-based approaches and gradient-free approaches. For the gradient-based approaches, the agents either estimate the gradient directions based on the measurements [5, 23, 27, 69, 87], or can measure the gradient directly using certain sensors [74]. Since we assume that each agent takes only one measurement of the field at each time instant, one agent needs to move several steps to collect measurements so that the gradient of the field can be estimated, or a group of agents need to share measurements and positions with each other to produce an estimate of the gradient, which requires communication among agents or between agents and a central computer. However, in real-world applications, we may face various limitations in terms of communication capability and computational load. Therefore, source-seeking algorithms that require less communication and computation are desirable.

In this chapter, we first introduce gradient-based source seeking using both individual agents and a group of collaborating agents. Then, we present a source seeking algorithm without explicit gradient estimation inspired by observations of fish schools [115].

5.1 Problem Formulation

Consider a group of N collaborating sensing agents that are seeking a minimum of an unknown scalar field $z(\mathbf{r})$, in which $\mathbf{r} \in R^2$ denotes a location in the field. Let $\mathbf{r}_i$ represent

the position and $\mathbf{v}_i$ represent the velocity of the ith agent. Suppose the motion of each agent in the group satisfies

$$\dot{\mathbf{r}}_i = \mathbf{v}_i, \quad i = 1, \cdots, N. \tag{48}$$

Denote the velocity of the group center as $\mathbf{v}_c$. Then, we derive $\mathbf{v}_c = \frac{1}{N}\sum_{i=1}^{N} \mathbf{v}_i$.

Suppose the field value satisfies $z_{\min} \leq z(\mathbf{r}) \leq z_{\max}$, in which $z_{\min} \geq 0$. Along the trajectories of the agents, the sensing agents take measurements of the field, which can be written as $y(\mathbf{r}_i) = z(\mathbf{r}_i) + w(\mathbf{r}_i), i = 1, \cdots, N$, in which $w(\mathbf{r}_i)$ is the noise term that may come from measuring process or the field.

The problem is to design controls for the velocities of the agents so that the group can move close to a local minimum in the field while maintaining a desired formation. More specifically, the goal is to design $\mathbf{v}_i$ so that: (1) $\frac{\mathbf{v}_c}{\|\mathbf{v}_c\|} \cdot \frac{\nabla z(\mathbf{r_c})}{\|\nabla z(\mathbf{r_c})\|}$ converges to -1 when $\| \nabla z(\mathbf{r_c}) \| \neq 0$, and (2) the relative displacement between agents $\mathbf{r}_i - \mathbf{r}_j$, where $j \neq i$, converges to a desired vector. Note that the first goal is invalid when $\| \nabla z(\mathbf{r_c}) \| = 0$, which indicates a singular point or saddle point in the field.

5.2 Gradient-based Source-Seeking

For gradient-based source-seeking, the agents produce estimates of the field gradient based on the measurements collected along their trajectories, and then follow the gradient direction to locate a minimum in the field.

If the agents are performing individual source-seeking, then, each agent estimates the gradient of the field based on its previous measurements, and moves according to the estimated field gradients as

$$\dot{\mathbf{r}}_{i,k} = -\delta_1 \frac{\nabla \hat{z}(\mathbf{r}_{i,k})}{\| \nabla \hat{z}(\mathbf{r}_{i,k}) \|}, \tag{49}$$

where $\nabla \hat{z}(\mathbf{r}_{i,k})$ is the estimated gradient of the field at position $\mathbf{r}_{i,k}$, and δ_1 is the step size.

In the following, we give a simple example of estimating the gradient of the field $\nabla z(\mathbf{r}_{i,k})$ by an individual agent at each time step k using the current and previous measurements. Denote the directional derivative of the field at position $\mathbf{r}_{i,k}$ in the direction h as

$D_h z(\mathbf{r}_{i,k})$, which satisfies $D_h z(\mathbf{r}_{i,k}) = \nabla z(\mathbf{r}_{i,k}) \cdot h$. If the successive positions of the agent are close enough, the gradient at the position $\mathbf{r}_{i,k}$ can be approximated by solving the following two equations.

$$y(\mathbf{r}_{i,k}) - y(\mathbf{r}_{i,k-1}) = \nabla \hat{z}(\mathbf{r}_{i,k}) \cdot (\mathbf{r}_{i,k} - \mathbf{r}_{i,k-1}), \tag{50}$$

$$y(\mathbf{r}_{i,k-1}) - y(\mathbf{r}_{i,k-2}) = \nabla \hat{z}(\mathbf{r}_{i,k}) \cdot (\mathbf{r}_{i,k-1} - \mathbf{r}_{i,k-2}). \tag{51}$$

If we define a matrix $\mathbf{R} = [\mathbf{r}_{i,k} - \mathbf{r}_{i,k-1}, \mathbf{r}_{i,k-1} - \mathbf{r}_{i,k-2}]^T$, then the solution to the above two equations is $\nabla \hat{z}(\mathbf{r}_{i,k}) = \mathbf{R}^{-1} \begin{pmatrix} y(\mathbf{r}_{i,k}) - y(\mathbf{r}_{i,k-1}) \\ y(\mathbf{r}_{i,k-1}) - y(\mathbf{r}_{i,k-2}) \end{pmatrix}$. If $\mathbf{r}_{i,k} - \mathbf{r}_{i,k-1} = \mathbf{r}_{i,k-1} - \mathbf{r}_{i,k-2}$, then $\mathbf{R}$ is singular and no valid estimates can be obtained by solving the above two equations. In this case, we let

$$\nabla \hat{z}(\mathbf{r}_{i,k}) = \frac{y(\mathbf{r}_{i,k}) - y(\mathbf{r}_{i,k-1})}{\|\mathbf{r}_{i,k} - \mathbf{r}_{i,k-1}\|^2} (\mathbf{r}_{i,k} - \mathbf{r}_{i,k-1}) + \delta, \tag{52}$$

where δ is a small perturbation that prevents the agent from moving along a straight line so that equation (50) and equation (51) will produce unique estimates of the field gradient. In the implementation of the algorithm, δ can be chosen as a Gaussian distributed random vector with zero mean and small variance.

For collaborating agents, a cooperative Kalman filter or H_∞ filter can be constructed as introduced in Chapter IV, which provide estimates of the field value and gradient at the group center. We direct the center of the group to follow the opposite direction of estimated field gradient

$$\dot{\mathbf{r}}_{c,k} = -\delta_1 \frac{\nabla z(\mathbf{r}_{c,k})}{\| \nabla z(\mathbf{r}_{c,k}) \|}. \tag{53}$$

Note that the gradient at any local minimum is zero. Therefore, once the formation center or individual agents reach a local minimum by moving along the opposite direction of the gradient, it will stay in the area containing the local minimum. The size of the area depends on the step size of movement.

5.3 Bio-inspired Gradient-free Source Seeking

Couzin's group [7] observed that fish groups are able to perform gradient tracking to locate darker (shaded) regions in complex light environments even if the field is time-varying. However, it is conjectured that each fish in a group have very poor or no gradient estimates. They principally measure the intensities of the light field and respond to the positions of other fish within their view. Based on the measurements, a fish in a group speeds up when the light intensity at its current position is relatively high and slows down as the light intensity decreases. In this way, the group is capable of aligning its trajectory with gradient directions and moves towards the shade as described in [7]. Once the group reaches the shade, the forward motion of the group becomes circular, in which some fish in the group reverse their directions of movement. The group circles around the shade until the position of the shade changes. Then, the group resumes the forward motion.

These data inspire us to investigate source-seeking for a group of sensing agents in a distributed fashion with no explicit gradient estimation [115]. The agents only have the knowledge of their own measurements, and they can observe relative distances from their neighboring agents. We choose a baseline for a group of agents, and decompose the velocity of each agent into two parts. The first part, which is perpendicular to the baseline, is chosen to be proportional to the measurements, agreeing with observations from fish groups. The second part, which is parallel to the baseline, can be designed to control the relative distances among the agents. This decomposition is leveraged to implement formation-maintaining strategies and source seeking behaviors for the entire group. We prove that the moving direction of a group will converge towards the gradient direction while the formation is maintained.

Our results on gradient-free source seeking reveal a strong connection with the well-known Braitenberg-style differential drive vehicles as introduced in [16], which have similar properties in that the movement of a wheel is directly controlled by the measurement of the sensor connected to it. Braitenberg-style source-seeking algorithms have been proposed

in studies as [60] and [73]. However, these algorithms are developed for one agent. The approaches we develop are for multi-agent systems. Our results suggest that by knowing only measurement information and the relative distances to other agents, a group of agents tend to behave like a Braitenberg-style vehicle.

5.3.1 Control of Two-agent Groups

We start with $N = 2$. We control the two agents to converge asymptotically to a constant formation with distance a between each other in steady state. Therefore, they can be considered as a rigid body with the center of mass being at $\mathbf{r}_c$. Define the inertial frame as X_I and Y_I. Let $\mathbf{q} = \mathbf{r}_2 - \mathbf{r}_1$, and define $\mathbf{q}^\perp$ to be the vector perpendicular to $\mathbf{q}$ that forms a right handed frame with $\mathbf{q}$. $\mathbf{q}$ and $\mathbf{q}^\perp$ intersects at $\mathbf{r}_c$. Set the origin of the rigid body frame at $\mathbf{r}_c$, and select X_B and Y_B to be aligned with $\mathbf{q}$ and $\mathbf{q}^\perp$. Denote the angle between X_B and X_I as $\theta \in [-\pi, \pi]$. Then, we obtain a rigid body rotation matrix $g = \begin{pmatrix} \cos\theta & -\sin\theta \\ \sin\theta & \cos\theta \end{pmatrix}$, and the angular velocity $\Omega = \begin{pmatrix} 0 & -\omega \\ \omega & 0 \end{pmatrix}$. For each agent, we decompose its velocity into two parts: $\mathbf{v}_i^\perp$, which is perpendicular to $\mathbf{q}$ and proportional to the measurements $y(\mathbf{r}_i)$, and $\mathbf{v}_i^{//}$, which is aligned with $\mathbf{q}$ and maintains formation. Then, $\mathbf{v}_i = \mathbf{v}_i^\perp + \mathbf{v}_i^{//}$. We will design $\mathbf{v}_i^\perp$ and $\mathbf{v}_i^{//}$ separately.

Fig. 3 illustrates the desired motion of the two-agent group. The two agents move in the same direction when they are seeking a source, as shown in the right of Figure 3. At this stage, the group is performing forward motion. Once the group approaches a local minimum of the field, one of the agents reverse its moving direction. Then, the group performs circular motion around the source, as shown in the left of Figure 3.

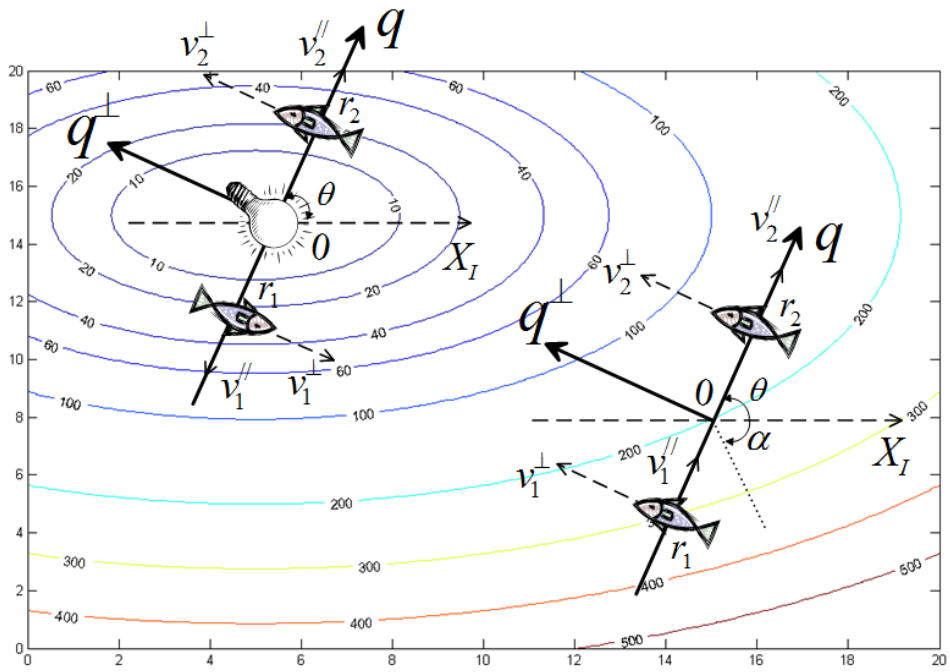

Figure 3: Desired motion of the two-agent group when seeking a source. Right: Forward motion. Left: Circular motion.

Let $\phi_i, i = 1,2$, be the angles between velocity $\mathbf{v}_i^{\perp}$ and X_I. We can write the perpendicular velocities as $\mathbf{v}_i^{\perp} = v_i^{\perp} \begin{pmatrix} \cos\phi_i \\ \sin\phi_i \end{pmatrix}$, where $v_i^{\perp}$ is the magnitude of $\mathbf{v}_i^{\perp}$. Similarly, $\mathbf{v}_i^{//} = v_i^{//} \begin{pmatrix} \cos\theta \\ \sin\theta \end{pmatrix}$. If the agents are performing forward motion, then, $\phi_1 = \phi_2 = \theta + \frac{\pi}{2}$. If the agents are performing circular motion, then, $\phi_1 = \theta + \frac{3\pi}{2}$ and $\phi_2 = \theta + \frac{\pi}{2}$. Inspired by the behaviors of fish schools, we design $v_i^{\perp}$ to be proportional to the measurements of the field. That is, when the measurements increase, the agents speed up. When the measurements decrease, the agents slow down.

$$v_i^{\perp} = ky(\mathbf{r}_i) + C, \quad i = 1,2, \tag{54}$$

where k and C are constants selected by design. In the direction that is aligned with $\mathbf{q}$, we aim to control the two agents to maintain a constant distance. Therefore, we design $v_i^{//}$,

$i = 1, 2$, as

$$v_1^{//} = k_p((\mathbf{r}_2 - \mathbf{r}_1) \cdot \mathbf{q} - a), \tag{55}$$

$$v_2^{//} = -k_p((\mathbf{r}_2 - \mathbf{r}_1) \cdot \mathbf{q} - a), \tag{56}$$

where a is the desired distance between the two agents. To prove the convergence of the controllers (55) and (56), we define a shape variable $s = (\mathbf{r}_2 - \mathbf{r}_1) \cdot \mathbf{q}$. From Equations (55) and (56), we calculate that

$$\dot{s} = 2(v_2^{//} - v_1^{//}) = -4k_p(s - a), \tag{57}$$

where $s = a$ is an asymptotically stable equilibrium. Therefore, the two agents will converge to a constant formation with a distance a between each other. Once $\mathbf{v}_i^{\perp}$ and $\mathbf{v}_i^{//}$ are determined, the velocities of the ith agent can be calculated as $\mathbf{v}_i = \mathbf{v}_i^{\perp} + \mathbf{v}_i^{//}$, which produces

$$\mathbf{v}_i = (ky(\mathbf{r}_i) + C) \begin{pmatrix} \cos\phi_i \\ \sin\phi_i \end{pmatrix} - k_p((\mathbf{r}_i - \mathbf{r}_j) \cdot \mathbf{q} - a) \begin{pmatrix} \cos\theta \\ \sin\theta \end{pmatrix}, \tag{58}$$

where $j = 1$ or 2, and $j \neq i$.

5.3.1.1 Forward Motion

We first discuss the forward motion of the group and prove that the first goal of source-seeking, the convergence of the moving direction of the group towards the gradient direction, can be achieved. In this case, $\phi_1 = \phi_2 = \theta + \frac{\pi}{2}$ are always satisfied, as illustrated in Figure 3. In this section, we investigate the situation in which noise in the measurements can be ignored, that is, $w(\mathbf{r}) = 0$. We will discuss the situation that the measurements are noisy in Section 5.3.1.3.

If there is no noise, the velocity of the formation center can be written as

$$\mathbf{v}_c = (\frac{1}{2}k(z(\mathbf{r}_1) + z(\mathbf{r}_2)) + C) \begin{pmatrix} -\sin\theta \\ \cos\theta \end{pmatrix}. \tag{59}$$

The angular velocity of the formation is

$$\dot{\theta} = \omega = \frac{v_2^{\perp} - v_1^{\perp}}{\| \mathbf{q} \|} = \frac{k(z(\mathbf{r}_2) - z(\mathbf{r}_1))}{\| \mathbf{q} \|}. \tag{60}$$

Denote the angle between the gradient direction $\nabla z(\mathbf{r}_c)$ and the inertial frame X_I as $\alpha \in [-\pi, \pi]$. If we consider only linear approximation of the field, then, we derive

$$z(\mathbf{r}_i) = z(\mathbf{r}_c) + \nabla z(\mathbf{r}_c) \cdot (\mathbf{r}_i - \mathbf{r}_c) + H.O.T, \tag{61}$$

where H.O.T represent higher order terms in the above Taylor expansion. From the linear approximation of the field, we derive

$$\begin{aligned} \dot{\theta} &\cong \frac{k}{\| \mathbf{q} \|} (\nabla z(\mathbf{r}_c) \cdot (\mathbf{r}_2 - \mathbf{r}_1)) = \frac{k}{\| \mathbf{q} \|} (\nabla z(\mathbf{r}_c) \cdot \mathbf{q}) \\ &= k \| \nabla z(\mathbf{r}_c) \| \left(\frac{\nabla z(\mathbf{r}_c)}{\| \nabla z(\mathbf{r}_c) \|} \cdot \frac{\mathbf{q}}{\| \mathbf{q} \|} \right) = -k \| \nabla z(\mathbf{r}_c) \| \sin(\theta - \alpha - \frac{\pi}{2}). \end{aligned} \tag{62}$$

Choose the state to be $\theta - \alpha$, then we obtain

$$\dot{\theta} - \dot{\alpha} = -k \| \nabla z(\mathbf{r}_c) \| \sin(\theta - \alpha - \frac{\pi}{2}) - \dot{\alpha}. \tag{63}$$

When $\| \nabla z(\mathbf{r}_c) \| \neq 0$, the above system has a stable equilibrium $\theta - \alpha = \frac{\pi}{2}$ and an unstable equilibrium $\theta - \alpha = -\frac{\pi}{2}$. Given the above system, we have the following proposition.

Proposition 5.3.1 *If the gradient direction α is constant, that is, $\dot{\alpha} = 0$, then, as $t \to \infty$, $lim_{t \to \infty} \theta(t) = \alpha + \frac{\pi}{2}$. If the rate of change $\dot{\alpha} \neq 0$ is considered as an input to the system (63), then $\theta - \alpha = \frac{\pi}{2}$ is an equilibrium of (63) that is input-to-state stable (ISS).*

Proof If $\dot{\alpha} = 0$, we choose a Lyapunov candidate function as

$$V(\theta) = -\ln(\cos(\frac{\theta - \alpha - \frac{\pi}{2}}{2})). \tag{64}$$

From $V(\theta)$, we have $V(0) \geq 0$. The equilibrium point of the Lyapunov function is $\alpha + \frac{\pi}{2}$.

We calculate

$$\begin{aligned}
\dot{V}(\theta) &= \tan(\frac{\theta-\alpha-\frac{\pi}{2}}{2})(\dot{\theta}-\dot{\alpha}) \\
&= -2k \parallel \nabla z(\mathbf{r}_c) \parallel \sin^2(\frac{\theta-\alpha-\frac{\pi}{2}}{2}) - \tan(\frac{\theta-\alpha-\frac{\pi}{2}}{2})\dot{\alpha} \\
&= -2k(1-\varepsilon) \parallel \nabla z(\mathbf{r}_c) \parallel \sin^2(\frac{\theta-\alpha-\frac{\pi}{2}}{2}) \\
&- 2k\varepsilon \parallel \nabla z(\mathbf{r}_c) \parallel \sin^2(\frac{\theta-\alpha-\frac{\pi}{2}}{2}) - \tan(\frac{\theta-\alpha-\frac{\pi}{2}}{2})\dot{\alpha} \\
&\leq -2k(1-\varepsilon) \parallel \nabla z(\mathbf{r}_c) \parallel \sin^2(\frac{\theta-\alpha-\frac{\pi}{2}}{2}), \qquad (65)
\end{aligned}$$

when $|\dot{\alpha}| \leq k\varepsilon \parallel \nabla z(\mathbf{r}_c) \parallel |\sin(\theta-\alpha-\frac{\pi}{2})|$ and $0<\varepsilon<1$. Therefore, according to Theorem 4.19 in [63], if $\dot{\alpha}$ is considered as the input, the system (63) is input-to-state stable (ISS). If the input $\dot{\alpha}=0$, θ converges to the equilibrium point $\alpha+\frac{\pi}{2}$. If the rate of change $\dot{\alpha}$ is bounded, then at the steady state, the deviation $|(\theta-\alpha-\frac{\pi}{2})|$ is also bounded. ■

Proposition 5.3.1 indicates that $\frac{\mathbf{v}_c}{\|\mathbf{v}_c\|} \cdot \frac{\nabla z(\mathbf{r_c})}{\|\nabla z(\mathbf{r_c})\|} = \cos(\theta+\frac{\pi}{2}-\alpha)$ converges to -1 as $t \to \infty$. The convergence of the moving direction of the group verifies the observations that fish groups are able to align their averaged motion with the gradient direction.

5.3.1.2 Circular Motion

When the two-agent group moves close to a local minimum of the field, it switches from forward motion to circular motion. The switching condition can be $\parallel \mathbf{v}_i^{\perp} \parallel < \varepsilon_1$, in which ε_1 is a positive constant. That is, when any agent senses that the forward speed is less than the threshold ε_1, it changes its moving direction. We will show that the circular motion can only be maintained around a point where $\parallel \nabla z(\mathbf{r}_c) \parallel = 0$.

In this case, the angles satisfy $\phi_1 = \theta + \frac{3\pi}{2}$ and $\phi_2 = \theta + \frac{\pi}{2}$. Then, we calculate

$$\begin{aligned}
\mathbf{v}_c &= \frac{1}{2}(\mathbf{v}_1 + \mathbf{v}_2) \qquad (66)\\
&= \frac{1}{2}k(z(\mathbf{r}_1) + C)\begin{pmatrix} \sin\theta \\ -\cos\theta \end{pmatrix} + \frac{1}{2}k(z(\mathbf{r}_2) + C)\begin{pmatrix} -\sin\theta \\ \cos\theta \end{pmatrix}\\
&= \frac{1}{2}k(\nabla z(\mathbf{r}_c)\cdot\mathbf{q})\begin{pmatrix} -\sin\theta \\ \cos\theta \end{pmatrix}\\
&= \frac{1}{2}k \parallel \mathbf{q} \parallel\parallel \nabla z(\mathbf{r}_c) \parallel \cos(\theta - \alpha)\begin{pmatrix} -\sin\theta \\ \cos\theta \end{pmatrix}. \qquad (67)
\end{aligned}$$

The angular velocity satisfies

$$\omega = \frac{v_2^{\perp} + v_1^{\perp}}{\parallel \mathbf{q} \parallel} = \frac{k(z(\mathbf{r}_2) + z(\mathbf{r}_1)) + 2C)}{\parallel \mathbf{q} \parallel}. \qquad (68)$$

If $\mathbf{v}_c = 0$, we must have $\parallel \nabla z(\mathbf{r}_c) \parallel = 0$ or $\cos(\theta - \alpha) = 0$. Consider $\cos(\theta - \alpha) = 0$, which indicates $\theta = \alpha \pm \frac{k\pi}{2}$, where k is an odd integer. Since $\omega \neq 0$ if $C \neq 0$, this case will not occur since $\theta = \alpha + \frac{k\pi}{2}$ cannot always be satisfied. Therefore, $\mathbf{v}_c = 0$ only when $\parallel \nabla z(\mathbf{r}_c) \parallel = 0$. This shows that circular motion can only sustain around a singular point.

5.3.1.3 Noisy Measurements

Usually, noise exists in the field or in the measuring process, which leads to uncertainties in the estimation of moving directions. If we consider $y(\mathbf{r}) = z(\mathbf{r}) + w(\mathbf{r})$, in which $w(\mathbf{r}) \neq 0$ represents the noise, then, Equations (59) and (62) become

$$\mathbf{v}_c = (\frac{1}{2}k(z(\mathbf{r}_1) + z(\mathbf{r}_2) + w(\mathbf{r}_1) + w(\mathbf{r}_2))) + C)\begin{pmatrix} -\sin\theta \\ \cos\theta \end{pmatrix}, \qquad (69)$$

and

$$\dot{\theta} = \frac{k}{\parallel \mathbf{q} \parallel}(\nabla z(\mathbf{r}_c)\cdot\mathbf{q} + w(\mathbf{r}_2) - w(\mathbf{r}_1)). \qquad (70)$$

Assume that $w(\mathbf{r})$ is zero mean Gaussian noise with variance σ^2. To show the convergence of the moving direction of the group, we examine the expected value and variance of

angle θ. We derive

$$d\theta = -k \parallel \nabla z(\mathbf{r}_c) \parallel \sin(\theta - \alpha - \frac{\pi}{2})dt + \frac{k\sigma}{\parallel \mathbf{q} \parallel}(d(w(\mathbf{r}_2)) - d(w(\mathbf{r}_1))), \tag{71}$$

where $d(w(\mathbf{r}_2)) - d(w(\mathbf{r}_1))$ is known as Brownian motion. Equation (71) yields

$$\frac{dE(\theta)}{dt} = -k \parallel \nabla z(\mathbf{r}_c) \parallel E(\sin(\theta - \alpha - \frac{\pi}{2})), \tag{72}$$

where the expectation E is taken with respect to the noise term. Let $e = \theta - \alpha - \frac{\pi}{2}$ and $\theta_0 = \alpha + \frac{\pi}{2}$. Assume e is small. Then, from Taylor expansion $\sin e = e - \frac{e^3}{3!} + \frac{e^5}{5!} + \cdots$, we obtain

$$\frac{dE(e)}{dt} = -k \parallel \nabla z(\mathbf{r}_c) \parallel E(e), \tag{73}$$

which indicates that $E(e) = 0$ is a stable equilibrium. Therefore, as $t \to \infty$, $E(\theta) = \alpha + \frac{\pi}{2}$, which proves the convergence of the expectation of the moving direction. Now, let's calculate the variance of θ. Define $\psi(e) = e^2$. Since we have

$$de = -k \parallel \nabla z(\mathbf{r}_c) \parallel edt + \frac{k\sigma}{\parallel \mathbf{q} \parallel}(d(w(\mathbf{r}_2)) - d(w(\mathbf{r}_1))), \tag{74}$$

then, according to Ito's differentiation rule [55], we derive

$$\begin{aligned} de^2 &= 2ede + 2(\frac{k\sigma}{\parallel \mathbf{q} \parallel})^2 dt \\ &= -2k \parallel \nabla z(\mathbf{r}_c) \parallel e^2 dt + 2(\frac{k\sigma}{\parallel \mathbf{q} \parallel})^2 dt + \frac{2ek\sigma}{\parallel \mathbf{q} \parallel}(d(w(\mathbf{r}_2)) - d(w(\mathbf{r}_1))), \end{aligned} \tag{75}$$

which yields

$$\frac{dE(e^2)}{dt} = -2k \parallel \nabla z(\mathbf{r}_c) \parallel E(e^2) + 2(\frac{k\sigma}{\parallel \mathbf{q} \parallel})^2. \tag{76}$$

As $t \to \infty$, $E(e^2) \to 2(\frac{k\sigma}{\|\mathbf{q}\|})^2$. Therefore, the variance of θ is $\frac{\sqrt{2}k\sigma}{\|\mathbf{q}\|}$, which indicates that as measurement noise increases, the variance of θ increases, and as the distance between the two agents $\parallel \mathbf{q} \parallel$ increases, the variance of θ decreases.

5.3.2 Generalization to N-agent Groups

We consider a group of N agents in the field seeking a local minimum. Arbitrarily select $\mathbf{q}$ as an unit vector that forms an angle θ with the inertial frame X_I. As illustrated in Figure 4,

we also decompose the velocities of the agents into two parts: $\mathbf{v}_i^{\perp}$, which is perpendicular to $\mathbf{q}$ and $\mathbf{v}_i^{//}$, which is aligned with $\mathbf{q}$. $\mathbf{v}_i^{\perp}$ and $\mathbf{v}_i^{//}$ can be designed in different ways. In this section, we discuss different designs for the formation control, and show the convergence of group motion towards the gradient direction.

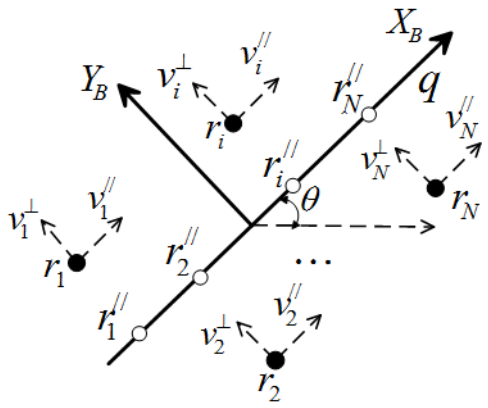

Figure 4: Decomposition of the velocities of the agents in a N-agent group.

5.3.2.1 Non-rigid Body Motion

We first design velocities of the agents so that the agents maintain only the relative positions to other agents in direction $\mathbf{q}$. In this case, we keep $\mathbf{v}_i^{\perp}$ the same as in the two-agent case, which is $\mathbf{v}_i^{\perp} = (kz(\mathbf{r}_i) + C)\begin{pmatrix} -\sin\theta \\ \cos\theta \end{pmatrix}, \quad i = 1, \cdots, N$. Note that using this design, the relative positions among agents may change in direction $\mathbf{q}^{\perp}$, which is perpendicular to $\mathbf{q}$.

Along direction $\mathbf{q}$, let $\mathbf{r}_i^{//}$ be the projection of location $\mathbf{r}_i$ onto vector $\mathbf{q}$, as illustrated in Figure 4. For agent i, we define set $\mathcal{N}_i$ to contain the closest agents to agent i to the right and to the left along direction $\mathbf{q}$. For example, as shown in Figure 4, $\mathcal{N}_1 = \{2\}$, $\mathcal{N}_i = \{i-1, i+1\}, i \neq 1, N$, and $\mathcal{N}_N = \{N-1\}$. The goal is to design $\mathbf{v}_i^{//}$ so that the relative distance from $\mathbf{r}_i^{//}$ to $\mathbf{r}_j^{//}, i \neq j$, converges to a constant a_{ij}^0. Furthermore, we require that $\mathbf{v}_c^{//} = \frac{1}{N}\sum_{i=1}^{N} \mathbf{v}_i^{//} = 0$. Therefore, we design $v_i^{//}$ as

$$v_i^{//} = k_p \sum_{j \in \mathcal{N}_i} ((\mathbf{r}_j - \mathbf{r}_i) \cdot \mathbf{q} - a_{j,i}^0), \tag{77}$$

where $a^0_{i,j} = -a^0_{j,i}$. To prove the convergence of the control (77), we define shape variables $s_i = (\mathbf{r}_{i+1} - \mathbf{r}_i) \cdot \mathbf{q}$, in which $i = 1, \cdots, N-1$. Then, for $i \neq 1, N$, we derive

$$\dot{s}_i = (\dot{\mathbf{r}}_{i+1} - \dot{\mathbf{r}}_i) \cdot \mathbf{q} = v^{//}_{i+1} - v^{//}_i = k_p(s_{i-1} - a^0_{i,i-1}) - 2k_p(s_i - a^0_{i+1,i}) + k_p(s_{i+1} - a^0_{i+2,i+1}). \tag{78}$$

For $i = 1$, we have

$$\dot{s}_1 = -2k_p(s_1 - a^0_{2,1}) + k_p(s_2 - a^0_{3,2}), \tag{79}$$

and for $i = N$, we have

$$\dot{s}_N = k_p(s_{N-2} - a^0_{N-1,N-2}) - 2k_p(s_{N-1} - a^0_{N,N-1}). \tag{80}$$

Denote $\mathbf{s} = \begin{pmatrix} s_1, & s_2, & \cdots, & s_{N-1} \end{pmatrix}^T$ and $\mathbf{a}^0 = \begin{pmatrix} a^0_{2,1}, & a^0_{3,2}, & \cdots, & a^0_{N,N-1}, a^0_{N,N-1} \end{pmatrix}^T$. Then, from Equations (79), (78), and (80), we obtain

$$\dot{\mathbf{s}} = k_p A(\mathbf{s} - \mathbf{a}^0), \tag{81}$$

where $A = \begin{pmatrix} -2 & 1 & 0 & \dots & 0 \\ 1 & -2 & 1 & \dots & 0 \\ 0 & & \ddots & & \vdots \\ \vdots & & 1 & -2 & 1 \\ 0 & \dots & 0 & 1 & -2 \end{pmatrix}$. The eigenvalues of A are $\lambda_i = -2 + 2\cos(\frac{i\pi}{N}) < 0$ for $i = 1, \cdots, N-1$. Therefore, system (81) is asymptotically stable. The shape variable $\mathbf{s}$ converges to $\mathbf{a}^0$ as $t \to \infty$. Then, the formation is stabilized.

Since each agent now has its velocity given by

$$\mathbf{v}_i = (kz(\mathbf{r}_i) + C) \begin{pmatrix} -\sin\theta \\ \cos\theta \end{pmatrix} + k_p \sum_{j \in \mathcal{N}_i} ((\mathbf{r}_j - \mathbf{r}_i) \cdot \mathbf{q} - a^0_{j,i}) \begin{pmatrix} \cos\theta \\ \sin\theta \end{pmatrix}, \tag{82}$$

and the parallel velocity of the center of the group is

$$\mathbf{v}^{//}_c = \frac{1}{N} \sum_{i=1}^{N} \mathbf{v}^{//}_i = 0, \tag{83}$$

we obtain the velocity of the formation center as

$$\mathbf{v}_c = (\frac{1}{N}k\sum_{i=1}^{N} z(\mathbf{r}_i) + C)\begin{pmatrix} -\sin\theta \\ \cos\theta \end{pmatrix}. \tag{84}$$

5.3.2.2 *Motion Under a Rigid Formation Controller*

We can also design a rigid formation controller, which controls the relative distances of the agents in direction $\mathbf{q}^\perp$. For this purpose, we replace the constant C in Equation (58) by a feedback control term.

Let $\mathbf{r}_i^\perp, i = 1, \cdots, N$ be the projections of locations $\mathbf{r}_i$ onto vector $\mathbf{q}^\perp$. Figure 5 illustrates the case that $N = 3$, in which $\mathbf{q}^\perp$ is chosen to start from location $\mathbf{r}_3$. Denote the desired distance between agent i and agent j in direction $\mathbf{q}^\perp$ as $b^0_{i,j}$, in which $b^0_{i,j} = -b^0_{j,i}$. Let $\mathcal{N}_i^\perp$ be the neighboring set of agent i along direction $\mathbf{q}^\perp$. Then we design

$$v_i^\perp = kz(\mathbf{r}_i) + k_d \sum_{j\in\mathcal{N}_i^\perp} ((\mathbf{r}_j - \mathbf{r}_i)\cdot\mathbf{q}^\perp - b^0_{j,i}), \tag{85}$$

where $i = 1, \cdots, N$.

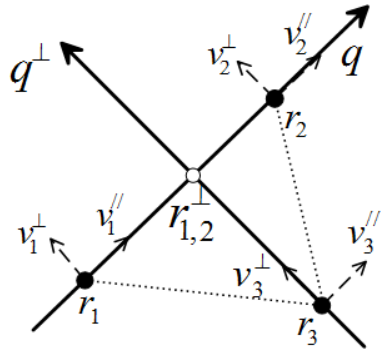

Figure 5: Decomposition of the velocities of the three-agent group.

Define shape variables $s_i^\perp = (\mathbf{r}_{i+1} - \mathbf{r}_i)\cdot\mathbf{q}^\perp$. Denote $\mathbf{s}^\perp = \begin{pmatrix} s_1^\perp, & s_2^\perp, & \cdots, & s_{N-1}^\perp \end{pmatrix}^T$ and $\mathbf{b}^0 = \begin{pmatrix} b^0_{2,1}, & b^0_{3,2}, & \cdots, & b^0_{N,N-1}, b^0_{N,N-1} \end{pmatrix}^T$. Let $\mathbf{z}$ be a column vector with the ith entry being $[z(\mathbf{r}_{i+1}) - z(\mathbf{r}_i)]$. Then, similar to the non-rigid body case, we obtain

$$\dot{\mathbf{s}}^\perp = k_p A(\mathbf{s}^\perp - \mathbf{b}^0) + k\mathbf{z}. \tag{86}$$

Starting from $t = 0$, the solution of the above system is

$$\mathbf{s}^{\perp}(t) = e^{k_p A t}(\mathbf{s}^{\perp}(0) - \mathbf{b}^0) + \mathbf{b}^0 + \int_0^t k e^{k_p A(t-\tau)} \mathbf{z}(\tau) d\tau. \tag{87}$$

Since $z_{\min} \leq z(\mathbf{r}) \leq z_{\max}$, $\mathbf{z}$ is bounded. Therefore, the solution satisfies

$$\begin{aligned} \| \mathbf{s}^{\perp}(t) - \mathbf{b}^0 \| &\leq e^{\lambda k_p t} \| \mathbf{s}^{\perp}(0) - \mathbf{b}^0 \| + k \| \mathbf{z}(\tau) \| \, | \int_0^t e^{\lambda k_p (t-\tau)} d\tau | \\ &\leq e^{\lambda k_p t} \| \mathbf{s}^{\perp}(0) - \mathbf{b}^0 \| + \frac{k}{|\lambda|} \sup_{0 \leq \tau \leq t} \| \mathbf{z}(\tau) \|, \end{aligned} \tag{88}$$

in which λ is the maximum eigenvalue of matrix A. Therefore, the system (86) is input-to-state stable (ISS)([63]), which implies that for any bounded $\mathbf{z}$, the shape variable $\mathbf{s}^{\perp}$ will be bounded, and if the input $\mathbf{z}$ converges to zero as $t \to 0$, $\mathbf{s}^{\perp} - \mathbf{b}^0$ will converge to 0. For $\mathbf{v}_i^{//}$, we design it to be the same form as in Equation (77). Then, we calculate

$$\mathbf{v}_c = \frac{1}{N} k \sum_{i=1}^{N} z(\mathbf{r}_i) \begin{pmatrix} -\sin\theta \\ \cos\theta \end{pmatrix}, \tag{89}$$

in which the velocities that control the formation cancel out.

We observe an interesting fact that from the ISS property of system (86), even though a rigid formation controller is used, the agents may not stay in a rigid formation due to the nonzero term $\mathbf{z}$, which seems to coincide with real life observations that fish don't tend to maintain a rigid formation. This insight may hint further investigations.

5.3.2.3 Rotation of the Group

To calculate the angular velocity of the group, we consider only the motion of the vector $\mathbf{q}$. Given two locations $\mathbf{r}_i^{//}$ and $\mathbf{r}_j^{//}$ along $\mathbf{q}$, then, in the non-rigid body case, we derive $\omega = -k \| \nabla z(\mathbf{r}_c) \| \sin(\theta - \alpha - \frac{\pi}{2})$, the convergence of which has been proven in Proposition 5.3.1. Therefore, the moving direction of the group converges to the gradient direction.

In rigid body motion, the angular velocity is obtained by

$$\begin{aligned} \dot{\theta} - \dot{\alpha} = -k \| \nabla z(\mathbf{r}_c) \| \sin(\theta - \alpha - \frac{\pi}{2}) + \frac{k_d}{\| \mathbf{q} \|} \Big(\sum_{l \in \mathscr{N}_i^{\perp}} ((\mathbf{r}_l - \mathbf{r}_i) \cdot \mathbf{q}^{\perp} - b_{l,i}^0) \\ - \sum_{l \in \mathscr{N}_j^{\perp}} ((\mathbf{r}_l - \mathbf{r}_j) \cdot \mathbf{q}^{\perp} - b_{l,j}^0) \Big) - \dot{\alpha}, \end{aligned} \tag{90}$$

Since the second term of system (90) is bounded, then, similar to Proposition 5.3.1, we can also prove that system (90) is input-to-state stable. Therefore, the formation may not align exactly with the gradient direction, but will nonetheless able to move in a direction to decrease their measurements.

5.4 Experiments

To verify our algorithms, we design a multi-agent exploration test-bed for a group of mobile robots performing source seeking tasks. In this section, we introduce the configuration of the test-bed and discuss the experimental results.

5.4.1 Experimental test-bed

Figure 6 shows the experimental test-bed that includes the following components:

5.4.1.1 Robots and sensors

We choose Khepera III robots from K-Team to implement the switching strategy. Khepera III is a round mobile robot running on two differential drive wheels and a sliding support. Each Khepera III robot has nine infrared (IR) sensors placed around it and two infra-red ground sensors placed on the bottom. We use the nine IR sensors around the robot to measure the ambient light intensity. The sensor readings are normalized to be within the range $[0, 5000]$. The higher the light intensity is, the **lower** the sensor reading is.

5.4.1.2 Localization system

As seen in Figure 6, the localization system consists of an overhead camera, a camera support and the LabVIEW vision system for providing the positions and orientations of the robots at each time step.

5.4.1.3 Central computer

A central computer is used to perform centralized control tasks. For centralized exploration tasks such as the gradient-based source-seeking using multiple agents, at each time step,

the localization system obtains the new positions and orientations of the robots and the robots collect new measurements of the field. These information can be sent to the central computer. Then the central computer calculates the new positions and orientations of the robots and sends the corresponding moving distances and turning angles back to the robots. All these communications are performed wirelessly.

5.4.1.4 Light field

We use a standard 40W incandescent light bulb to serve as a light source that generates a light field unknown to the robots. The field is about 2.8 meters long and 1.6 meters wide. The light intensity decreases when the distance from the light source increases, which indicates that the location of the light bulb hosts the maximum of the intensity of the light field. Therefore, seeking for the maximum of the light field corresponds to finding the minimum of the measured field.

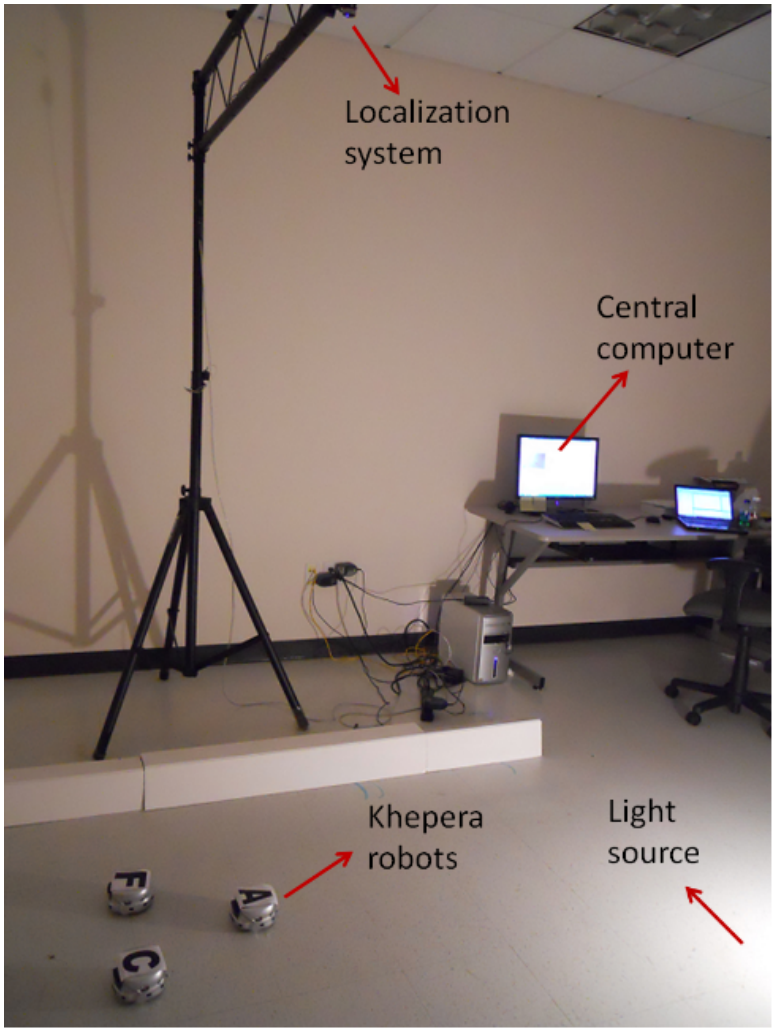

Figure 6: The experimental setting.

5.4.2 Experimental Results

We deploy two Khepera III robots that perform gradient-free light source-seeking in the field. The velocities of the robots are determined by Equation (58), and are translated into step sizes in the experiment, Once one robot detects that $\| \mathbf{v}_i^{\perp} \| < \varepsilon_1$, it changes direction so that the two-agent group starts circular motion. Figure 7 shows the snapshots of two agents moving towards the light source, and Figure 8 demonstrates the trajectories of the two robots. The two figures shows that the two robots maintain a desired distance and converge to the light source.

In addition to the experiments, we also simulate eight agents in a scalar field seeking a minimum of the field. Figure 9 demonstrates the trajectories of the eight agents in non-rigid body motion, in which blue dots are the positions of the agents. The formation is plotted every 30 steps. Since the agents control only the relative distances from other agents along direction **q**, which corresponds to the yellow vector in the figure, they do not maintain a solid formation. As suggested by the figure, since the velocities of the agents depend on the measurements of the field, when the field value is high, the agents move faster, resulting in a larger step size. Figure 10 illustrates the relative distances between neighboring agents in direction **q** as the agent group moves in the field, which shows the convergence of the relative distances to constant values.

Figure 7: Snapshots of the trajectories of two agents seeking a light source.

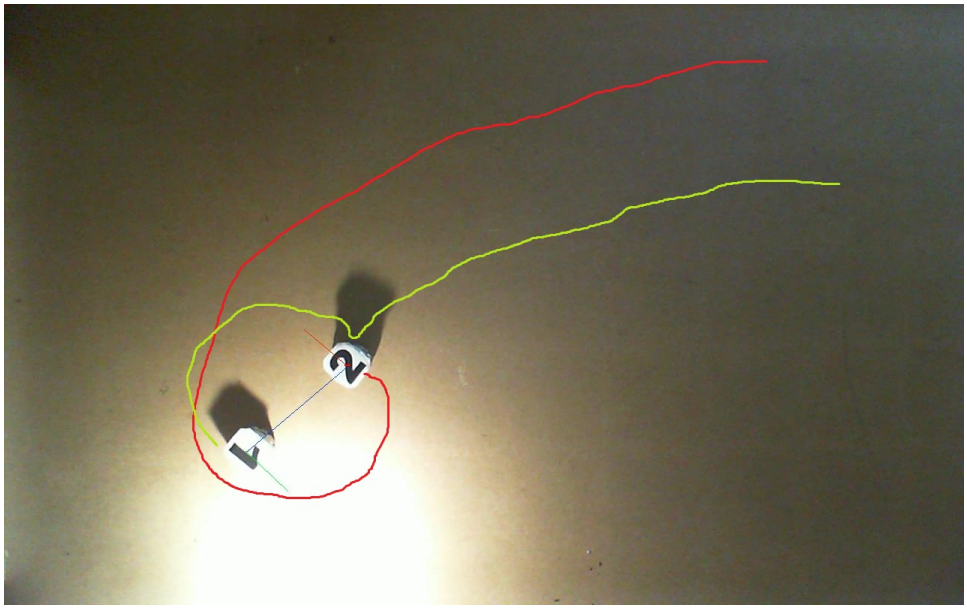

Figure 8: Trajectories of two agents seeking a light source.

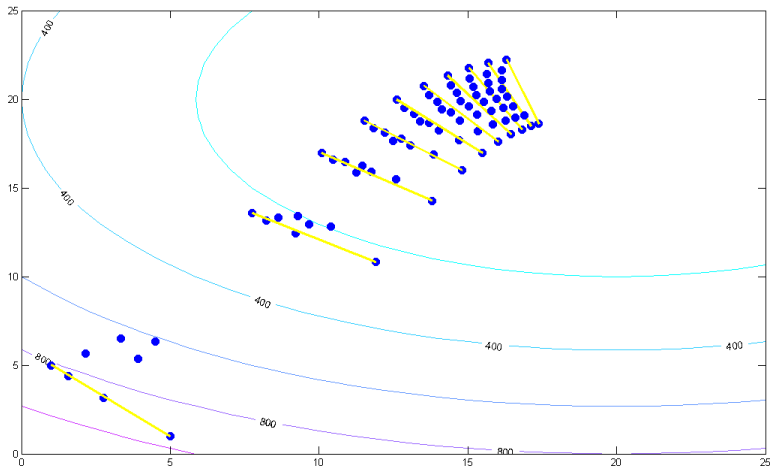

Figure 9: Trajectories of an eight-agent group seeking a minimum in a field. The group is performing non-rigid body motion.

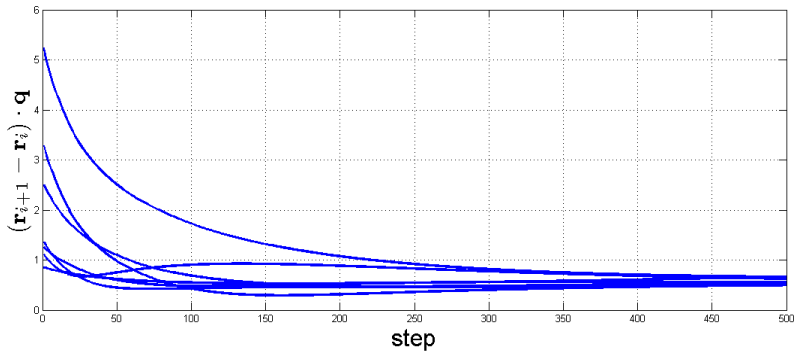

Figure 10: Relative distances among neighboring agents in direction **q**.

5.5 Conclusion

Inspired by the behaviors of fish groups, we develop source-seeking algorithms for a group of sensing agents with no explicit gradient estimation. By decomposing the velocity of each agent into two parts and designing each part as feedback control, we control the moving direction of the group to converge to gradient directions while formation is maintained. Our results show that a group of sensing agents are able to emulate the source seeking behaviors of a fish group.

CHAPTER VI

A SWITCHING STRATEGY IN COOPERATIVE EXPLORATION

In typical scenarios of exploration of scalar fields, a cooperative group of agents are expected to perform better than a single agent [5, 19, 34]. However, increasing the number of agents results in rising cost, communication delay, and computational complexity. Therefore, the exploration behavior of each agent does not have to be fixed. Biologists have observed switching between individual and cooperative behaviors in certain species of fish [109]. It is speculated that fish in a group collaborate with each other when they are not confident with the information gathered individually. A switching behavior model based on the level of confidence of individual fish has been studied. Simulation results in [109] show striking similarities to real fish data.

Inspired by the results in [109], we propose a switching strategy that allows a group of agents to switch between individual exploration and cooperative exploration. The switching conditions between those two stages are related to the speed of convergence and the signal-to-noise ratio (SNR) [114, 117, 121]. The flowchart of the switching strategy is illustrated in Figure 11. As shown in the chart, the agents check the switching conditions at each time step both in the individual exploration mode and in the cooperative exploration mode. Once the switching conditions are satisfied, the agents switch to the other mode.

The switching strategy strikes a balance between exploration complexity and exploration performance in terms of convergence rate and exploration cost, which may enable more flexibility in autonomy compared to fixed strategies. We first demonstrate the switching strategy in source-seeking problems. The agents perform the source-seeking task according to the gradient-based algorithms introduced in Chapter V. Other than the source seeking problem, the switching strategy can also be applied to other exploration tasks for

multi-agent systems such as target tracking as long as a cost function related to convergence rate is defined.

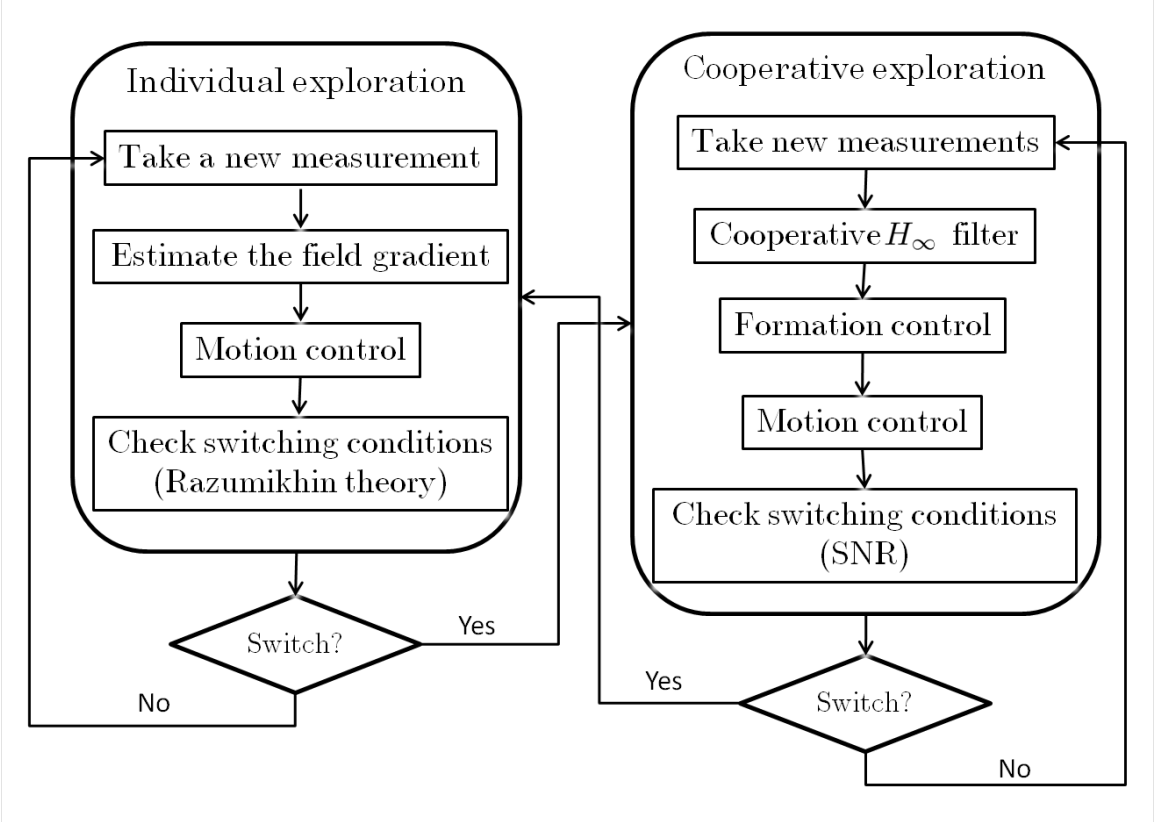

Figure 11: The flowchart of the switching strategy.

6.1 Individual Exploration to Cooperative Exploration

In the individual exploration phase, we suppose the agents estimate the field gradient utilizing the time-series measurements, as introduced in Chapter V, and move according to the estimated gradient direction. If the noise level gets higher, the steps of the agents can become incoherent, which leads to high probability of false-walks. Therefore, the estimates of the gradient directions will become more noisy, which may prevent the agents from finding the right direction. Therefore, we propose a switching condition based on the Razumikhin theorem [44, 46] for the agents to check whether they can keep individual exploration and find a local minimum.

We first restate the Razumikhin theorem for the asymptotic stability of time-delay systems [46] without proof.

Suppose $\mathbb{R} = (-\infty, \infty)$, $\mathbb{R}^n$ is an n-dimensional linear vector space with norm $\|\cdot\|$, $C([a,b],\mathbb{R}^n)$ is the Banach space of continuous functions which maps the interval $[a,b]$ into $\mathbb{R}^n$ with the topology of uniform convergence. Let $[a,b] = [-r,0]$, in which $r \geq 0$ is a given real number. Then, $C = C([-r,0],\mathbb{R}^n)$. Denote the norm of an element ϕ in C as $|\phi| = sup_{-r\leq\theta\leq}|\phi(\theta)|$. If

$$\tau \in \mathbb{R}, A \geq 0, \quad \text{and} \quad x \in C([-\tau - r, \tau + A, \mathbb{R}^n]),$$

then, for any $t \in [\tau, \tau + A]$, $x_t \in C$ is defined as $x_t(\theta) = x(t+\theta), -r \leq \theta \leq 0$. Suppose D is a subset of $\mathbb{R} \times C$ and $f : D \to \mathbb{R}^n$ is a given function. Let "$\cdot$" denote the right-hand derivative. Then, the relation

$$\dot{x}(t) = f(t, x_t) \tag{91}$$

is a retarded functional differential equation(RFDE) on D. If there exist $\tau \in \mathbb{R}$ and $A > 0$ such that $x \in C([\tau - r, \tau + A], \mathbb{R}^n)$, and for $t \in [\tau, \tau + A]$, $(t, x_t) \in D$ and $x(t)$ satisfies Equation (91), then, x is a solution of Equation (91) on $[\tau - r, \tau + A]$ [46]. The Razumikhin theory is stated as follows.

Theorem 6.1.1 *(Theorem 4.1 in [46]) Suppose $f : \mathbb{R} \times C \to \mathbb{R}^n$ takes $\mathbb{R} \times$ (bounded sets of C) into bounded sets of $\mathbb{R}^n$ and consider the RFDE(f). Suppose $\alpha_1, \alpha_2, \omega : \mathbb{R}^+ \to \mathbb{R}^+$ are continuous, nondecreasing functions, $\alpha_1(u), \alpha_2(u)$ positive for $u > 0$, $\alpha_1(0) = \alpha_2(0) = 0$, α_2 strictly increasing. If there is a continuous function $V : \mathbb{R} \times \mathbb{R}^n \to \mathbb{R}$ such that*

$$\alpha_1(\|x\|) \leq V(t,x) \leq \alpha_2(\|x\|), \quad t \in \mathbb{R}, x \in \mathbb{R}^n, \tag{92}$$

and

$$\dot{V}(t, \phi(0)) \leq -\omega(\|\phi(0)\|), \quad \text{if} \quad V((t+\theta), \phi(\theta)) \leq V(t, \phi(0)), \tag{93}$$

for $\theta \in [-r, 0]$, then the solution $x = 0$ of the RFDE(f) is uniformly stable.

Theorem 6.1.2 *(Theorem 4.2 in [46]) Suppose all the conditions of Theorem 6.1.1 are satisfied and in addition* $\omega(u) > 0$ *if* $u > 0$*. If there is a continuous nondecreasing function* $g(u) > u$ *for* $u > 0$ *such that Condition 93 is strengthened to*

$$\dot{V}(t,\phi(0)) \leq -\omega(\|\phi(0)\|), \quad \textit{if} \quad V((t+\theta),\phi(\theta)) \leq g(V(t,\phi(0))) \tag{94}$$

for $\theta \in [-r,0]$*, then the solution* $x = 0$ *of the RFDE*(f) *is uniformly asymptotically stable. If* $\alpha_1(u) \to \infty$ *as* $u \to \infty$*, then the solution* $x = 0$ *is also a global attractor for the RFDE*(f)*.*

For discrete systems, condition (94) becomes [36]

$$V(k+1,x(k+1)) - V(k,x(k)) \leq -\omega(\|x(k)\|), \tag{95}$$

whenever $V((k+\theta),x(k+\theta)) \leq g(V(k,x(k)))$ for all $\theta \in [-r,0]$.

Now consider a single sensing agent. For simplicity, we drop the subscript i used to index the agent in the following arguments. We suppose that the agent has a memory with finite length r, where $r \in \mathbf{Z}^+$. The memory is used to store the measurements $y(\mathbf{r}_{k+s})$ where s is a non-positive integer such that $-r \leq s \leq 0$. Based on the discrete time Razumikhin theorem, we have the following proposition.

Proposition 6.1.3 *Suppose the field value* $z(\mathbf{r}_k)$ *satisfy* $z_{\min} \leq z(\mathbf{r}_k) \leq z_{\max}, \forall k$*. Let* $\bar{y}(\mathbf{r}_k) = \max_{s\in[-r,0]} y(\mathbf{r}_{k+s})$ *where* $r \in \mathbf{Z}^+$ *and* $y(\mathbf{r}_k)$ *is the measurement at time step k. If* $y(\mathbf{r}_{k+1}) - y(\mathbf{r}_k) \leq -\rho y(\mathbf{r}_k) + \rho z_{\min}$ *whenever* $(1+\varepsilon)y(\mathbf{r}_k) \geq \bar{y}(\mathbf{r}_k) + \varepsilon z_{\min}$*, where* $\rho, \varepsilon > 0$ *are infinitesimal constants, then* $y(\mathbf{r}_k)$ *will converge to* $z_{\min}$ *as* $k \to \infty$*.*

Proof Define a new variable

$$y_k = y(\mathbf{r}_k) - z_{min} \geq 0.$$

Then, we have $0 \leq y_k \leq y_{max}$. Define $\bar{y}_k = \max_{s\in[-r,0]} y_{k+s}$. Then, the condition (95) becomes

$$V(k+1,y_{k+1}) - V(k,y_k) \leq -\omega(y_k), \tag{96}$$

whenever $V(k,\bar{y}_k) \leq g(V(k,x(k)))$. Choose $V(k,y_k) = y_k \in [0, y_{max}]$, $g(V(k,y_k)) = (1+\varepsilon)y_k$, and $w(y_k) = \rho y_k = \rho y(\mathbf{r}_k) - \rho z_{\min}$, where $\varepsilon > 0$ and ρ are infinitesimal constants. Since we have $V(k+1,y_{k+1}) - V(k,y_k) = y(\mathbf{r}_{k+1}) - y(\mathbf{r}_k)$, condition (96) becomes

$$y(\mathbf{r}_{k+1}) - y(\mathbf{r}_k) \leq -\rho y(\mathbf{r}_k) + \rho z_{\min} \tag{97}$$

whenever $\bar{y}_k \leq (1+\varepsilon)y_k$, which can be rewritten as

$$\bar{y}(\mathbf{r}_k) + \varepsilon z_{\min} \leq (1+\varepsilon)y(\mathbf{r}_k). \tag{98}$$

Therefore, according to the Razumikhin theorem, if for all $k \in [r,\infty)$, the measurements satisfy $y(\mathbf{r}_{k+1}) - y(\mathbf{r}_k) \leq -\rho y(\mathbf{r}_k) + \rho z_{\min}$ whenever $(1+\varepsilon)y(\mathbf{r}_k) \geq \bar{y}(\mathbf{r}_k) + \varepsilon z_{\min}$, then y_k converge to 0 as $k \to \infty$. This fact implies that $y(\mathbf{r}_k)$ converge to $z_{\min}$ as $k \to \infty$. ■

Given the above proposition, we propose the following exploration algorithm for individual exploration.

Algorithm 6.1.4 *Suppose an agent is searching for a local minimum of an unknown field, where the field value satisfies $z_{\min} \leq z(\mathbf{r}_k) \leq z_{\max}$. Let $\bar{y}(\mathbf{r}_k) = \max_{s\in[-r,0]} y(\mathbf{r}_{k+s})$, where r is the memory length of the agent.*

S.1 At step $k \geq r$, the agent takes a measurement of the field $y(\mathbf{r}_k)$. Then estimates the field gradient $\nabla z(\mathbf{r}_k)$ by solving the equations (50) and (51).

S.2 The agent moves in the opposite direction of the estimated gradient according to $\dot{\mathbf{r}}_k = -\nabla\hat{z}(\mathbf{r}_k)$ or uses other strategies to reduce the measured field value. At step $k+1$, the agent takes a new measurement $y(\mathbf{r}_{k+1})$.

S.3 At step $k+1$, the agent checks whether $(1+\varepsilon)y(\mathbf{r}_k) \geq \bar{y}(\mathbf{r}_k) + \varepsilon z_{\min}$ is satisfied or not. If yes, the agent checks the value of $y(\mathbf{r}_{k+1}) - y(\mathbf{r}_k)$. If $y(\mathbf{r}_{k+1}) - y(\mathbf{r}_k) \leq -\rho y(\mathbf{r}_k) + \rho z_{\min}$, it keeps individual exploration. Otherwise, it requires to switch to cooperative exploration. If for all $k > 0$, $y(\mathbf{r}_{k+1}) - y(\mathbf{r}_k) \leq -\rho y(\mathbf{r}_k) + \rho z_{\min}$ whenever $(1+\varepsilon)y(\mathbf{r}_k) \geq \bar{y}(\mathbf{r}_k) + \varepsilon z_{\min}$, the agent will converge to a local minimum $z_{\min}$ according to Proposition 6.1.3.

According to Proposition 6.1.3 and Algorithm 6.1.4, the switching conditions from individual exploration to cooperative exploration can be stated as: (1) at time step $k+1$, check if $(1+\varepsilon)y(\mathbf{r}_k) \geq \bar{y}(\mathbf{r}_k) + \varepsilon z_{\min}$. If (1) is satisfied, then (2) check if $y(\mathbf{r}_{k+1}) - y(\mathbf{r}_k) > -\rho y(\mathbf{r}_k) + \rho z_{\min}$. Once an agent detects that both switching conditions are satisfied at step $k+1$, it notifies other agents, then all agents switch to cooperative exploration upon request. This ensures that all agents behave consistently in the cooperative exploration phase.

6.2 Cooperative Exploration to Individual Exploration

According to the information dynamics for cooperative exploration introduced in Chapter IV, when all the agents are moving in a formation, which is treated as a "super-agent", a cooperative filter is producing estimates of field values and gradients at the formation center. Then the convergence of the cooperative exploration algorithm is dictated by the same sufficient conditions for convergence of the individual exploration algorithm. Define $\bar{z}(\mathbf{r}_{c,k}) = \max_{s\in[-r_c,0]} z(\mathbf{r}_{c,k+s})$, where r_c is the memory length of the "super-agent" that can be considered as the average of the memory lengths of all the individual agents in the formation. For simplicity and without loss of generality, we assume that all the agents have the same memory lengths. As long as (1) $(1+\varepsilon)z(\mathbf{r}_{c,k}) \geq \bar{z}(\mathbf{r}_{c,k}) + \varepsilon z_{\min}$ and (2) $z(\mathbf{r}_{c,k+1}) - z(\mathbf{r}_{c,k}) > -\rho z(\mathbf{r}_{c,k}) + \rho z_{\min}$ are not satisfied, the formation will converge to a local minimum of the field.

One reason that the collaborating sensing agents outperform individual agents is that at each step, the cooperative filter provides the filtered field value by combining measurements from N agents, which serves as an effective way of noise reduction while a single agent can only make use of the time-series measurements with no reduction of noises. When the field is time-varying and the noise level reduces to the extent that a single agent is able to generate accurate gradient estimates, the cooperative sensing agents should break out the formation and start individual exploration again.

We utilize the signal-to-noise ratio (SNR) to serve as the switching condition from

cooperative exploration to individual exploration. If we define the signal-to-noise ratio obtained by the ith agent at the step k as

$$\beta_{i,k} = 10\log_{10} \sum_{\xi=0}^{r} \frac{\hat{y}^2(\mathbf{r}_{i,k-\xi})}{(y(\mathbf{r}_{i,k-\xi}) - \hat{y}(\mathbf{r}_{i,k-\xi}))^2}, i = 1, \cdots, N, \tag{99}$$

where $\hat{y}(\mathbf{r}_{i,k})$ is the estimated field value obtained by

$$\hat{y}_{i,k} = z(\mathbf{r}_{c,k}) + (\mathbf{r}_{i,k} - \mathbf{r}_{c,k})^T \nabla z(\mathbf{r}_{c,k}), \tag{100}$$

then, we have the following algorithm for the agents to decide when to switch from cooperative exploration back to individual exploration.

Algorithm 6.2.1 *Define the average SNR at time step k as* $\bar{\beta}_k = \frac{1}{N}\sum_{i=1}^{N} \beta_{i,k}$. *Suppose that at time* T_s, *the agents have switched to cooperative exploration. Then for* $k > T_s + r_c$, *where* r_c *is the memory length of the super agent, the cooperative agents switch back to individual exploration if* $\bar{\beta}_k > \mu \bar{\beta}_{T_s + r_c}$, *where* $\mu > 1$ *is a constant.*

The constant μ is chosen by design. A larger μ tends to prevent the agents from switching to individual exploration since the SNR needs to increase by a large amount to satisfy Algorithm 6.2.1. If μ is small, the agents switch to individual exploration as soon as they detect the noise reduces by a small amount. However, if the agents can not individually converge to a field minimum, they have to switch back to cooperative exploration again, which increases the exploration effort and cost. If that happens, one may increase μ so that a larger threshold can be set.

6.3 Experiments

6.3.1 Switching with Fixed Number of Agents

Since the field minimum is unknown to the robots and $\rho > 0$ and $\varepsilon > 0$ in Algorithm 6.1.4 are infinitesimal constants, we approximate ρ and ε by 0 so that the condition $y(\mathbf{r}_{k+1}) - y(\mathbf{r}_k) \leq -\rho y(\mathbf{r}_k) + \rho z_{\min}$ whenever $(1+\varepsilon)y(\mathbf{r}_k) \geq \bar{y}(\mathbf{r}_k) + \varepsilon z_{\min}$ is simplified to $y(\mathbf{r}_{k+1}) - p_k < 0$ whenever $y(\mathbf{r}_k) > \bar{p}_k$. If we consider the derivation from the Razumikhin theorem

to Proposition 4.2.2, the simplified condition corresponds to the Razumikhin theorem on stability, not asymptotic stability. Therefore, under the simplified condition, the agents can only be guaranteed to stay near a local minimum, not converge to a local minimum. In the experiments, because of the disturbances and noises in the field and measuring process, we still observe the convergence to the field minimum, which is not surprising since the conditions in the Razumkhin Theorem is sufficient but not necessary.

We deploy three Khepera III robots in the light field, which are labeled as "A", "F" and "C", respectively. Figure 12 shows the trajectories of the three robots searching for the light source with the switching strategy from one trial with the memory length $r = 5$. The information collected are plotted in Figure 13, in which the green (solid with dot marker), red (dashed with dot marker), and yellow (dotted with dot marker) lines indicate the measurements taken by robots A, F, and C, respectively and the blue line (dashed with triangular marker) indicates the filtered field values at the formation center after they switched to cooperative exploration. At first few steps, each robot explores the field independently. After several steps, individual exploration is abandoned because of high noise strength, then they switch to cooperative exploration and find the light source.

In this experiment, at step $k = 13$, robot A detects that $p_{13} > \max_{s\in[-5,0]} p_{13+s}$. According to the switching conditions from individual exploration to cooperative exploration, the robot needs to check if $p_{14} > p_{13}$ at step 14. At step $k = 14$, the robot takes a new measurement and detects that $p_{14} > p_{13}$. In this case, the switching conditions in Algorithm 6.1.4 are satisfied and robot A decides to switch to cooperative exploration. It sends a switching signal to the central computer through wireless connection and the central computer broadcasts a signal to all the robots once it received the switching signal from robot A. Due to the communication delay, at step $k = 16$, all the robots receive the signal from the central computer and start to cooperate. Since we do not actively control the existing noises, the robots never detect that the field noise level decreases to the extent that they can switch back to individual exploration. They keep exploring the field cooperatively and

locate the field minimum in around 50 steps. Other parameters in these experiments are as follows: the formation size $a = 0.2$m, the noise attenuation level $\gamma = 3$, the weighting matrices $Q = I$, $W = 0.01I$, and $V = 0.01I$.

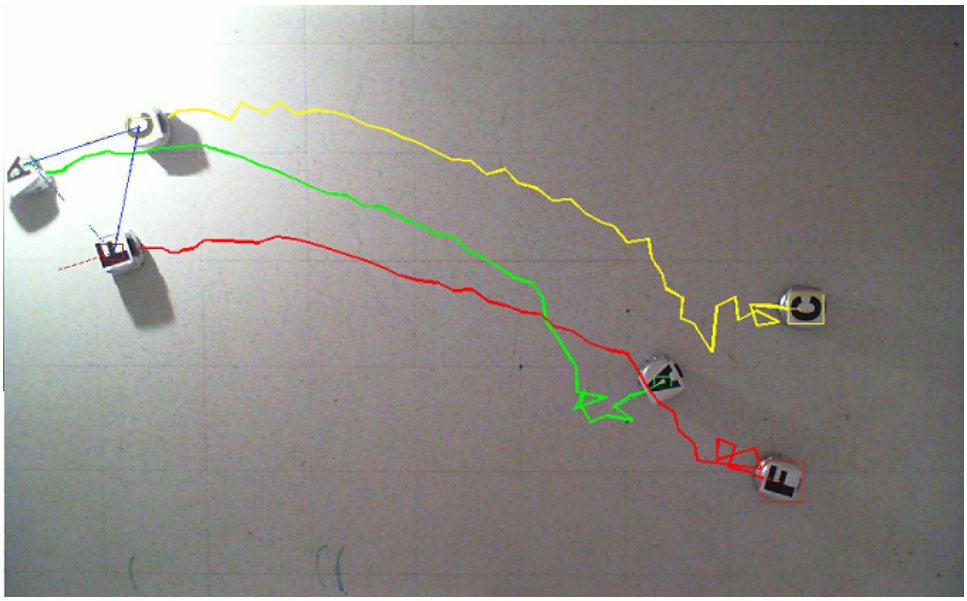

Figure 12: Trajectories of three robots seeking for the light source with the switching strategy.

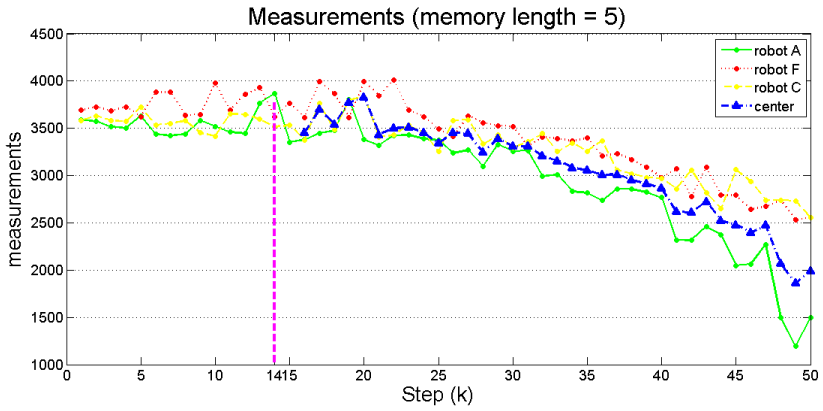

Figure 13: Measurements when memory length is 5. At step $k = 16$, the robots switch to cooperation.

6.3.1.1 *Effects of the memory length r*

To illustrate the influence of the memory length on the exploration behavior of the robots, we conduct other two experiments with different memory lengths. Figure 14 and Figure 15 show the measurements corresponding to the memory lengths 10 and 20. As seen in Figure 14, at step $k = 27$, robot F checks that the switching conditions are satisfied and at the same step the robots switch to cooperative exploration. In around 60 steps, the robots reach the light source. In Figure 15, the memory length $r = 20$. At step $k = 57$, robot A sends out the switching signal to the central computer and at step $k = 58$, the robots switch to cooperative exploration. They take around 80 steps to find the light source.

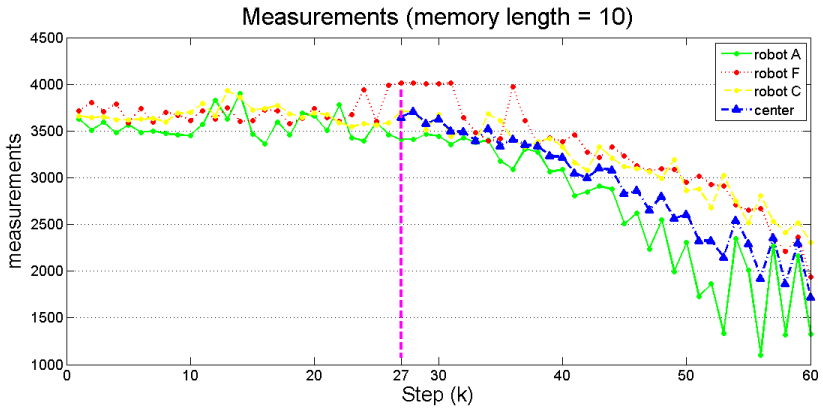

Figure 14: Measurements when memory length is 10. At step $k = 27$, the robots switch to cooperation.

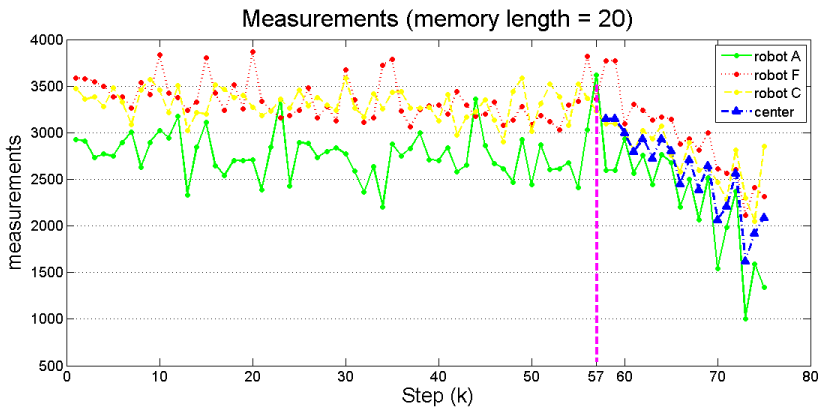

Figure 15: Measurements when memory length is 20. At step $k = 57$, the robots switch to cooperation.

The three trials with different memory lengths indicate that the memory length r plays an important role in the switching strategy. For a given field, if the noise level is high so that it is hard for the robots to find the source by themselves, the shorter the memory length is, the earlier the robots realize the situation and switch to cooperative exploration. On the other hand, a longer memory indicates higher noise tolerance. In situations that the cooperative exploration cost is high so that it is preferable for robots to explore the field individually, longer memory lengths give more chances to the robots to explore the field by their own.

Figure 16 shows the measurements taken by one robot in another experiment. In this trial, the memory length is set to be 60, which is long enough for the robot not to switch to cooperative exploration. We can see from the figure that even though the measurements are noisy, since the switching conditions are not satisfied with $r = 60$, the robot is able to find the light source after around 100 steps, which verifies the fact we discussed previously that as long as the switching conditions are not satisfied, a robot moves towards a local minimum of a field.

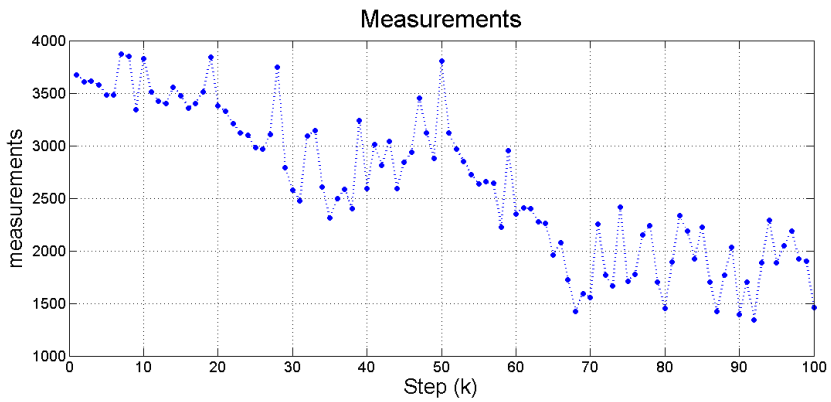

Figure 16: Measurements taken by one robot with memory length $r = 60$.

6.3.1.2 Effects of the noise attenuation level γ

Figure 17 illustrates the traces of the error bound P_k of the H_∞ filter associated with different noise attenuation levels when the robots are in the cooperative exploration phase. In these experiments, we also set $a = 0.2$m, $Q = I$, $W = 0.01I$, and $V = 0.01I$. Given the parameters and from the sufficient conditions (138), we can calculate that if $\gamma^2 > \max(\frac{\sigma_1^2\sigma_3^2}{N}, \frac{2\sigma_1^2\sigma_3^2}{aN}) = \max(\frac{0.01}{3}, \frac{2\times 0.01}{0.2\times 3}) = 0.033$, which implies $\gamma > 0.1826$, then the cooperative H_∞ filter will converge. In Figure 17, we can see that, when $\gamma > 0.1826$, the noise bound P_k converges to a steady state value P^s. Actually, since (138) is only a sufficient condition for convergence, when $\gamma < 0.1826$, the cooperative H_∞ filter may converge as well. We have tested that when $\gamma > 0.045$, the cooperative H_∞ filter converges. Only when $\gamma < 0.045$, the cooperative H_∞ filter becomes unstable.

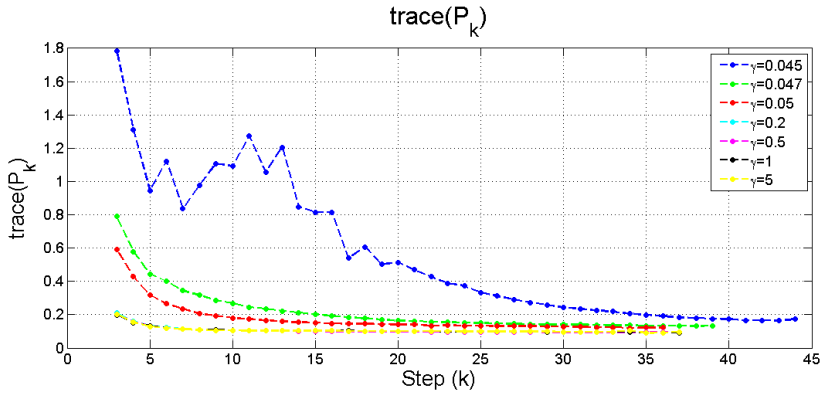

Figure 17: Trace(P_k) when the noise attenuation level γ of the H_∞ filter varies.

6.3.1.3 Effects of the formation size a

Figure 18 illustrates the trace of the error bound P_k of the H_∞ filter associated with different formation sizes when the robots are in the cooperative exploration phase. In these experiments, we set the noise attenuation level $\gamma = 3$, the weighting matrices $Q = I$, $W = 0.01I$, and $V = 0.01I$. Equation (32) also indicates that as the formation size a increases, the trace of P^s decreases. We can clearly see the tendency in Figure 18.

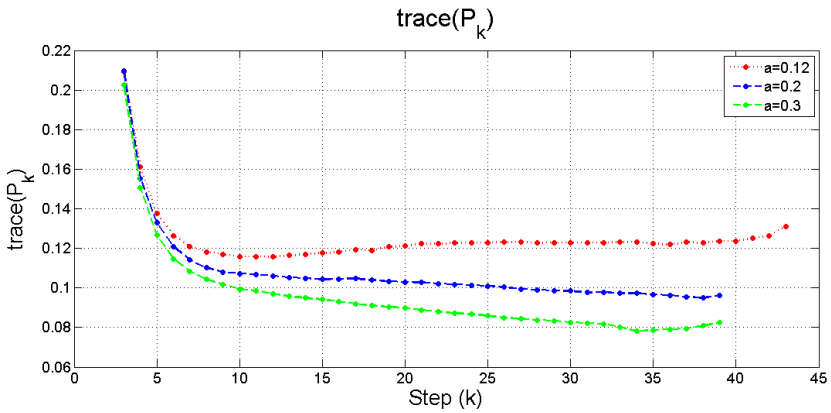

Figure 18: Trace(P_k) when the distance between each pair of the robots varies.

6.3.1.4 Comparison with purely individual exploration

As we discussed before, Figure 16 shows the measurements taken by one robot without switching to cooperative exploration. We can also consider this experiment as the robot

exploring the field with purely individual exploration strategy. As we can see from the figure, the convergence rate is slower compared to the experiment with switching strategy, as shown in Figure 13, Figure 14, and Figure 15. Therefore, with the switching strategy, we can achieve a higher rate of convergence.

6.3.1.5 Comparison with purely cooperative exploration

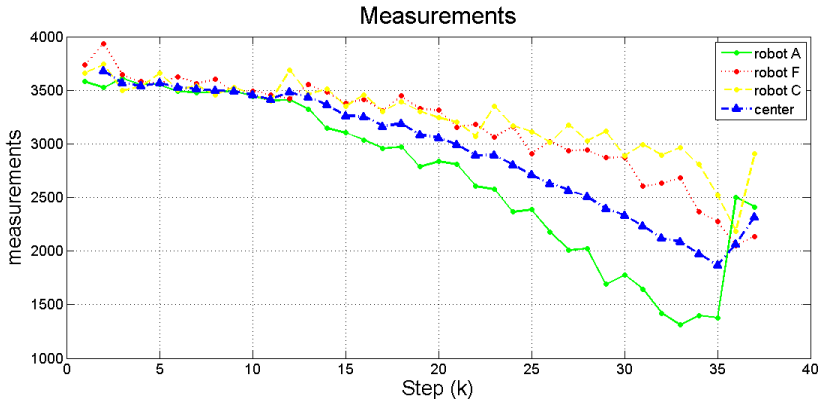

Figure 19: Measurements taken by three robots with purely cooperative exploration.

Figure 19 shows the measurements taken by three robots in an experiment with purely cooperative exploration strategy. The settings are the same as the experiments we introduced before with the formation size $a = 0.35m$. As illustrated in the figure, the formation formed by the robots converges to the light source in fewer steps. However, since cooperative exploration is associated with increased cost such as communication and computation, in fields with lower noise levels, the switching strategy can allow the agents to seek the source individually without collaborating if the switching conditions are not satisfied. Thus, the cost can be reduced.

6.3.2 Complementary Simulation Results

In the experiments, once the robots switch to cooperative exploration, they do not switch back to individual exploration because the noises are not under our control and remain at a constant level. To justify our switching condition from cooperative exploration to

individual exploration, we simulate three sensing agents searching for a minimum of a two dimensional scalar field that is corrupted by time-varying uniformly distributed noises. The field is generated according to $z = (x-10)^2 + 2(y-10)^2$. We assume that at step $k = 80$, the noise level in the field increases from 5% to 30% and at step $k = 250$, the noise level reduces from 30% to 5%. We choose the memory length $r = 20$ in algorithm 1 and $\mu_1 = 1.3$ in algorithm 3.

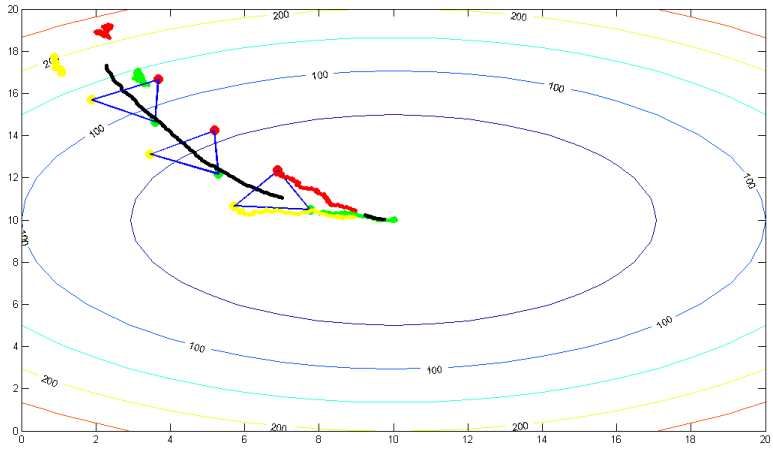

Figure 20: The trajectories of the sensing agents. The green, red, and yellow lines indicate the trajectories of the agents in the individual exploration phase and the black line indicates the trajectory of the formation center in the cooperative exploration phase.

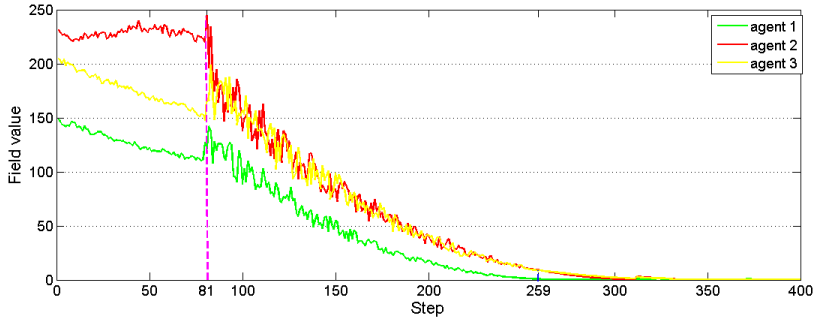

Figure 21: Measurements taken by the agents. The agents switch to cooperative exploration at $k = 81$ and switch back to individual exploration at $k = 259$.

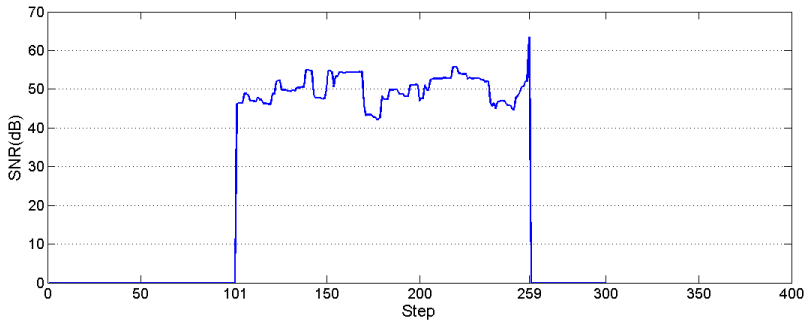

Figure 22: The average signal-to-noise ratio. When $k > 101$ and $k < 259$, the agents calculate the SNR. After $k = 259$, the agents switch back to individual exploration.

Figure 20 illustrates the exploration process of the three sensing agents. The agents form a symmetric formation. The colored lines are trajectories of the three agents when they are performing individual exploration. The black line is the trajectory of the formation center when the agents are collaborating. Figure 21 shows the filtered field values measured by each agent with different colored lines corresponding to different agents in Figure 20. Figure 22 shows the estimated SNR when the agents are performing cooperative exploration. The figures indicate that the agents start from individual exploration. At step $k = 86$, they switch to cooperative exploration. Thus, $T_s = 86$. When $k > T_s + r = 106$, the SNR is computed and at $k = 259$, the agents find that $\bar{\beta}_k > 1.3\bar{\beta}_{T_s+r}$, so they switch back to individual exploration and succeed in locating the field minimum in around 300 steps.

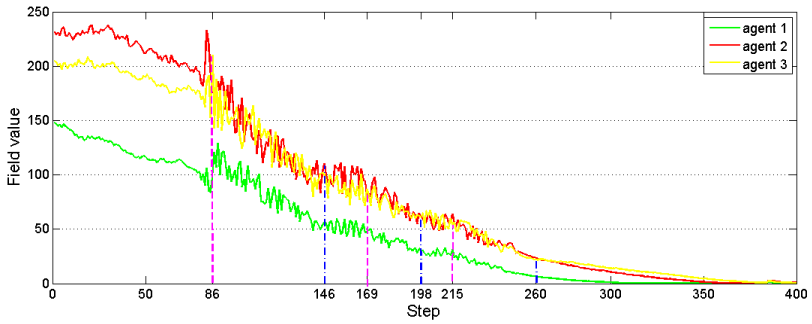

Figure 23: Measurements taken by the agents. The agents switch to cooperative exploration at $k = 86, 169$, and 215 and switch back to individual exploration at $k = 146, 198$, and 260.

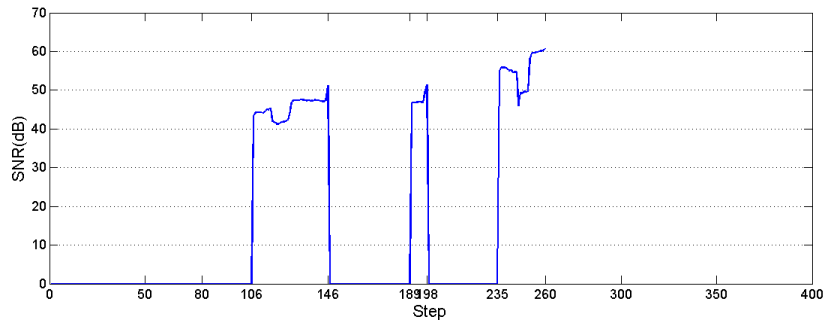

Figure 24: The average signal-to-noise ratio estimated by the agents.

If we set μ_1 to be a smaller value and keep other settings the same as the first simulation, we can observe from the simulation results that the switchings between individual exploration and cooperative exploration happen several times during one trial. Figure 23 indicates the measurements taken by the agents. In this simulation, we choose $\mu_1 = 1.1$ and $\varepsilon = 0.05$. The agents switch to cooperative exploration at $k = 86, 169$, and 215 and switch back to individual exploration at $k = 146, 198$, and 260. Figure 24 shows the corresponding SNR calculated in this trial. In this simulation, the agents take around 400 steps to converge to the field minimum. We can see that the larger μ_1 tends to keep the agents in the cooperative exploration phase and increase the rate of convergence of the exploration behavior.

6.3.3 Self-Organization

Using the proposed switching strategy, the agents can switch to cooperative exploration once they detect that the convergence rate to a local minimum is not satisfactory. However, if we are provided with N agents, where N is sufficiently large number, does it mean that when a few agents in the group require collaboration, all the other agents need to respond to their requirements and collaborate with them? Obviously, the answer is no. As introduced in Chapter V, if the noise $w(\mathbf{r})$ in the measurements is assumed to be Gaussian, then, Algorithm 4.4.4 provides an approach to estimate the minimum number of agents required to guarantee coherent steps of the group. Thus, lower probability of false-walks can be achieved.

Based on Algorithm 4.4.4 , we modify Algorithm 6.1.4 so that once one agent in a group requires collaboration, it estimates the minimum number of agents $N_{\min}$ simultaneously. Then, only $N_{\min}$ agents switch to cooperative exploration. Other agents can be saved to other exploration tasks. The modified algorithm is as follows.

Algorithm 6.3.1 *Suppose a group of N agents are searching for a local minimum of an unknown field, where the field value satisfies* $z_{\min} \leq z(\mathbf{r}_k) \leq z_{\max}$. *Let* $\bar{y}(\mathbf{r}_k) = \max_{s\in[-r,0]} y(\mathbf{r}_{k+s})$, *where r is the memory length of the agent. Given* $\varepsilon > 0$ *and* $0 < p < 1$,

S.1 At step $k \geq r$, *the ith agent takes a measurement of the field* $y(\mathbf{r}_{i,k})$. *Then estimates the field gradient* $\nabla z(\mathbf{r}_{i,k})$ *by solving the equations (50) and (51).*

S.2 The ith agent moves in the opposite direction of the estimated gradient according to $\dot{\mathbf{r}}_{i,k} = -\nabla\hat{z}(\mathbf{r}_{i,k})$ *or uses other strategies to reduce the measured field value. At step* $k+1$, *the agent takes a new measurement* $y(\mathbf{r}_{k+1})$.

S.3 At step $k+1$, *the agent checks whether* $(1+\varepsilon)y(\mathbf{r}_{i,k}) \geq \bar{y}(\mathbf{r}_{i,k}) + \varepsilon z_{\min}$ *is satisfied or not. If yes, the agent checks the value of* $y(\mathbf{r}_{i,k+1}) - y(\mathbf{r}_{i,k})$. *If* $y(\mathbf{r}_{i,k+1}) - y(\mathbf{r}_{i,k}) \leq -\rho y(\mathbf{r}_{i,k}) + \rho z_{\min}$, *it keeps individual exploration. Go to step S.6. Otherwise, go to step S.4.*

S.4 At step $k+1$, the ith agent estimates the field noise variance by

$$\hat{\sigma}_3^2 = \frac{1}{k+1}\sum_{j=1}^{k+1}(y(\mathbf{r}_{i,j}) - \frac{1}{k+1}\sum_{l=1}^{k+1} y(\mathbf{r}_{i,l}))^2, \tag{101}$$

and estimates the number of the agents required to guarantee coherent steps by

$$N_{\min} > \frac{16\hat{\sigma}_3{}^4}{m^2(\frac{(|z(\mathbf{r}_{i,k+1}) - z(\mathbf{r}_{i,k})| - \varepsilon)}{\mathrm{erf}^{-1}(p)})^4 - 4\hat{\sigma}_3^4}, \tag{102}$$

Then the ith agent forms a group of $N_{\min}$ with the $N_{\min}-1$ agents closest to it. The distance between the ith and jth agents is measured by $d_{i,j} = |\mathbf{r}_{i,k} - \mathbf{r}_{j,k}|$. If $N < N_{\min}$, all the agents form a group with N agents.

S.5 From $k+1$, the group performs cooperative exploration. A cooperative filter is constructed to produce estimates of the field value and gradient at the formation center. The remaining agents continue individual exploration.

S.6 For agents in individual exploration mode, if $|y(\mathbf{r}_{i,k}) - z_{\min}| < \eta$, in which η is a constant depending on the choice of the step size, stop. For collaborating agent-groups, if $|y(\mathbf{r}_{c,k}) - z_{\min}| < \eta$, stop.

The performance of the self-organizing algorithm 6.3.1 has been verified in experiments. When one agent wants collaboration, it sends the requirement to the central computer and estimates σ_3 and $N_{\min}$ according to Equations (101) and (102). Then, the central computer sends switching signals to the $N_{\min}-1$ robots that are closest to the agent that requires collaborating. According to the switching conditions, only the robot that moves towards a local minimum with an unsatisfactory convergence rate will initiate collaboration. In the cooperative exploration stage, the central computer broadcasts the estimated moving directions to the robots. The robots move according to the received information.

In the first trial, we set $p = 0.9$, $\varepsilon = 50$, and $m = 1.5$, and choose a step size of $\delta_1 = 5cm$ for the robots. Following Algorithm 4.4.4, at step $k = 8$, robot "G" first requires collaboration since it is not converging to the source. Robot "G" estimates $\sigma_2 = 341.0085$

and $N_{\min} > 2.8429$. Therefore, $N_{\min} = 3$. The closest two robots to Robot "G", robots "O" and "N", together with Robot "G" form a symmetric formation and they are able to converge to the light source. Since the estimation results indicate that three robots are enough to guarantee coherent steps with an explorative probability of 90%, the other two robots perform individual exploration all the time. We can also assign other tasks to the remaining two robots. Figure 25 shows the trajectories of the five robots and Figure 26 shows the measurements. In another trial, we increase the desired explorable probability p to 0.91, the estimated minimum number becomes $N_{\min} = 4$. The blue line with triangles are the filtered field values at the center of the formation, and the vertical dark blue lines indicate the time step, at which switching occurs.

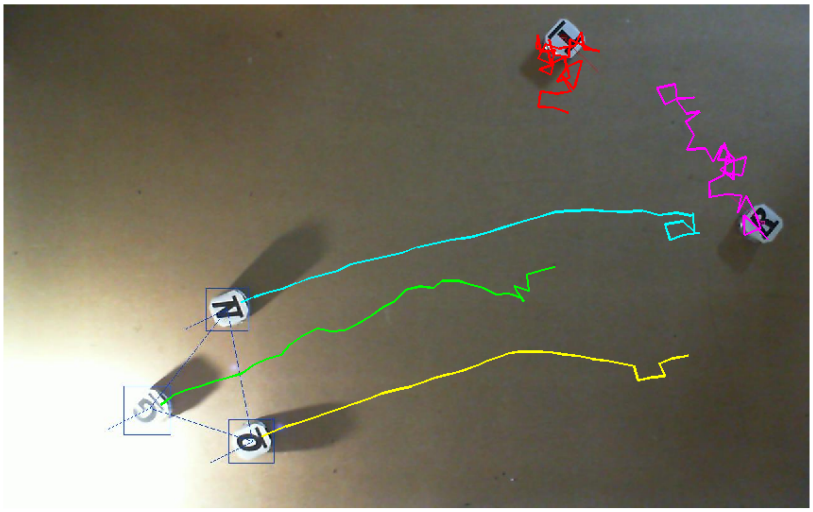

Figure 25: Trajectories of five Khepera III robots. $N_{\min} = 3$. Robots "G," "O," and "N" form a three-robot group.

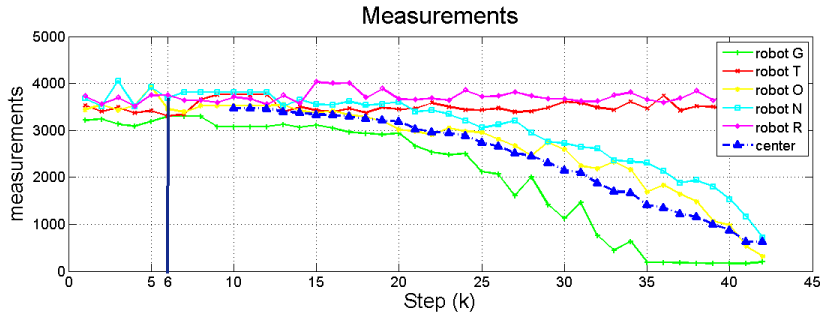

Figure 26: Measurements of five Khepera III robots in the first ($N_{\min} = 3$) experiment.

As we discussed in Section 4.4, as the number of agents N increases, the error in the cooperative Kalman filter decreases, as shown in Figure 27, in which the blue, green, and red lines correspond to the traces of the error covariance matrix of the cooperative Kalman filter when three, four, and five robots are in a group, respectively.

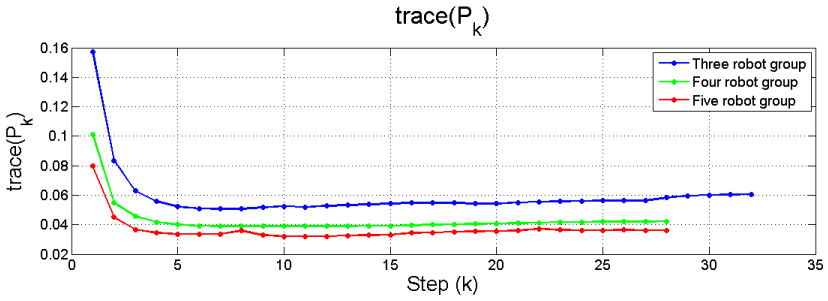

Figure 27: Traces of the cooperative Kalman filter when three, four, and five robots are performing cooperative exploration.

6.4 Another Application: Target Tracking

Other than the source seeking problem, the switching strategy can also be applied to other exploration tasks such as target tracking as long as a cost function related to convergence rate is defined. In this section, we introduce the target tracking problem and apply the switching strategy.

6.4.1 Tracking Model

Suppose a target is moving in a two dimensional plane with a constant velocity. Define $\mathbf{r}_T = (x_T, y_T)$ as the Cartesian coordinates of the target, and let $\dot{\mathbf{r}}_T = (\dot{x}_T, \dot{y}_T)$ represent the velocity of the target. N sensing agents mounted with bearings-only sensors are used in tracking the target. Because of the limited number of sensing agents and the limited sensing range of each sensing agent, the sensing agents are controlled to move in a group to keep track of the target. Denote the position of the ith agent as $\mathbf{r}_i = (x_i, y_i)$ and the corresponding bearing measurement as $\theta_i, i = 1, \cdots, N$. Assume that the sensing agents move in a constant speed that is identical to the speed of the target. In addition, each sensing agent is aware of the positions of all other agents.

Given the settings, at the kth time instant, the geometry of the target tracking is illustrated in Figure 28, in which $\mathbf{r}_{i,k}$ represents the position of the ith sensing agent, $\mathbf{r}_{T,k}$ represents the position of the target, and $\theta_{i,k}$ is the bearing from the ith agent to the target.

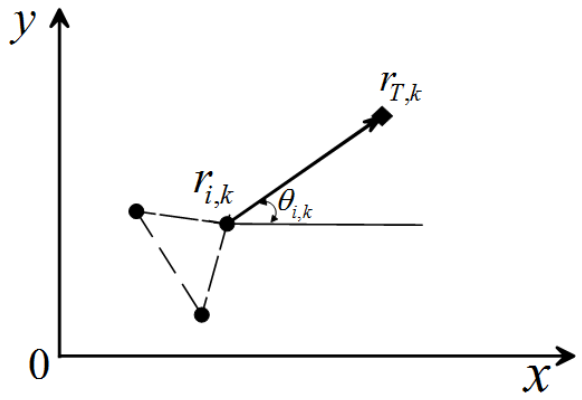

Figure 28: Bearings-only target tracking geometry in two-dimension.

The objective of the target tracking problem is to (1) estimate the state of the moving target, e.g. position and velocity from the bearings-only measurements taken by the N sensing agents, and (2) control the sensing agents to keep track of of the target while remaining in a desired formation.

At each time instant, the bearing measurement of the ith sensing agent is

$$\theta_{i,k} = \arctan \frac{y_{T,k} - y_{i,k}}{x_{T,k} - x_{i,k}} + w_{i,k}, \tag{103}$$

where $w_{i,k} \sim \mathcal{N}(0, \sigma_w^2)$ is assumed to be mutually independent zero-mean Gaussian noise with variance σ_w^2. Choose the state of the target to be $\mathbf{s} = [x_T, y_T, \dot{x}_T, \dot{y}_T]$. Let $h(\mathbf{s}_k)$ be a $N \times 1$ observation matrix with the ith row defined by $\theta_{i,k}$, that is,

$$h(\mathbf{s}_k) = [\arctan \frac{y_{T,k} - y_{1,k}}{x_{T,k} - x_{1,k}}, \cdots, \arctan \frac{y_{T,k} - y_{N,k}}{x_{T,k} - x_{N,k}}]^T, \tag{104}$$

and let $\mathbf{y}_k = col(\theta_{1,k}, \cdots, \theta_{N,k}) \in \mathscr{R}^N$ be the measurement vector consisting of all the measurements collected from the N collaborating agents at time k. Then, the measurement equation for the N sensing agents is

$$\mathbf{y}_k = h(\mathbf{s}_k) + \mathbf{w}_k. \tag{105}$$

The covariance of the noise vector $\mathbf{w}_k$ is given by $R = \sigma_w^2 \mathbf{I}$, in which $\mathbf{I}$ is a $N \times N$ dimensional identity matrix. Therefore, the measurement vector $\mathbf{y}_k$ is a normally distributed random vector with mean $h(\mathbf{s}_k)$ and covariance matrix R, i.e., $\mathbf{y}_k \sim \mathcal{N}(h(\mathbf{s}_k), R)$.

The evolution of the target state is described by the dynamic model of a target. Most tracking algorithms are model based assuming the knowledge of the target motion is available. We choose a constant-velocity model to describe the motion of the target, which is

$$\mathbf{s}_{k+1} = F_k \mathbf{s}_k + \mathbf{v}_k, \tag{106}$$

where $F_k = \begin{pmatrix} 1 & 0 & T & 0 \\ 0 & 1 & 0 & T \\ 0 & 0 & 1 & 0 \\ 0 & 0 & 0 & 1 \end{pmatrix}$ is the state transition matrix, T is the sampling rate, $\mathbf{v}_k \sim \mathcal{N}(0, Q)$ is uncorrelated, zero-mean Gaussian noise processes with covariance matrices Q. For mathematical simplification, we assume that he noise terms $\mathbf{v}_k$ and $\mathbf{w}_k$ satisfy:

$E(\mathbf{v}_k\mathbf{v}_j^T) = Q\delta_{k,j}, E(\mathbf{w}_k\mathbf{w}_j^T) = R\delta_{k,j}$, and $E(\mathbf{v}_k\mathbf{w}_j^T) = 0$. The uncertainty in the target state estimates will be influenced by the uncertainty of the bearing measurements and the positions of the sensing agents with respect to the target.

6.4.2 Extended Kalman Filter

Since the measurement equation (105) is nonlinear, we apply the extended Kalman filter (EKF) [100] to estimate the state of the target. Compared to particle filters, extended Kalman filter requires less computational load, which produces more efficient estimates.

Define $\mathbf{H}_k$ to be the Jacobian of the measurement vector with respect to the state of the target. We derive $\mathbf{H}_k = \nabla_{\mathbf{s}} h(\mathbf{s}_k) = \begin{pmatrix} \frac{\partial \theta_{1,k}}{\partial \mathbf{s}} & \dots & \frac{\partial \theta_{N,k}}{\partial \mathbf{s}} \end{pmatrix}^T$, the ith row of which is

$$\mathbf{H}_{i,k} = \begin{pmatrix} -\frac{y_{T,k}-y_{i,k}}{(x_{T,k}-x_{i,k})^2+(y_{T,k}-y_{i,k})^2} & \frac{x_{T,k}-x_{i,k}}{(x_{T,k}-x_{i,k})^2+(y_{T,k}-y_{i,k})^2} & 0 & 0 \end{pmatrix}, \tag{107}$$

Two steps are consisted in the extended Kalman filter: prediction and update. Denote P_k as the error covariance matrix of the extended Kalman filter, and K_k as the Kalman gain. Given state equation (106) and measurement equation (105), the equations of the EKF are listed below:

$$\begin{aligned} \hat{\mathbf{s}}_k^- &= F_k\hat{\mathbf{s}}_{k-1}, \\ P_k^- &= F_kP_{k-1}F_k^T + Q_{k-1}, \\ K_k &= P_k^-\mathbf{H}_{k|\hat{\mathbf{s}}_k^-}^T(\mathbf{H}_{k|\hat{\mathbf{s}}_k^-}P_k^-\mathbf{H}_{k|\hat{\mathbf{s}}_k^-}^T + R_k)^{-1}, \\ P_k &= (I - K_k\mathbf{H}_{k|\hat{\mathbf{s}}_k^-})P_k^-, \\ \hat{\mathbf{s}}_k &= \hat{\mathbf{s}}_k^- + K_k(\mathbf{y}_k - h(\hat{\mathbf{s}}_k^-)), \end{aligned} \tag{108}$$

where $\mathbf{H}_{k|\hat{\mathbf{s}}_k^-}$ is the Jacobian $\mathbf{H}_k$ given the predicted state based on the measurements at step $k-1$. Consider the linearized system

$$\mathbf{s}_{k+1} = F_k\mathbf{s}_k + \mathbf{v}_k, \tag{109}$$

$$\mathbf{y}_k = \mathbf{H}_k\mathbf{s}_k + \mathbf{w}_k. \tag{110}$$

If only one agent is used in tracking the target, $N = 1$. Then, the observation matrix becomes $\mathbf{H}_k = \begin{pmatrix} -\frac{y_{T,k}-y_{1,k}}{(x_{T,k}-x_{1,k})^2+(y_{T,k}-y_{i,k})^2} & \frac{x_{T,k}-x_{1,k}}{(x_{T,k}-x_{1,k})^2+(y_{T,k}-y_{i,k})^2} & 0 & 0 \end{pmatrix}$, which implies that the system is unobservable. In fact, for the state of a moving target to be observable to a sensing agent, the sensing agent must execute a proper maneuver, e.g. changes the heading or accelerates, as described in [86, 101]. Since we assume that the speed of the sensing agents are the same of the target, we always let $N \geq 2$.

6.4.3 Formation and Motion Control

In this section, we first introduce the optimal formation that the agent group is required to maintain, then, we discuss the motion control design for the group. Formation control is achieved by using the same technique as introduced in Chapter V.

6.4.3.1 Optimal Formation

The Fisher information matrix (FIM) describes the amount of information that the measurement $\mathbf{y}_k$ carries about the unobservable state $\mathbf{s}_k$. It is calculated in [78] that the FIM is

$$I(\mathbf{s}_k) = \nabla_{\mathbf{s}} h(\mathbf{s}_k)^T R^{-1} \nabla_{\mathbf{s}} h(\mathbf{s}_k). \tag{111}$$

Recall the error covariance matrix P_k in the extended Kalman filter, which can also be written as

$$P_k^{-1} = (P_k^-)^{-1} + \mathbf{H}_{k|\hat{\mathbf{s}}_k^-}^T R^{-1} \mathbf{H}_{k|\hat{\mathbf{s}}_k^-}. \tag{112}$$

The second term of P_k^{-1} can be recognized as the Fisher information matrix since

$$I(\hat{\mathbf{s}}_k^-) = \nabla_{\mathbf{s}} h(\hat{\mathbf{s}}_k^-)^T R^{-1} \nabla_{\mathbf{s}} h(\hat{\mathbf{s}}_k^-) = \mathbf{H}_{k|\hat{\mathbf{s}}_k^-}^T R^{-1} \mathbf{H}_{k|\hat{\mathbf{s}}_k^-}. \tag{113}$$

Therefore, equation (112) becomes

$$P_k^{-1} = (P_k^-)^{-1} + I(\hat{\mathbf{s}}_k^-). \tag{114}$$

Hence, reducing the estimating error in the extended Kalman filter can be translated into increasing the Fisher information. The Cramer-Rao lower bound (CRLB) states that the

variance of any unbiased estimator is bounded by the inverse of the Fisher information [59]. As stated in [11, 33, 78, 135], an agent configuration over the space of all angle positions θ_i, $\forall i \in \{1, \cdots, N\}$ is optimal if the configuration maximizes the determinant of Fisher information matrix, or minimizes the Cramer-Rao lower bound.

Define the distance from the target to the ith sensing agent as $d_i = \|\mathbf{r}_T - \mathbf{r}_i\|$. We derive that

$$I(\mathbf{s}) = \frac{1}{\sigma_w^2} \begin{pmatrix} \sum_{i=1}^N \frac{1}{d_i^2} \sin^2\theta_i & -\sum_{i=1}^N \frac{1}{2d_i^2} \sin 2\theta_i & 0 & 0 \\ -\sum_{i=1}^N \frac{1}{2d_i^2} \sin 2\theta_i & \sum_{i=1}^N \frac{1}{d_i^2} \cos^2\theta_i & 0 & 0 \\ 0 & 0 & 0 & 0 \\ 0 & 0 & 0 & 0 \end{pmatrix} = \frac{1}{\sigma_w^2} \begin{pmatrix} I'(\mathbf{s}) & \mathbf{0} \\ \mathbf{0} & \mathbf{0} \end{pmatrix}, \quad (115)$$

in which $\mathbf{0}$ is a 2×2 matrix. If we only consider the Fisher information of the position measurements, that is, $I'(\mathbf{s})$, then, the optimal formation can be obtained by solving the following two equations simultaneously [11, 33, 78, 135]

$$\sum_{i=1}^N \frac{1}{d_i^2} \sin 2\theta_i = 0, \text{ and } \sum_{i=1}^N \frac{1}{d_i^2} \cos 2\theta_i = 0. \quad (116)$$

In addition, θ_i can be found if and only if $\frac{1}{d_j^2} \leq \sum_{i=1, i\neq j}^N \frac{1}{d_i^2}$ for all $j \in \{1, \cdots, N\}$. It is also proved in [135] that if there are only indices permutation, agents flipping about the target, or global rotation, reflection of combined, the two placements $\{\theta_i\}_{i=1}^N$ and $\{\theta_i'\}_{i=1}^N$ are equivalent.

In [11, 33, 78, 135], the target that is being localized by sensors is static, and d_i are considered as the sensor ranges, which are fixed. If the sensor ranges are identical, i.e., $d_i = d_j, \forall i, j \in \{1, \cdots, N\}, i \neq j$, the angles between adjacent sensing agents can be calculated as $\theta_{i,j} = \frac{2\pi}{N}$. Figure 29 (a) illustrates an example of an optimal formation of three sensing agents with identical distances d_i from the target. In this case, $\theta_{1,2} = \theta_{2,3} = \theta_{3,1} = \frac{2\pi}{3}$.

In this study, the sensing agents are tracking a moving target, and may not start from locations close to the target. Therefore, the agents may not be controlled to be placed around the target. We solve this problem by flipping sensor agents about the target so that

all the agents are in the same side with regard to the target. In addition, we do not assume that each sensing agent has fixed sensing range. We assume that the sensing agents can take bearing measurements regardless of the distances from the target, which indicates that d_i may change before the distances between the sensing agents and the target converge. Thus, the optimal formation evolves with the change of the distances d_i.

Figure 29 (b) illustrates an optimal formation of three sensing agents by flipping the second agent about the target in Figure 29 (a). As shown in the figure, the dashed lines connecting three sensing agents form a triangular formation. Note that the calculation of the optimal formation only determines θ_i, which indicates that the formation size in terms of the distance between agents depends on d_i. Then, we can observe from Figure 29 (b) that, as the distances from agents to the target decrease, i.e., decrease d_i, the formation size in terms of the distances between agents decreases.

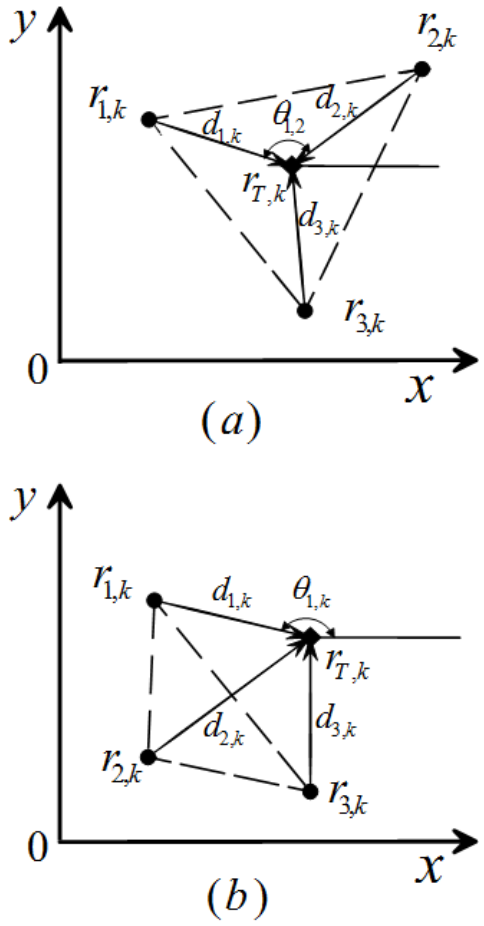

Figure 29: Bearings-only target tracking geometry in two-dimension. (a) Optimal symmetric formation when $N = 3$. (b) Optimal formation when the position of one agent is flipped with respect to the position of the target.

6.4.3.2 Group Motion Planning

Define a simple convex quadratic cost function

$$V_{c,k} = \frac{1}{2}(\mathbf{r}_{c,k} - \mathbf{r}_{T,k})^T M(\mathbf{r}_{c,k} - \mathbf{r}_{T,k}), \tag{117}$$

where M is a symmetric matrix. Equation (117) yields

$$\nabla V_{c,k} = M(\mathbf{r}_{c,k} - \mathbf{r}_{T,k}). \tag{118}$$

Let the agent group move towards the target along the gradient of $V_{c,k}$.

$$\mathbf{r}_{c,k+1} = \mathbf{r}_{c,k} - \frac{\nabla V_{c,k}}{|\nabla V_{c,k}|} v = \mathbf{r}_{c,k} - \frac{\mathbf{r}_{c,k} - \mathbf{r}_{T,k}}{|\mathbf{r}_{c,k} - \mathbf{r}_{T,k}|} v, \tag{119}$$

where v is the speed of the agent, which is assumed to be constant. The agent moves in the direction that reduces the value of the cost function until it gets sufficient close to the target.

6.4.4 The Switching Strategy

A switching strategy similar to Algorithm 6.1.4 is applied to the target tracking problem. There are two differences: (1) The agents check a cost function as in Equation (117) instead of the measurements of the field to decide whether to switch to cooperative exploration; and (2) In the tracking process, the N agents first form $\frac{N}{2}$ two-agent groups. The two-agent groups keep tracking the target until the switching conditions are satisfied. Then, the two-agent groups form larger groups (e.g., four-agent group), the larger groups start to check the switching conditions, and continue the process: keep tracking or switch to larger groups. The algorithm is as follows.

Algorithm 6.4.1 *Suppose N sensing agents with memory length r are tracking a moving target. N is an even number. The N agents form $\frac{N}{2}$ two-agent groups at step $k = 0$. At step k, do the following:*

S1. Each agent takes a bearings-only measurement $\theta_{i,k}$ of the target.

S2. Each two-agent group obtains the state estimation produced by the extended Kalman filter.

S3. Given the state estimation, each two-agent group calculates the value of the cost function $V_{c,k}$ (117) and moves towards the target according to equation (119); If $k = T_{terminal}$, in which $T_{terminal}$ is the terminal time, stop.

S4. If $k \leq r$, go to step S1. Otherwise, continue to step S5.

S5. If $\bar{V}_{c,k} \leq K_2 V_{c,k}$, go to step S1. Otherwise, continue to step S6;

S6. The agent group moves one step further, and obtain a new cost function value $V_{c,k+1}$. Then, the group checks the value of $V_{c,k+1} - V_{c,k}$. If $V_{c,k+1} - V_{c,k} \leq K_1 V_{c,k}$, then, it remains in the two-agent group. Go to step S1. Otherwise, continue to step S7;

S7. The group requires to switch to larger groups with more agents by sending switching signals to other groups.

Under the above algorithm, if for all $k > 0$, $V_{c,k+1} - V_{c,k} \leq K_1 V_{c,k}$ whenever $\bar{V}_{c,k} \leq K_2 V_{c,k}$, the distance between the agent group and the target will converge to a constant. According to Algorithm 6.4.1, the switching conditions from smaller groups to larger groups can be stated as: (1) $\bar{V}_{c,k} \leq K_2 V_{c,k}$, and (2) $V_{c,k+1} - V_{c,k} \leq K_1 V_{c,k}$. Once a two-agent group detects that both switching conditions are satisfied, it notifies other two-agent groups, then all two-agent groups switch to cooperative tracking upon request. All the agents form a N-agent group with similar formation control laws and motion control laws developed in previous sections. This ensures that all agents behave consistently in the cooperative tracking mode.

6.4.5 Simulation Results

We simulate a group of agents tracking a target moving in constant velocities. In the simulations, we choose $T = 0.1$, $\sigma_w = 0.4$, and $\sigma_v = 0.2$. At each time step, the sensing agents take bearings-only measurements from the target. A central controller collects the measurements and runs an extended Kalman filter that produces state estimates, which are used in calculating the motion control laws and formation control laws. We obtain optimal formations according to Equation (116). In the case of two-agent groups, the state of the target is unobservable if the target is located on the line that connects the two sensing agents. Therefore, we choose another form of optimal formation that the two lines connecting each agent and the target are perpendicular. Figures 30 and 31 illustrate the tracking results of

a two-agent group and a four-agent group, respectively. In the figures, we use different colored dots to represent the positions of the agents and plot the agent formations every 50 steps. The red lines are the trajectories of the moving target, and the black lines are the trajectories of the center of the groups. As illustrated in the figures, as the formation moves closer to the target, the size of the optimal formation reduces. The green dots illustrate the estimated positions of the moving target produced by the extended Kalman filter. The green dots in the two figures indicate that the error in the estimates is reduced by increasing the number of agents in a group.

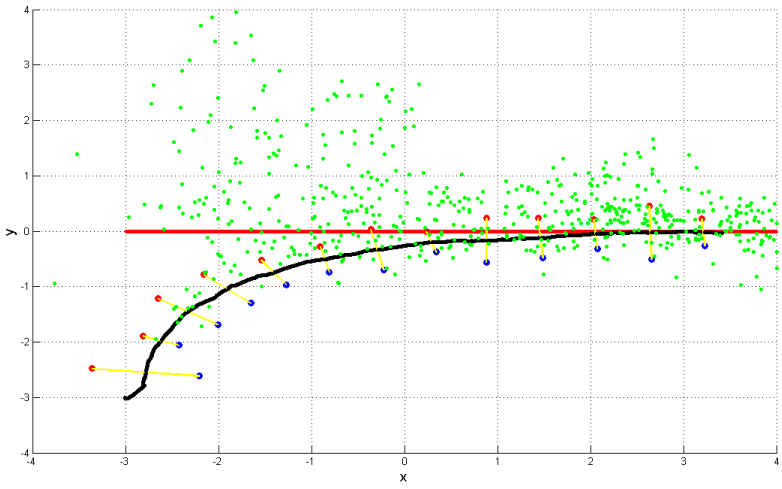

Figure 30: The trajectory of a two-agent group tracking a moving target. The red line and black line represent the trajectory of the moving target and the center of the group, respectively. The green dots illustrate the estimated positions of the moving target produced by the extended Kalman filter.

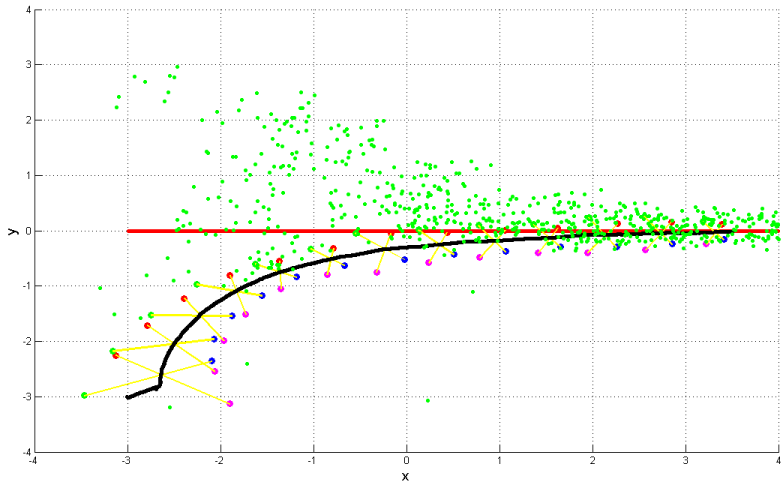

Figure 31: The trajectory of a four-agent group tracking a moving target. The red line and black line represent the trajectory of the moving target and the center of the group, respectively. The green dots illustrate the estimated positions of the moving target produced by the extended Kalman filter.

We then implement the switching strategy using four sensing agents. As illustrated in Figure 32, we first let the four agents form two two-agent groups and track the moving target using the techniques introduced previously. The blue and cyan dots are trajectories of the two two-agent groups, and the magenta and yellow dots are the estimated positions of the target by the two two-agent groups, respectively. The two-agent groups check the switching conditions at each time step while moving towards the target based on the estimated target positions. Once the switching conditions are satisfied, which indicates that the convergence to the constant distance from the target is not guaranteed, the two two-agent groups join together and form a four-agent group. In this simulation, the switching occurs at step $k = 65$. The black dots are the trajectories of the four-agent group, and the green dots are the estimated positions of the target. Figure 33 shows the estimated speed by the four-agent group. The red line is the real speed of the target, which is 0.1. Figure 34 shows the relative distance between the center of the four-agent group and the moving

target, which indicates that the relative distance converges.

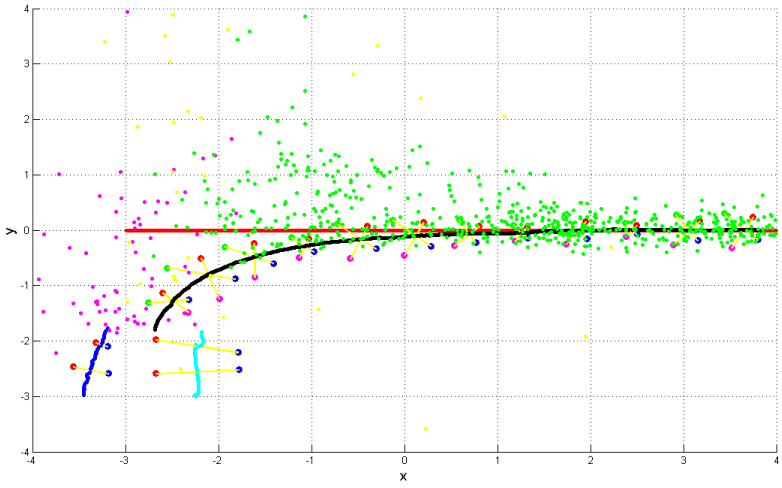

Figure 32: The trajectories of the agent groups and the estimates in the switching strategy. The red line and black line represent the trajectory of the moving target and the center of the group, respectively. The green dots illustrate the estimated positions of the moving target produced by the extended Kalman filter.

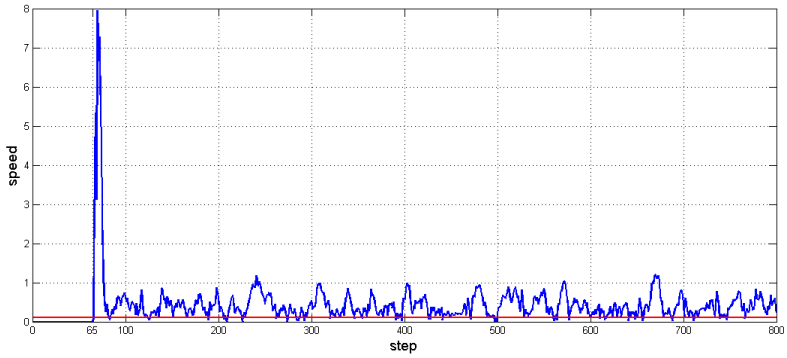

Figure 33: The estimated speed of the target after switching to a four-agent group.

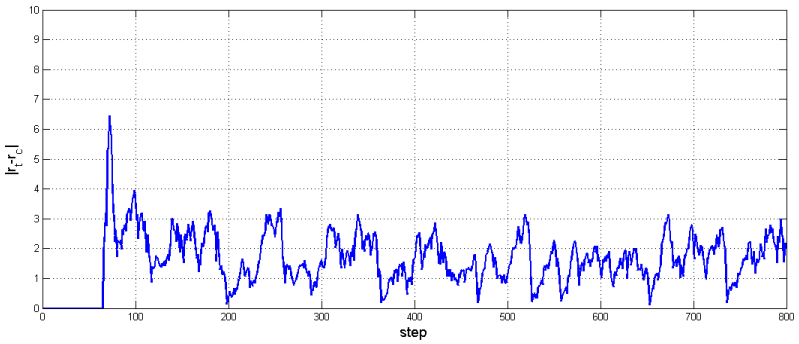

Figure 34: The relative distance between the four-agent group and the target.

CHAPTER VII

EXPLORATION IN 3D FIELDS

The structure of 3D scalar fields is of great importance to exploration tasks in the air by unmanned aerial vehicles (UAV) and underwater by autonomous underwater vehicles (AUV). The development of mobile sensor networks that are able to track small scale features in a three dimensional space takes the research to a new direction. To this end, we develop control and filtering algorithms for a mobile sensor network to cooperatively detect and track a desired curve on a desired level surface in an unknown 3D scalar field while moving in a formation [116]. In this way, the local structure of the field can be estimated from the measurements taken by all the agents. We propose an algorithm that allows the mobile sensor network to estimate principal curvatures and principal directions for lines of curvature using the measurements of the agents. In addition, we theoretically justify the minimum number of agents that can be utilized to accomplish the exploration task of detecting and tracking a line of curvature on a level surface.

7.1 Curve Tracking on a Level Surface

7.1.1 Curve Tracking Dynamics

At each time instant, for a 3D scalar field, consider a level surface with the level value $z(\mathbf{r}_c)$ passing through the formation center $\mathbf{r}_c$. The gradients of the 3D scalar field are perpendicular to the level surfaces. At the formation center $\mathbf{r}_c$, a unit normal vector $\mathbf{n}$, which is perpendicular to the surface can be defined as $\mathbf{n} = \frac{\nabla z(\mathbf{r}_c)}{\|\nabla z(\mathbf{r}_c)\|}$, in which $\nabla z(\mathbf{r}_c)$ is the gradient of the field at $\mathbf{r}_c$. When the formation is moving in the field at unit speed, its velocity vector is a unit vector $\mathbf{X}_1$. The field value $z(\mathbf{r}_c)$, which is estimated by the

cooperative Kalman filter, is changing with respect to time:

$$\dot{z}(\mathbf{r}_c) = \nabla z(\mathbf{r}_c) \cdot \frac{d\mathbf{r}_c}{dt} = \nabla z(\mathbf{r}_c) \cdot \mathbf{X}_1 = \|\nabla z(\mathbf{r}_c)\| \mathbf{n} \cdot \mathbf{X}_1. \tag{120}$$

Suppose $\gamma(s)$ is a curve passing through the formation center $\mathbf{r}_c$ that lies on the level surface, where s is the arc-length parameter. Then a right-handed orthonormal frame $(\mathbf{x}_1, \mathbf{x}_2, \mathbf{n})$ for the curve is established where $\mathbf{x}_1$ is the unit tangent vector to the curve and $\mathbf{x}_2$ is defined by $\mathbf{n} \times \mathbf{x}_1$. To describe the trajectory traced by the formation center moving with unit speed, a natural frame [12] can be established. Let $\mathbf{X}_1$ be the unit tangent vector to the trajectory of the formation center, and let $\mathbf{N}_c$ and $\mathbf{X}_2$ be unit normal vectors to the trajectory that are parallel transported along the trajectory from an arbitrarily chosen initial configuration so that $\mathbf{X}_1$, $\mathbf{X}_2$, and $\mathbf{N}_c$ always form an orthornormal basis of $\mathbf{R}^3$. Figure 35 illustrates the frame $[\mathbf{x}_1, \mathbf{x}_2, \mathbf{n}]$ of the curve $\gamma(s)$ on a level surface that passing through the formation center and the frame $[\mathbf{X}_1, \mathbf{X}_2, \mathbf{N}]$ of the formation center trajectory.

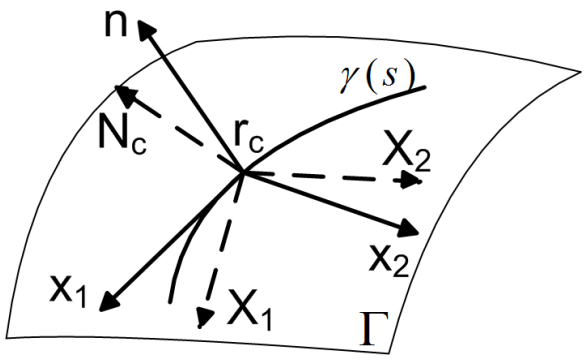

Figure 35: The frame $[\mathbf{x}_1, \mathbf{x}_2, \mathbf{n}]$ of a curve $\gamma(s)$ on a level surface that is passing through the formation center and the natural frame $[\mathbf{X}_1, \mathbf{X}_2, \mathbf{N}]$ of the trajectory of the formation center.

There are two sets of dynamic equations that are similar to the well-known Frenet-Serret equations [32] that describe the changes of the two frames, one set for the curve $\gamma(s)$ on the level surface, and the other for the trajectory of the formation center. We list the two

sets of equations side by side as follows

$$\begin{aligned}
\dot{\gamma} &= \alpha \mathbf{x}_1 & \dot{\mathbf{r}}_c &= \mathbf{X}_1 \\
\dot{\mathbf{x}}_1 &= \alpha \kappa_n \mathbf{n} + \alpha \kappa_g \mathbf{x}_2 & \dot{\mathbf{X}}_1 &= u\mathbf{N}_c + v\mathbf{X}_2 \\
\dot{\mathbf{x}}_2 &= -\alpha \kappa_g \mathbf{x}_1 + \alpha \tau_g \mathbf{n} & \dot{\mathbf{X}}_2 &= -v\mathbf{X}_1 \\
\dot{\mathbf{n}} &= -\alpha \kappa_n \mathbf{x}_1 - \alpha \tau_g \mathbf{x}_2 & \dot{\mathbf{N}}_c &= -u\mathbf{X}_1.
\end{aligned} \tag{121}$$

The term $\alpha = ds/dt$ is the instantaneous rate of change for the curve length of $\gamma(s)$ when the formation center moves. The terms κ_n, κ_g and τ_g are the normal curvature, the geodesic curvature, and the geodesic torsion of the curve $\gamma(s)$ on the level surface. We will discuss their geometric meaning in more detail in Section 7.2.1. The terms u and v are the steering controls for the formation center moving at the unit speed.

7.1.2 Steering Control Law Design

We define the steering control problem for the formation center as follows:

Problem 7.1.1 *Consider the motion of the formation center $\mathbf{r}_c$ moving at unit speed and the following assumptions about the 3D scalar field:*

- *A1 Suppose there exists a unique level surface $\Gamma(\mathbf{r}_c)$ passing through $\mathbf{r}_c$ along the trajectory of $\mathbf{r}_c$.*
- *A2 Suppose a unit tangent vector to a curve $\gamma(s) \in \Gamma(\mathbf{r}_c)$ passing through $\mathbf{r}_c$ is well defined at $\mathbf{r}_c$ and known as $\mathbf{x}_1$. This implies that $\mathbf{x}_1$ is known or accurately measured at every point of the trajectory of $\mathbf{r}_c$.*
- *A3 Suppose the curvatures ($\kappa_n(s)$, $\kappa_g(s)$, $\tau_g(s)$) are bounded and known at $\mathbf{r}_c$ for the curve $\gamma(s)$. This implies that the curvatures are known or accurately measured at every point of the trajectory of $\mathbf{r}_c$.*

Given a desired field value C, design the steering control laws u and v so that the formation center converges to the level surface with value C and moves along the curve $\gamma(s)$ with

the tangent direction $\mathbf{x}_1$. *In other words, as* $t \to \infty$, *the goal is to achieve* $z(\mathbf{r}_c) \to C$ *and* $\mathbf{X}_1 \to \mathbf{x}_1$.

Remark 7.1.2 *Assumptions (A2) and (A3) usually do not specify a unique curve on a level surface to track. Instead, we aim to track one out of a class of curves with desired curvatures and tangent directions. We will use the formation to estimate the tangent* $\mathbf{x}_1$ *and the curvatures. In Section 7.2, we will show that the lines of curvature of a surface can be traced in this setting.*

The relative displacement between the two frames at the formation center can be described by a set of "shape variables" [58] [130] as $((\mathbf{x}_1 \cdot \mathbf{X}_1), (\mathbf{x}_2 \cdot \mathbf{X}_1), (\mathbf{n} \cdot \mathbf{X}_1), z(\mathbf{r}_c))$. Define two 3×3 matrices $g_1 = (\mathbf{x}_1, \mathbf{x}_2, \mathbf{n})$ and $g_2 = (\mathbf{X}_1, \mathbf{X}_2, \mathbf{N}_c)$. From the fact that $g_1, g_2 \in SO(3)$, we have the orthonormality conditions that $g_1^T g_1 = \mathbf{I}_{3\times 3}$, $g_2^T g_2 = \mathbf{I}_{3\times 3}$ and $(g_1^T g_2)(g_1^T g_2)^T = \mathbf{I}_{3\times 3}$ [3]. Hence, the last equation and the orthonomality of the frames give

$$\begin{aligned}
&(\mathbf{x}_2 \cdot \mathbf{N}_c)(\mathbf{x}_1 \cdot \mathbf{N}_c) + (\mathbf{x}_2 \cdot \mathbf{X}_2)(\mathbf{x}_1 \cdot \mathbf{X}_2) = -(\mathbf{x}_2 \cdot \mathbf{X}_1)(\mathbf{x}_1 \cdot \mathbf{X}_1), \\
&(\mathbf{x}_1 \cdot \mathbf{N}_c)(\mathbf{n} \cdot \mathbf{N}_c) + (\mathbf{x}_1 \cdot \mathbf{X}_2)(\mathbf{n} \cdot \mathbf{X}_2) = -(\mathbf{x}_1 \cdot \mathbf{X}_1)(\mathbf{n} \cdot \mathbf{X}_1), \\
&(\mathbf{x}_1 \cdot \mathbf{X}_2)^2 + (\mathbf{x}_1 \cdot \mathbf{N}_c)^2 = 1 - (\mathbf{x}_1 \cdot \mathbf{X}_1)^2.
\end{aligned} \tag{122}$$

These identities will be used to simplify the dynamics of the shape variables.

From the equation $\dot{\mathbf{X}}_1 = u\mathbf{N}_c + v\mathbf{X}_2$, we can derive that $u = \dot{\mathbf{X}}_1 \cdot \mathbf{N}_c$ and $v = \dot{\mathbf{X}}_1 \cdot \mathbf{X}_2$. Since $\mathbf{x}_1, \mathbf{x}_2$ and $\mathbf{n}$ form an orthogonal basis of $\mathbf{R}^3$, $\dot{\mathbf{X}}_1$ can be expressed by the linear combination of $\mathbf{x}_1, \mathbf{x}_2$ and $\mathbf{n}$ as $\dot{\mathbf{X}}_1 = a_1\mathbf{x}_1 + a_2\mathbf{x}_2 + a_3\mathbf{n}$, where a_1, a_2 and a_3 are scalars that depend on the dynamics of the formation center and the curve. Hence, u and v can be represented as

$$\begin{aligned}
u &= a_1(\mathbf{x}_1 \cdot \mathbf{N}_c) + a_2(\mathbf{x}_2 \cdot \mathbf{N}_c) + a_3(\mathbf{n} \cdot \mathbf{N}_c), \\
v &= a_1(\mathbf{x}_1 \cdot \mathbf{X}_2) + a_2(\mathbf{x}_2 \cdot \mathbf{X}_2) + a_3(\mathbf{n} \cdot \mathbf{X}_2).
\end{aligned} \tag{123}$$

The design of u and v becomes finding the parameters (a_1, a_2, a_3). With u and v as in (123), we can obtain that

$$\begin{aligned}\frac{d(\mathbf{x}_1 \cdot \mathbf{X}_1)}{dt} &= \dot{\mathbf{x}}_1 \cdot \mathbf{X}_1 + \mathbf{x}_1 \cdot \dot{\mathbf{X}}_1 \\ &= (\alpha\kappa_n \mathbf{n} + \alpha\kappa_g \mathbf{x}_2) \cdot \mathbf{X}_1 + \mathbf{x}_1 \cdot (u\mathbf{N}_c + v\mathbf{X}_2) \\ &= \alpha\kappa_n(\mathbf{n} \cdot \mathbf{X}_1) + \alpha\kappa_g(\mathbf{x}_2 \cdot \mathbf{X}_1) + a_1((\mathbf{x}_1 \cdot \mathbf{N}_c)^2 + (\mathbf{x}_1 \cdot \mathbf{X}_2)^2) \\ &+ a_2((\mathbf{x}_2 \cdot \mathbf{N}_c)(\mathbf{x}_1 \cdot \mathbf{N}_c) + (\mathbf{x}_2 \cdot \mathbf{X}_2)(\mathbf{x}_1 \cdot \mathbf{X}_2)) \\ &+ a_3((\mathbf{n} \cdot \mathbf{N}_c)(\mathbf{x}_1 \cdot \mathbf{N}_c) + (\mathbf{n} \cdot \mathbf{X}_2)(\mathbf{x}_1 \cdot \mathbf{X}_2)). \end{aligned} \tag{124}$$

Applying the identities in (122), $\frac{d(\mathbf{x}_1 \cdot \mathbf{X}_1)}{dt}$ becomes

$$\begin{aligned}\frac{d(\mathbf{x}_1 \cdot \mathbf{X}_1)}{dt} &= \alpha\kappa_n(\mathbf{n} \cdot \mathbf{X}_1) + \alpha\kappa_g(\mathbf{x}_2 \cdot \mathbf{X}_1) + a_1(1 - (\mathbf{x}_1 \cdot \mathbf{X}_1)^2) \\ &- a_2(\mathbf{x}_2 \cdot \mathbf{X}_1)(\mathbf{x}_1 \cdot \mathbf{X}_1) - a_3(\mathbf{x}_1 \cdot \mathbf{X}_1)(\mathbf{n} \cdot \mathbf{X}_1) \end{aligned} \tag{125}$$

which only depends on the shape variables. Applying similar calculations to $\frac{d(\mathbf{x}_2 \cdot \mathbf{X}_1)}{dt}$ and $\frac{d(\mathbf{n} \cdot \mathbf{X}_1)}{dt}$ gives us

$$\begin{aligned}\frac{d(\mathbf{x}_2 \cdot \mathbf{X}_1)}{dt} &= -\alpha\kappa_g(\mathbf{x}_1 \cdot \mathbf{X}_1) + \alpha\tau_g(\mathbf{n} \cdot \mathbf{X}_1) - a_1(\mathbf{x}_1 \cdot \mathbf{X}_1)(\mathbf{x}_2 \cdot \mathbf{X}_1) \\ &+ a_2(1 - (\mathbf{x}_2 \cdot \mathbf{X}_1)^2) - a_3(\mathbf{x}_2 \cdot \mathbf{X}_1)(\mathbf{n} \cdot \mathbf{X}_1), \end{aligned} \tag{126}$$

$$\begin{aligned}\frac{d(\mathbf{n} \cdot \mathbf{X}_1)}{dt} &= -\alpha\kappa_n(\mathbf{x}_1 \cdot \mathbf{X}_1) - \alpha\tau_g(\mathbf{x}_2 \cdot \mathbf{X}_1) - a_1(\mathbf{x}_1 \cdot \mathbf{X}_1)(\mathbf{n} \cdot \mathbf{X}_1) \\ &- a_2(\mathbf{x}_2 \cdot \mathbf{X}_1)(\mathbf{n} \cdot \mathbf{X}_1) + a_3(1 - (\mathbf{n} \cdot \mathbf{X}_1)^2). \end{aligned} \tag{127}$$

If the control laws u and v (e.g. a_1, a_2, and a_3) are designed as feedback laws using only the shape variables, we can then focus on analyzing the closed-loop dynamics of the shape variables described by the equations (120), (125)-(127) as a time-varying nonlinear system. We want to stabilize the equilibrium of the closed-loop dynamics that corresponds to the desired tracking behavior.

Suppose the scalar field has extrema $z_{min} < z_{max}$. Consider a Lyapunov candidate function that is analogous to the one chosen in [58]:

$$V(\mathbf{x}_1, \mathbf{X}_1, z(\mathbf{r}_c)) = -\ln(\mathbf{x}_1 \cdot \mathbf{X}_1) + h(z(\mathbf{r}_c)), \tag{128}$$

where $h(z(\mathbf{r}_c))$ satisfies the following assumptions:

B1 $h(z(\mathbf{r}_c))$ is continuously differentiable on (z_{min}, z_{max}) and $f(z(\mathbf{r}_c)) = \frac{dh}{dz(\mathbf{r}_c)}$ is a Lipschitz continuous function.

B2 $f(C) = 0$, and $f(z(\mathbf{r}_c)) \neq 0$ if $z(\mathbf{r}_c) \neq C$ where C is the desired level surface value.

B3 $\lim_{z(\mathbf{r}_c)\to z_{min}} h(z(\mathbf{r}_c)) = \infty$, $\lim_{z(\mathbf{r}_c)\to z_{max}} h(z(\mathbf{r}_c)) = \infty$, and there exists $\tilde{z}(\mathbf{r}_c)$ such that $h(\tilde{z}(\mathbf{r}_c) = 0$.

The term $\ln(\mathbf{x}_1 \cdot \mathbf{X}_1)$ in the Lyapunov function aims to align the moving direction of the formation center with the tangent direction of the curve on the level surface. We will prove that as long as we set $\mathbf{x}_1 \cdot \mathbf{X}_1 > 0$ initially, $0 < \mathbf{x}_1 \cdot \mathbf{X}_1 \leq 1$ all the time, which makes the term $-\ln(\mathbf{x}_1 \cdot \mathbf{X}_1) \geq 0$ for $0 < \mathbf{x}_1 \cdot \mathbf{X}_1 \leq 1$. The other term $h(z(\mathbf{r}_c))$ serves to control the agent to stay on a desired level surface. The derivative of the Lyapunov candidate function can be calculated as

$$\dot{V}(\mathbf{x}_1, \mathbf{X}_1, z(\mathbf{r}_c)) = -\frac{1}{\mathbf{x}_1 \cdot \mathbf{X}_1}\frac{d(\mathbf{x}_1 \cdot \mathbf{X}_1)}{dt} + f(z(\mathbf{r}_c))\dot{z}(\mathbf{r}_c) \tag{129}$$

If we choose $a_1 = \mu, a_2 = \frac{\alpha\kappa_g}{\mathbf{x}_1 \cdot \mathbf{X}_1}$, and $a_3 = \frac{\alpha\kappa_n}{\mathbf{x}_1 \cdot \mathbf{X}_1} - f(z(\mathbf{r}_c))\|\nabla z(\mathbf{r}_c)\|$, where μ is a positive constant and plug (a_1, a_2, a_3) into u and v in equation (123), we get

$$\begin{aligned} u &= \mu(\mathbf{x}_1 \cdot \mathbf{N}_c) + \frac{\alpha\kappa_g}{\mathbf{x}_1 \cdot \mathbf{X}_1}(\mathbf{x}_2 \cdot \mathbf{N}_c) + \frac{\alpha\kappa_n}{\mathbf{x}_1 \cdot \mathbf{X}_1}(\mathbf{n} \cdot \mathbf{N}_c) - f(z(\mathbf{r}_c))\|\nabla z(\mathbf{r}_c)\|(\mathbf{n} \cdot \mathbf{N}_c), \\ v &= \mu(\mathbf{x}_1 \cdot \mathbf{X}_2) + \frac{\alpha\kappa_g}{\mathbf{x}_1 \cdot \mathbf{X}_1}(\mathbf{x}_2 \cdot \mathbf{X}_2) + \frac{\alpha\kappa_n}{\mathbf{x}_1 \cdot \mathbf{X}_1}(\mathbf{n} \cdot \mathbf{X}_2) - f(z(\mathbf{r}_c))\|\nabla z(\mathbf{r}_c)\|(\mathbf{n} \cdot \mathbf{X}_2). \end{aligned} \tag{130}$$

If we plug a_1, a_2 and a_3 into (125) and then use (120), we can calculate that

$$\dot{V}(\mathbf{x}_1, \mathbf{X}_1, z(\mathbf{r}_c)) = -\frac{\mu}{\mathbf{x}_1 \cdot \mathbf{X}_1}(1 - (\mathbf{x}_1 \cdot \mathbf{X}_1)^2) \leq 0 \quad \text{for} \quad 0 < \mathbf{x}_1 \cdot \mathbf{X}_1 \leq 0. \tag{131}$$

We have the following proposition.

Proposition 7.1.3 *Consider a smooth scalar field and the formation center satisfying assumptions (A1-A3) and the following additional assumptions:*

A4 All level surfaces are compact.

A5 The field has isolated extrema at a finite set of points $\mathbf{R}_{sup}$*. Suppose the infimums are all equal to* z_{min} *and the supremums are all equal to* z_{max}*.*

Let the desired level value $C \in (z_{min}, z_{max})$ *be given. Then under the control laws u and v in equations* (130) *with assumptions (B1-B3), as* $t \to \infty$*, we have* $\mathbf{X}_1 \to \mathbf{x}_1$ *and* $z(\mathbf{r}_c) \to C$ *from all initial states satisfying* $\mathbf{x}_1 \cdot \mathbf{X}_1 > 0$ *and* $\mathbf{r}_c(t_0) \notin \mathbf{R}_{sup}$*.*

Proof Consider the Lyapunov candidate function $V(\mathbf{x}_1, \mathbf{X}_1, z(\mathbf{r}_c))$ in (128) and $\dot{V}(\mathbf{x}_1, \mathbf{X}_1, z(\mathbf{r}_c))$ in (131). Since $V(\mathbf{x}_1, \mathbf{X}_1, z(\mathbf{r}_c)) \to \infty$ as $\mathbf{x}_1 \cdot \mathbf{X}_1 \to 0$, $z(\mathbf{r}_c) \to z_{max}$, or $z(\mathbf{r}_c) \to z_{min}$, if the trajectory of the formation center initially satisfies $\mathbf{x}_1 \cdot \mathbf{X}_1 > 0$ and $z(\mathbf{r}_c) \in (z_{min}, z_{max})$, then the trajectory will stay in a compact sub-level set of the Lyapunov function $V(\mathbf{x}_1, \mathbf{X}_1, z(\mathbf{r}_c))$. Let E be the following set within the sub-level set where $\dot{V}(\mathbf{x}_1, \mathbf{X}_1, z(\mathbf{r}_c)) = 0$:

$$E = \{((\mathbf{x}_1 \cdot \mathbf{X}_1), (\mathbf{x}_2 \cdot \mathbf{X}_1), (\mathbf{n} \cdot \mathbf{X}_1), z(\mathbf{r}_c)) | (\mathbf{x}_1 \cdot \mathbf{X}_1) = 1, (\mathbf{x}_2 \cdot \mathbf{X}_1) = 0, (\mathbf{n} \cdot \mathbf{X}_1) = 0\}. \quad (132)$$

Because the closed-loop system is time-varying, we can not apply the classical LaSalle's Invariance Principle. Instead, we apply LaSalle-Yoshizawa Theorem (Theorem 8.4 in [63] and Theorem 4.7 in [110]) to claim that the trajectory will converge to the set E when $t \to \infty$. At points in E, the closed loop system becomes

$$\dot{z}(\mathbf{r}_c) = 0, \ \frac{d(\mathbf{x}_1 \cdot \mathbf{X}_1)}{dt} = 0, \ \frac{d(\mathbf{x}_2 \cdot \mathbf{X}_1)}{dt} = 0, \frac{d(\mathbf{n} \cdot \mathbf{X}_1)}{dt} = -f(z(\mathbf{r}_c))\|\nabla z(\mathbf{r}_c)\|. \quad (133)$$

In the current context, $\mathbf{n} \cdot \mathbf{X}_1 = 0$ on set E and we have shown that the dynamics will converge to set E, hence $\mathbf{n} \cdot \mathbf{X}_1 \to 0$. According to the Barbalat Lemma (Lemma 8.2 in [63]), if $f(z(\mathbf{r}_c))\|\nabla z(\mathbf{r}_c)\|$ is uniformly continuous and $\mathbf{n} \cdot \mathbf{X}_1 \to 0$, then $\frac{d(\mathbf{n} \cdot \mathbf{X}_1)}{dt} \to 0$ must hold. Since all level surfaces are compact and the field is smooth, it is straightforward to show that $\|\nabla z(\mathbf{r}_c)\|$ is uniformly continuous along smooth curves with bounded curvatures on the level surfaces. Therefore, we conclude that $f(z(\mathbf{r}_c))\|\nabla z(\mathbf{r}_c)\| = 0$, which implies that $f(z(\mathbf{r}_c)) = 0$ on E. This means the tangent vector $\mathbf{X}_1$ to the trajectory of the formation center will be aligned with the known tangent vector $\mathbf{x}_1$ along the curve and the field value at the formation center will converge to the desired constant value C. ■

7.2 Curvature Estimation Using Formations

For exploration problems, the field that is going to be explored is unknown. Assumptions (A2) and (A3) can only be satisfied based on estimates made by sensing agents. We consider a special case, which is to detect and track one of the lines of curvature on a desired level surface [113]. We design a formation formed by N agents so that by combining the measurements taken by all of the agents, the curvatures and the directions of a line of curvature can be estimated.

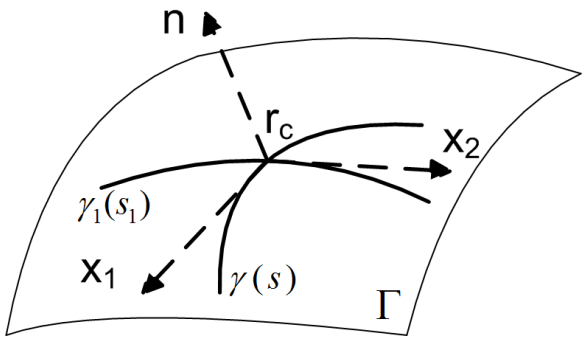

Figure 36: Two curves on a level surface Γ. $\mathbf{x}_1$ and $\mathbf{x}_2$ are the tangent vectors of $\gamma(s)$ and $\gamma_1(s_1)$. $\mathbf{n}$ is the normal vector to Γ at $\mathbf{r}_c$.

7.2.1 Principal Curvatures and Directions

We start with reviewing the definition of the lines of curvature briefly [81]. As shown in Figure 36, $\gamma(s)$ is a curve that lies on a smooth surface Γ, which can be described by the equations (121) (left). $\gamma_1(s_1)$ is another curve which also lies on Γ and intersects with $\gamma(s)$ at the point $\mathbf{r}_c$. As introduced in Section 3.1, the frame $(\mathbf{x}_1, \mathbf{x}_2, \mathbf{n})$ is used to describe the curve $\gamma(s)$. If the curve $\gamma_1(s_1)$ has $\mathbf{x}_2$ as its unit tangent vector at $\mathbf{r}_c$, then at the same point $\mathbf{r}_c$, the frame for $\gamma_1(s_1)$ is $(\mathbf{x}_2, -\mathbf{x}_1, \mathbf{n})$.

Suppose κ_n and κ_{1n} are the normal curvatures of $\gamma(s)$ and $\gamma_1(s_1)$ at the point $\mathbf{r}_c$, which are also known as the directional curvatures of the surface Γ at $\mathbf{r}_c$ in the directions $\mathbf{x}_1$ and $\mathbf{x}_2$. Among all possible directional curvatures of the surface Γ at $\mathbf{r}_c$, if κ_n takes the maximum value along $\mathbf{x}_1$, then κ_n is one of the principal curvatures and $\mathbf{x}_1$ is the corresponding

principal direction of Γ at $\mathbf{r}_c$. Since $\mathbf{x}_1$ and $\mathbf{x}_2$ are perpendicular to each other, then $\mathbf{x}_2$ is another principal direction and κ_{1n} is the corresponding principal curvature with the minimum value among all directional curvatures of Γ at $\mathbf{r}_c$. Note that the principal directions may not be unique for some smooth surfaces such as a sphere. If the tangent direction $\mathbf{x}_1$ of $\gamma(s)$ at each point is a principal direction at that point, then $\gamma(s)$ is a line of curvature of the surface Γ. Another important property of lines of curvature is that the geodesic torsion τ_g is zero. Examples of the lines of curvature are the meridians and circles of latitude of a surface of revolution, such as a cylinder.

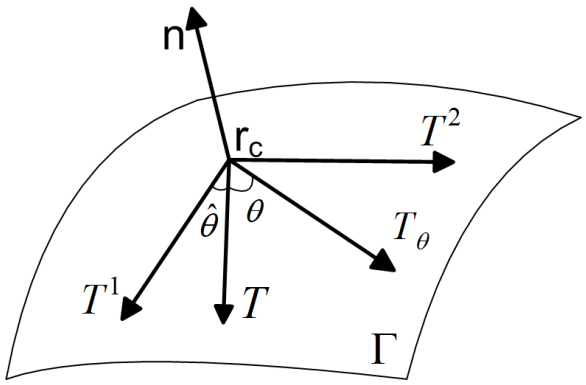

Figure 37: $\mathbf{T}^1$ and $\mathbf{T}^2$ are the two principal directions of the surface at $\mathbf{r}_c$. $\mathbf{T}$ and $\mathbf{T}_\theta$ are two arbitrarily chosen tangent vectors that form certain angles with $\mathbf{T}^1$. $\mathbf{n}$ is the normal vector to the surface at $\mathbf{r}_c$.

7.2.2 Taubin's Algorithm

To estimate the principal directions and the principal curvatures of a line of curvature on a level surface, we introduce the curvature estimation algorithm described by Taubin in [106]. As shown in Figure 37, let $\mathbf{T}^1$ and $\mathbf{T}^2$ denote the two principal directions of the surface Γ at the point $\mathbf{r}_c$ with corresponding principal curvatures κ^1 and κ^2 where $\kappa^1 > \kappa^2$. Choose an arbitrary unit tangent vector $\mathbf{T}$ to the surface at $\mathbf{r}_c$ that forms an angle $\hat{\theta}$ with $\mathbf{T}^1$ where $\hat{\theta}$ is unknown. For $-\pi < \theta < \pi$, define another unit tangent vector $\mathbf{T}_\theta$ to the surface at $\mathbf{r}_c$ that forms an angle θ with $\mathbf{T}$. Let $\kappa_p(\mathbf{T}_\theta)$ be the directional curvature associated with the

direction $\mathbf{T}_\theta$. Then a symmetric matrix $\mathbf{M}_p$ can be constructed by an integral formula as

$$\mathbf{M}_p = \frac{1}{2\pi}\int_{-\pi}^{+\pi} \kappa_p(\mathbf{T}_\theta)\mathbf{T}_\theta\mathbf{T}_\theta^T d\theta. \tag{134}$$

It can be shown that the principal directions and the unit normal vector are the eigenvectors of $\mathbf{M}_p$, which can be computed by diagonalizing $\mathbf{M}_p$ as

$$\mathbf{M}_p = \begin{pmatrix} \mathbf{T}^1 & \mathbf{T}^2 & \mathbf{n} \end{pmatrix} \begin{pmatrix} \lambda_1 & 0 & 0 \\ 0 & \lambda_2 & 0 \\ 0 & 0 & 0 \end{pmatrix} \begin{pmatrix} \mathbf{T}^1 & \mathbf{T}^2 & \mathbf{n} \end{pmatrix}^T, \tag{135}$$

where λ_1 and λ_2 are the two non-zero eigenvalues of $\mathbf{M}_p$. It is further shown in [106] that the principal curvatures can be calculated as $\kappa^1 = 3\lambda_1 - \lambda_2$ and $\kappa^2 = 3\lambda_2 - \lambda_1$.

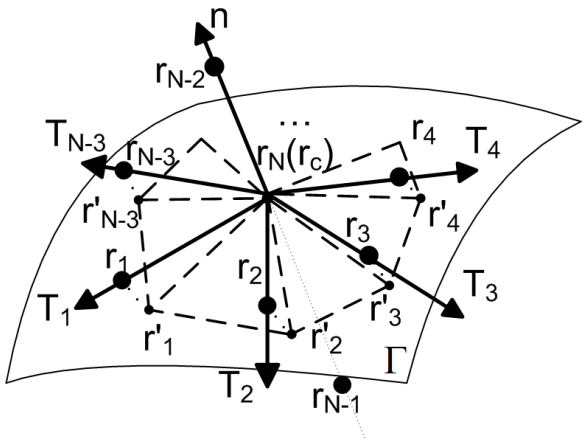

Figure 38: $\mathbf{r}_c$ is the center of the formation. $\mathbf{r}'_i, i = 1,\cdots,N-3$ are points on the level surface obtained by searching along either the negative or positive direction of the normal vector $\mathbf{n}$ starting from $\mathbf{r}_i, i = 1,\cdots,N-3$. $\mathbf{T}_i, i = 1,\cdots,N-3$ are projections of $\mathbf{r}'_i - \mathbf{r}_c$ to the tangent plane of Γ at $\mathbf{r}_c$.

We introduce a *discretized Taubin's algorithm* for estimating curvatures using formations. We arrange a formation formed by N agents as illustrated in Fig 38. We allocate $N-3$ agents on a plane in a circular fashion, among which we arbitrarily select one as $\mathbf{r}_1$ and label the others $\mathbf{r}_2,\cdots,\mathbf{r}_{N-3}$ counter-clockwisely. The remaining three agents are allocated along a line perpendicular to the plane with the Nth agent located at the center of the

formation formed by the $N-3$ agents and the agents $N-1$ and $N-2$ located symmetrically on the opposite sides of the plane. The position of the Nth agent $\mathbf{r}_N$ overlaps with the formation center $\mathbf{r}_c$. Note that this configuration requires $N > 4$. If $N = 5$, the first two agents only form a line instead of a plane. The formation can be stabilized with the cooperative control laws based on the Jacobi vectors. With the formation control law, the $N-3$ agents can be controlled to lie on the tangent plane of $\Gamma(\mathbf{r}_c)$ and agents $\mathbf{r}_{N-2}, \mathbf{r}_{N-1}$, and $\mathbf{r}_N$ can be controlled to be aligned with the direction of $\mathbf{n}$ by correctly selecting $\mathbf{q}_i^0, i = 1, \cdots, N-1$. We assume that all such formation control goals have been achieved.

The discretized Taubin's algorithm is as follows.

Algorithm 7.2.1 *Denote $\hat{\mathbf{n}}$ as the estimate of $\mathbf{n}$. Starting from $\mathbf{r}_1$,...,$\mathbf{r}_{N-3}$ and searching along the positive or negative directions of $\hat{\mathbf{n}}$ obtained at the previous time instant, we can find $\mathbf{r}'_1, ..., \mathbf{r}'_{N-3}$, which lie on the level surface $\Gamma(\mathbf{r}_c)$ and divide $\Gamma(\mathbf{r}_c)$ into $N-3$ triangular faces. We label the triangular faces as $f_i, i = 1, \cdots, N-3$. The unit vectors $\mathbf{T}_i, i = 1, ..., N-3$ represent the projections of the vectors $\mathbf{r}'_i - \mathbf{r}_c$ to the tangent plane of the surface $\Gamma(\mathbf{r}_c)$. With this setting, the steps to estimate the principal curvatures and principal directions with N agents are as follows:*

S.1 estimate the unit normal vector $\mathbf{n}$ at $\mathbf{r}_c$. Let $\mathbf{n}_{f_i}$ be the unit normal vector to the face f_i. For $i = 1, \cdots, N-4$, $\mathbf{n}_{f_i} = \frac{\mathbf{r}_i - \mathbf{r}_c}{\|\mathbf{r}_i - \mathbf{r}_c\|} \times \frac{\mathbf{r}_{i+1} - \mathbf{r}_c}{\|\mathbf{r}_{i+1} - \mathbf{r}_c\|}$. For the face f_{N-3}, $\mathbf{n}_{f_{N-3}} = \frac{\mathbf{r}_{N-3} - \mathbf{r}_c}{\|\mathbf{r}_{N-3} - \mathbf{r}_c\|} \times \frac{\mathbf{r}_1 - \mathbf{r}_c}{\|\mathbf{r}_1 - \mathbf{r}_c\|}$. Then $\mathbf{n}$ can be estimated by $\hat{\mathbf{n}} = \frac{\sum_{i=1}^{N-3} |f_k| \mathbf{n}_{f_i}}{\|\sum_{i=1}^{N-3} |f_i| \mathbf{n}_{f_i}\|}$, where $|f_i|$ are the areas of the faces f_i.

S.2 compute the projections $\mathbf{T}_i$. Since the tangent plane of $\Gamma(\mathbf{r}_c)$ at $\mathbf{r}_c$ is perpendicular to $\hat{\mathbf{n}}$, $\mathbf{T}_i$ can be estimated using $\mathbf{T}_i = \frac{(\mathbf{r}'_i - \mathbf{r}_c) - ((\mathbf{r}'_i - \mathbf{r}_c) \cdot \hat{\mathbf{n}}) \hat{\mathbf{n}}}{\|(\mathbf{r}'_i - \mathbf{r}_c) - ((\mathbf{r}'_i - \mathbf{r}_c) \cdot \hat{\mathbf{n}}) \hat{\mathbf{n}}\|}$.

S.3 approximate the matrix $\mathbf{M}_p$ in (134) as

$$\mathbf{M}_v = \sum_{i=1}^{N-3} \omega_i \kappa_i \mathbf{T}_i \mathbf{T}_i^T, \tag{136}$$

where ω_i are the weights that depend on $|f_i|$ and satisfy $\sum \omega_i = 1$. κ_i are the directional curvatures associated with $\mathbf{T}_i$ and are approximated by $\kappa_i = \frac{2\hat{\mathbf{n}}^T(\mathbf{r}_i' - \mathbf{r}_c)}{\|\mathbf{r}_i' - \mathbf{r}_c\|^2}$.

S.4 diagonalize $\mathbf{M}_v$ to obtain the estimated principal directions $\hat{\mathbf{T}}^1$ and $\hat{\mathbf{T}}^2$, as well as the estimated principal curvatures $\hat{\kappa}^1$ and $\hat{\kappa}^2$. Therefore, the frame of a line of curvature that is associated with the larger principal curvature can be estimated by $\hat{\mathbf{x}}_1 = \hat{\mathbf{T}}^1$, $\hat{\mathbf{x}}_2 = \hat{\mathbf{T}}^2$ and $\hat{\kappa}_n = \hat{\kappa}^1$.

Remark 7.2.2 *In the step (2), the projections $\mathbf{T}_i$ can be approximated by $\mathbf{r}_i - \mathbf{r}_c$ when the formation converges and the agents $1, \cdots, N-3$ stay in the tangent plane of the surface at the position $\mathbf{r}_c$.*

7.2.3 Geodesic Curvature Estimation

The geodesic curvature measures how a curve is curving in the surface M. The geodesic curvature κ_g, the normal curvature κ_n, and the Frenet-Serret curvature κ of a curve are related by

$$\kappa^2 = \kappa_n^2 + \kappa_g^2. \tag{137}$$

Algorithm 7.2.3 *Knowing the consecutive positions of the formation center $\mathbf{r}_{c,k-2}, \mathbf{r}_{c,k-1}, \mathbf{r}_{c,k}$ and $\mathbf{r}_{c,k+1}$,*

S.1 compute the unit tangent vector to the trajectory of $\gamma(s)$ at time instant k, which should be aligned with $\mathbf{x}_1$ that can be approximated by $\hat{\mathbf{T}}_k = \frac{\mathbf{r}_{c,k+1} - \mathbf{r}_{c,k-1}}{\|\mathbf{r}_{c,k+1} - \mathbf{r}_{c,k-1}\|}$.

S.2 compute the Frenet-Serret curvature. With the estimated tangent vectors $\hat{\mathbf{T}}_k$ and $\hat{\mathbf{T}}_{k-1}$, the Frenet-Serrat curvature κ can be estimated as $\hat{\kappa} = \frac{\arccos(\hat{\mathbf{T}}_k \cdot \hat{\mathbf{T}}_{k-1})}{\|\mathbf{r}_{c,k} - \mathbf{r}_{c,k-1}\|}$.

S.3 estimate the geodesic curvature. Since we have obtained $\hat{\kappa}_n$, the geodesic curvature κ_g can be calculated by $\hat{\kappa}_g = \sqrt{\hat{\kappa}^2 - \hat{\kappa}_n^2}$.

Until now, we have estimated all the information needed by assumptions (A2) and (A3) for tracking a line of curvature with $\hat{\tau}_g = 0$.

7.2.4 Constraints on Agent Quantity and Formation Design

The discretized Taubin's algorithm approximates the integral formula for $\mathbf{M}_p$ with a finite sum that computes $\mathbf{M}_v$. The number of agents and the formation will affect the estimation accuracy. Under this concern, we discuss the constraints on the agent quantity. For $\Gamma(\mathbf{r}_c)$, assume that there exist two unique principal directions $\mathbf{T}^1 \in T_c\Gamma$ and $\mathbf{T}^2 \in T_c\Gamma$ where $T_c\Gamma$ is the tangent plane of $\Gamma(\mathbf{r}_c)$ at $\mathbf{r}_c$. With the configuration shown in Figure 38, denote the angle from the vector $\mathbf{T}_1$ to $\mathbf{T}_i, i = 1, \cdots, N-3$ as $\theta_i \in (-\pi, \pi]$. Under this setting, $\theta_1 = 0$. Define a set $\Omega = \{\mathbf{T} | \mathbf{T} \in T_c\Gamma, \mathbf{T} \neq \mathbf{T}^1, \mathbf{T} \neq \mathbf{T}^2, \|\mathbf{T}\| = 1\}$. We assume that the tangent vector $\mathbf{T}_1$ is selected so that $\mathbf{T}_1 \in \Omega$. With this configuration, we propose the following proposition.

Proposition 7.2.4 *Consider a formation with N agents as illustrated in Figure 38 with the assumptions that* $\mathbf{T}_1 \in \Omega$ *and that the surface* $\Gamma(\mathbf{r}_c)$ *has two unique principal directions at* $\mathbf{r}_c$. *Then the following statements hold for the discretized Taubin's algorithm 7.2.1;*

1. *the algorithm provide nonsingular estimates of principal curvatures and principal directions if and only if*
$$\sum_{i=1}^{N-3} \omega_i \kappa_i \sin 2\theta_i \neq 0, \tag{138}$$
where θ_i *is the angle between* $\mathbf{T}_i$ *and* $\mathbf{T}_1$, *and* $\theta_1 = 0$.

2. $N \geq 6$ *must be satisfied to avoid singularity in the estimates. If the formation is symmetric, then* $N \neq 7$.

Proof for Statement (1). Choose $\mathbf{T}_1$ and the corresponding orthonormal vector $\mathbf{T}_1^{\perp}$ as the basis of the tangent plane, then $\mathbf{T}_i$ can be written as: $\mathbf{T}_i = \mathbf{T}_1 \cos\theta_i + \mathbf{T}_1^{\perp} \sin\theta_i,\ i = 1, 2, ..., N-3$. Substitute $\mathbf{T}_i$ into equation (136), we can obtain

$$\begin{aligned}\mathbf{M}_v = \sum_{i=1}^{N-3} \omega_i \kappa_i (&\mathbf{T}_1 \mathbf{T}_1^T \cos^2\theta_i + \mathbf{T}_1 (\mathbf{T}_1^{\perp})^T \cos\theta_i \sin\theta_i \\ &+ \mathbf{T}_1^{\perp} \mathbf{T}_1^T \cos\theta_i \sin\theta_i + \mathbf{T}_1^{\perp} (\mathbf{T}_1^{\perp})^T \sin^2\theta_i).\end{aligned} \tag{139}$$

Suppose $\hat{\mathbf{T}}^1$ is one of the estimated principal directions that can be expressed as $\hat{\mathbf{T}}^1 = \mathbf{T}_1 \cos\hat{\theta} + \mathbf{T}_1^{\perp} \sin\hat{\theta}$ where $\hat{\theta} \in (-\frac{\pi}{2}, \frac{\pi}{2}]$ is the angle between $\hat{\mathbf{T}}^1$ and $\mathbf{T}_1$. Then according to Taubin's algorithm, we can write down the following relationship:

$$\mathbf{M}_v \hat{\mathbf{T}}^1 = \hat{\lambda}_1 \hat{\mathbf{T}}^1 = \mathbf{T}_1 \hat{\lambda}_1 \cos\hat{\theta} + \mathbf{T}_1^{\perp} \hat{\lambda}_1 \sin\hat{\theta}, \tag{140}$$

where $\hat{\lambda}_1$ is the eigenvalue corresponding to $\hat{\mathbf{T}}^1$. On the other hand, $\mathbf{M}_v \hat{\mathbf{T}}^1 = \mathbf{M}_v(\mathbf{T}_1 \cos\hat{\theta} + \mathbf{T}_1^{\perp} \sin\hat{\theta})$. Substitute $\mathbf{M}_v$ in equation (139) into the above equation and use the relationship $\mathbf{T}_1^T \mathbf{T}_1 = (\mathbf{T}_1^{\perp})^T \mathbf{T}_1^{\perp} = 1$ and $(\mathbf{T}_1^{\perp})^T \mathbf{T}_1 = \mathbf{T}_1^T \mathbf{T}_1^{\perp} = 0$, $\mathbf{M}_v \hat{\mathbf{T}}^1$ can be calculated as

$$\begin{aligned} \mathbf{M}_v \hat{\mathbf{T}}^1 = {} & \mathbf{T}_1 [\sum_{i=1}^{N-3} \omega_i \kappa_i (\cos^2\theta_i \cos\hat{\theta} + \frac{1}{2} \sin 2\theta_i \sin\hat{\theta})] \\ & + \mathbf{T}_1^{\perp} [\sum_{i=1}^{N-3} \omega_i \kappa_i (\sin^2\theta_i \sin\hat{\theta} + \frac{1}{2} \sin 2\theta_i \cos\hat{\theta})]. \end{aligned} \tag{141}$$

Hence, comparing with equation (140), we have

$$\begin{aligned} \hat{\lambda}_1 &= \sum_{i=1}^{N-3} \omega_i \kappa_i \cos^2\theta_i + \frac{1}{2} \sum_{i=1}^{N-3} \omega_i \kappa_i \sin 2\theta_i \tan\hat{\theta} \\ &= \sum_{i=1}^{N-3} \omega_i \kappa_i \sin^2\theta_i + \frac{1}{2} \sum_{i=1}^{N-3} \omega_i \kappa_i \sin 2\theta_i \cot\hat{\theta}. \end{aligned} \tag{142}$$

Suppose $\sum_{i=1}^{N-2} \omega_i \kappa_i \sin 2\theta_i \neq 0$, then the above two equations give well defined solutions for $\hat{\theta}$ that satisfy:

$$\tan^2\hat{\theta} + \frac{2\sum_{i=1}^{N-3} \omega_i \kappa_i \cos 2\theta_i}{\sum_{i=1}^{N-3} \omega_i \kappa_i \sin 2\theta_i} \tan\hat{\theta} - 1 = 0. \tag{143}$$

For each solution $\hat{\theta}$, the estimated eigenvector $\hat{\mathbf{T}}^1$ has the form of $\mathbf{T}_1 \cos\hat{\theta} + \mathbf{T}_1^{\perp} \sin\hat{\theta}$. This finishes the proof for the sufficient condition. From the relationship $\mathbf{T}_1^T \mathbf{T}_1 = 1$ and $(\mathbf{T}_1^{\perp})^T \mathbf{T}_1 = 0$, we also have

$$\mathbf{M}_v \mathbf{T}_1 = \mathbf{T}_1 \sum_{i=1}^{N-3} \omega_i \kappa_i \cos^2\theta_i + \frac{1}{2} \mathbf{T}_1^{\perp} \sum_{i=1}^{N-3} \omega_i \kappa_i \sin 2\theta_i. \tag{144}$$

We now use proof by contradiction to show the necessity. Suppose the term $\sum_{i=1}^{N-3} \omega_i \kappa_i \sin 2\theta_i$ sums to zero, then $\mathbf{M}_v \mathbf{T}_1 = \mathbf{T}_1 \sum_{i=1}^{N-3} \omega_i \kappa_i \cos^2\theta_i = \lambda_1 \mathbf{T}_1$, where λ_1 is a scalar. From equation (144), we can see that $\mathbf{T}_1$ is one of the eigenvectors of $\mathbf{M}_v$ and λ_1 is the corresponding

eigenvalue. According to Taubin's algorithm, this results in $\mathbf{T}_1$ being one of the principal directions. However, $\mathbf{T}_1$ is not aligned with any principal directions since $\mathbf{T}_1 \in \Omega$. This contradiction means that Taubin's algorithm can produce estimates of principal directions only if $\sum_{i=1}^{N-3} \omega_i \kappa_i \sin 2\theta_i \neq 0$.

Proof for Statement (2). Consider a symmetric formation where the angles between $\mathbf{T}_1$ and $\mathbf{T}_i, i = 1, \cdots, N-3$ can be expressed as $\theta_i = \frac{2\pi}{N-3}(i-1)$. When $N = 5$, according to our formation design, agents 1 and 2 form a line and the agent 5 is located at the center of the line, which always gives us a symmetric formation. From the relationship $\sum_{i=1}^{N-3} \omega_i \kappa_i \sin 2\theta_i = \sum_{i=1}^{N-3} \omega_i \kappa_i \sin(\frac{4\pi}{N-3}(i-1))$, we can obtain that for $N = 5$, $\omega_1 \kappa_1 \sin 0 + \omega_2 \kappa_2 \sin 2\pi = 0$. In addition, when $N = 7$, we have $\omega_1 \kappa_1 \sin 0 + \omega_2 \kappa_2 \sin \pi + \omega_3 \kappa_3 \sin 2\pi + \omega_4 \kappa_4 \sin 3\pi = 0$. The summations will be zero regardless of the labeling of the sensor platforms and the values of $\omega_i \kappa_i$, which violates the condition (138). This fact indicates that we can not deploy five or seven agents arranged in the symmetric formation to implement Taubin's algorithm.

When $N = 6$, if the assumptions of the proposition are satisfied, the estimated $\hat{\theta}$ can be solved from

$$\tan^2 \hat{\theta} + \frac{2(\omega_1 \kappa_1 + \omega_2 \kappa_2 \cos(2\theta_2) + \omega_3 \kappa_3 \cos(2\theta_3))}{\omega_2 \kappa_2 \sin(2\theta_2) + \omega_3 \kappa_3 \sin(2\theta_3)} \tan \hat{\theta} - 1 = 0. \tag{145}$$

Therefore, the minimum number of agents that can be utilized without producing singular estimates is six. ■

Notice that for the symmetric formation, because of the relationship: $\sum_{i=1}^{N-3} \sin \frac{4\pi}{N-3}(i-1) = 0, \forall N \geq 6$, the condition (138) in Proposition 7.2.4 is violated if the term $\omega_i \kappa_i$ are identical. Since we assume that for the smooth surface $\Gamma(\mathbf{r}_c)$, there exist two unique principal directions $\mathbf{T}^1$ and $\mathbf{T}^2$, we can select ω_i so that $\omega_i \kappa_i$ are not identical. For example, $\omega_i = 1, i = 1, \cdots, N-3$.

Remark 7.2.5 *Proposition 7.2.4 suggests that when we design a formation using N agents*

as illustrated in Figure 38 to implement the discretized Taubin's algorithm to provide estimates of the principal directions and principal curvatures on a level surface, more than six agents should be used. In addition, we can not use seven agents in a symmetric formation to implement Taubin's algorithm.

7.3 Cooperative Hessian Estimation

As seen in the state equation (9) and the measurement equation (10) in Chapter IV, the Hessian matrix of the field at the formation center needs to be estimated in order to enable a cooperative filter. As shown in Figure 36, $\gamma(s)$ and $\gamma_1(s_1)$ are two intersecting curves on a level surface Γ. We can write down the dynamic equations for $\gamma(s)$ and $\gamma_1(s_1)$ side by side,

$$\begin{aligned} \mathbf{x}_1' &= \kappa_n \mathbf{n} + \kappa_g \mathbf{x}_2 & \mathbf{x}_2' &= \kappa_{1n}\mathbf{n} - \kappa_{1g}\mathbf{x}_1 \\ \mathbf{x}_2' &= -\kappa_g \mathbf{x}_1 + \tau_g \mathbf{n} & \mathbf{x}_1' &= \kappa_{1g}\mathbf{x}_2 - \tau_{1g}\mathbf{n}, \\ \mathbf{n}' &= -\kappa_n \mathbf{x}_1 - \tau_g \mathbf{x}_2 & \mathbf{n}' &= -\kappa_{1n}\mathbf{x}_2 + \tau_{1g}\mathbf{x}_1. \end{aligned} \tag{146}$$

where $'$ represents the derivative with respect to the arc-length parameter s or s_1 and κ_{1n}, κ_{1g} and τ_{1g} are the normal curvature, the geodesic curvature and geodesic torsion of $\alpha_1(s_1)$, respectively.

From the fact that the gradients of the surface are always perpendicular to the tangent plane, we have the following relationships:

$$\begin{aligned} \nabla z(\mathbf{r}_c) \cdot \mathbf{x}_1 &= 0, \\ \nabla z(\mathbf{r}_c) \cdot \mathbf{x}_2 &= 0, \\ \nabla z(\mathbf{r}_c) \cdot \mathbf{n} &= \|\nabla z(\mathbf{r}_c)\|. \end{aligned} \tag{147}$$

If we take derivatives on both sides of $\nabla z(\mathbf{r}_c) \cdot \mathbf{x}_1 = 0$ with respect to s and use the relationship

$$\frac{d}{ds}\nabla z(\mathbf{r}_c) = \mathbf{x}_1^T \nabla^2 z(\mathbf{r}_c), \tag{148}$$

we obtain

$$\mathbf{x}_1^T \nabla^2 z(\mathbf{r}_c)\mathbf{x}_1 + \|\nabla z(\mathbf{r}_c)\|\mathbf{n} \cdot (\kappa_n \mathbf{n} + \kappa_g \mathbf{x}_2) = 0. \tag{149}$$

In the frame described in equation (146) (left) for the curve $\gamma(s)$, since $\mathbf{x}_1$ is a unit vector along the $\mathbf{x}_1$ axis, and $\mathbf{x}_1, \mathbf{x}_2$ are perpendicular to each other, from the equation (149), we have

$$\partial_{x_1 x_1} z(\mathbf{r}_c) = -\|\nabla z(\mathbf{r}_c)\| \kappa_n. \tag{150}$$

Therefore, the estimate of the first element of Hessian matrix is given by

$$H_{c(11)} = \partial_{x_1 x_1} z(\mathbf{r}_c) = -\|\nabla z(\mathbf{r}_c)\| \kappa_n. \tag{151}$$

Also, if we take derivatives on both sides of $\nabla z(\mathbf{r}_c) \cdot \mathbf{x}_2 = 0$ and $\nabla z(\mathbf{r}_c) \cdot \mathbf{n} = \|\nabla z(\mathbf{r}_c)\|$, similar calculations can be conducted, which give us the estimates of $H_{c(12)}$ and $H_{c(13)}$:

$$\begin{aligned} H_{c(12)} &= -\|\nabla z(\mathbf{r}_c)\| \tau_g, \\ H_{c(13)} &= \frac{d}{ds} \|\nabla z(\mathbf{r}_c)\|. \end{aligned} \tag{152}$$

Use the similar steps to analyze the curve $\alpha_1(s_1)$, we estimate $H_{c(22)}$, $H_{c(21)}$ and $H_{c(23)}$ as

$$\begin{aligned} H_{c(22)} &= -\|\nabla z(\mathbf{r}_c)\| \kappa_{1n}, \\ H_{c(21)} &= -\|\nabla z(\mathbf{r}_c)\| \tau_{1g}, \\ H_{c(23)} &= \frac{d}{ds_1} \|\nabla z(\mathbf{r}_c)\|. \end{aligned} \tag{153}$$

Since the field is considered to be smooth, the Hessian matrix is symmetric. Therefore, $H_{c(13)} = H_{c(31)} = \frac{d}{ds}\|\nabla z(\mathbf{r}_c)\|$ and $H_{c(23)} = H_{c(32)} = \frac{d}{ds_1}\|\nabla z(\mathbf{r}_c)\|$. In addition, from the relationship $H_{c(12)} = H_{c(21)}$, we have $\tau_g = \tau_{1g}$. Note again that if $\gamma(s)$ and $\gamma_1(s_1)$ are lines of curvature on a surface, the geodesic torsion $\tau_g = \tau_{1g} = 0$, which means $H_{c(12)} = H_{c(21)} = 0$. Note that $\kappa_n = \hat{\kappa}^1$ and $\kappa_{1n} = \hat{\kappa}^2$. With the formation designed in the previous section, the last element of the Hessian $H_{c(33)}$ can be approximated by

$$H_{c,(33)} = \frac{\frac{z_{N-1} - z_N}{\|\mathbf{r}_{N-1} - \mathbf{r}_N\|} - \frac{z_N - z_{N-2}}{\|\mathbf{r}_N - \mathbf{r}_{N-2}\|}}{\|\mathbf{r}_{N-1} - \mathbf{r}_{N-2}\|}. \tag{154}$$

7.4 Simulation Results

We demonstrate the cooperative exploration algorithm utilizing six agents. We assume that the measurements taken and the positions are shared among all the agents. At each

time instant, the agents take new measurements of the field, then the cooperative Kalman filter, the curvature estimation and the Hessian estimation are computed to find the steering control forces u and v as described in Section 7.1. Meanwhile, the formation shape control forces are also calculated.

In the simulation illustrated in Figure 39 and Figure 40, three of the six agents (two are plotted as triangles and one is plotted as a circle) lie in the tangent plane of a level surface passing through the formation center and form a symmetric triangular formation. The distance between each pair of the three agents in the plane is 0.6. The other three agents (rectangular markers) are lying in a line perpendicular to the tangent plane with the sixth agent sitting in the formation center. To satisfy the constraints discussed in Section 7.2.4, we control the orientation of the formation so that none of the vectors connecting an agent to the formation center aligns with any principal directions of the level surface. This is accomplished by selecting the Jacobi vectors $\mathbf{q}_i$ and $\mathbf{q}_i^0, i = 1, \cdots, N-1$ so that the vector connecting the agent one (the circle) and the formation center forms an angle $\frac{\pi}{8}$ with the estimated principal direction associated with the larger principal curvature.

The goal is to detect and track one of the lines of curvature on a desired level surface in an unknown 3D scalar field with 5% i.i.d. Gaussian noise. The unknown fields are composed of cylindrical level surfaces and ellipsoidal level surfaces. We only plot one of the level surfaces on each figure with the level value $C = 20$ and set it as the desired level value that the formation center should converge to. The lines of curvature with the larger principal curvatures for both level surfaces are shown by the circles on the level surfaces in the figure. The thick lines are the trajectories of the formation center. The initial positions of the formation center are at the position $(4.3, 0, 0)$, which are -0.2 off the desired level surfaces. The six agents converge to a constant formation while the formation center moves to the desired level surfaces, and track one of the lines of curvature.

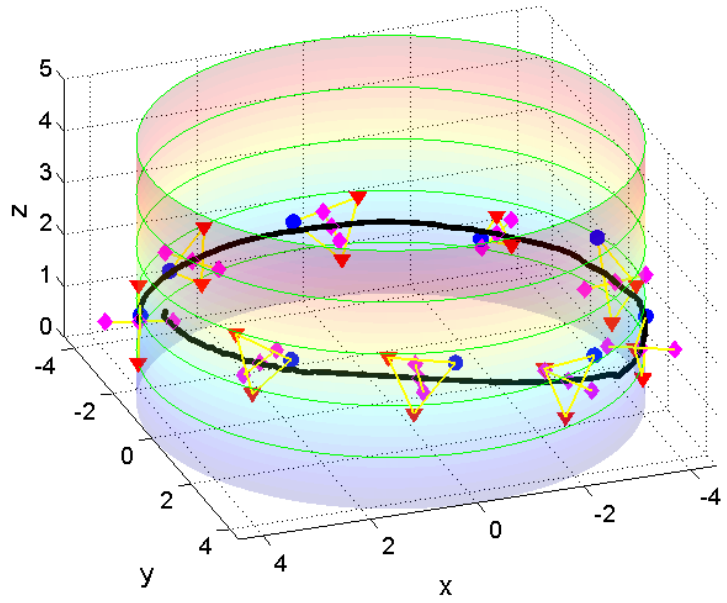

Figure 39: Detecting and tracking a line of curvature on a cylinder by six agents. The desired level value C = 20.

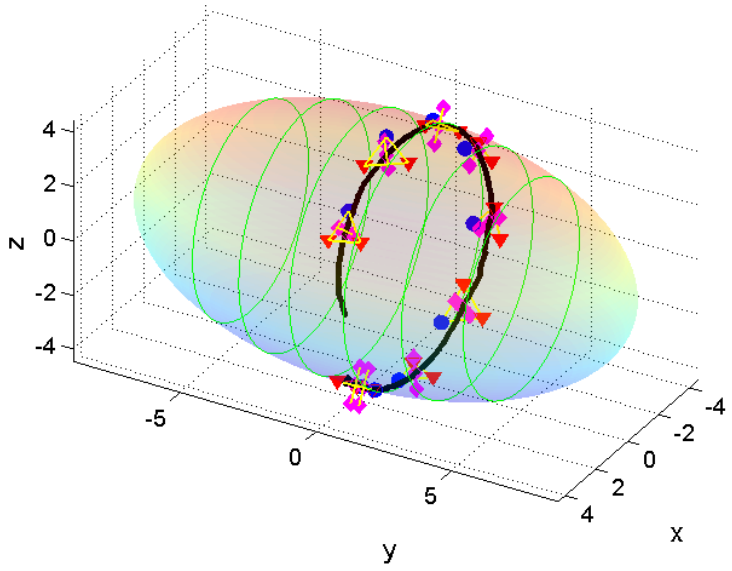

Figure 40: Detecting and tracking a line of curvature on a ellipsoid by six agents. The desired level value C = 20.

Denote the angle between $\mathbf{T}^1$ and the inertial frame as β and the angle between $\hat{\mathbf{T}}_1$ and

the inertial frame as $\hat{\beta}$. To compare the estimated principal directions with the actual principal directions, we plot $\beta - \hat{\beta}$ in Figure 41. We can tell that with three agents estimating the principal directions, the error is within ± 20 degree.

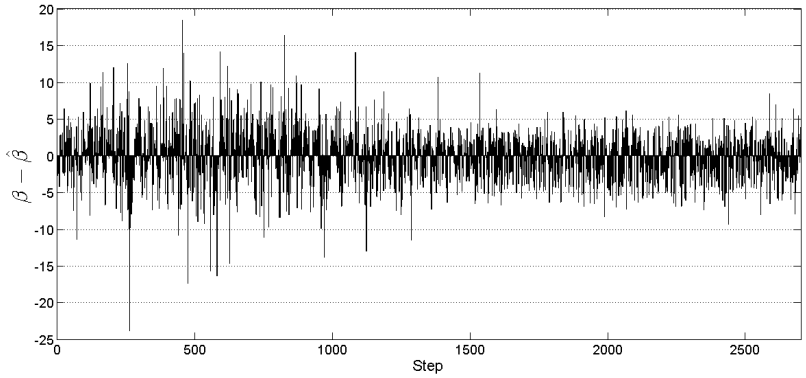

Figure 41: Estimation error between $\hat{\beta}$ and β.

7.5 Conclusion

We develop steering control laws that are able to control a formation formed by N agents to move to a desired level surface and track a class of curves in a 3D scalar field. We have shown that a discretized Taubin's algorithm, the Hessian estimation and the cooperative Kalman filter can be combined to allow a group of agents to perform cooperative exploration of 3D level surfaces by tracking lines of curvature.

CHAPTER VIII

CONCLUDING REMARKS AND FUTURE RESEARCH

8.1 Conclusion

The main contributions of this thesis include platform independent mathematical models for the coupled motion-sensing dynamics of MSN and biologically-inspired provably convergent cooperative control and filtering algorithms for MSN exploring unknown scalar fields in both 2D and 3D spaces. We introduce a novel model of behaviors of mobile agents that leads to fundamental theoretical results for evaluating the feasibility and difficulty of exploring a field using MSN. Under this framework, we propose and implement source-seeking algorithms using MSN inspired by behaviors of fish schools. To balance the cost and performance in exploration tasks, a novel switching strategy, which allows the mobile sensing agents to switch between individual and cooperative exploration, is developed. Compared to fixed strategies, the switching strategy brings in more flexibility in engineering design. To reveal the geometry of 3D spaces, we introduce a control and sensing co-design for MSN to detect and track a line of curvature on a desired level surface. The detailed contribution of this thesis is summarized as follows.

- *Coherent steps of mobile sensing agents in explorable fields.* We develop fundamental theoretical results that describe exploration behaviors of mobile sensing agents in a noisy scalar field by introducing notions of coherent and incoherent steps, and propose criteria for evaluating the feasibility and difficulty of exploring the field by establishing the notion of local explorability, which analyzes the tendency that such field would induce false-walks for a sensing agent. We are able to connect the variance of Gaussian noise with the success rate for coherent steps of mobile sensing agents, and explain why gradient following and level curve tracking are desirable

strategies in exploration. We also theoretically justify the minimum number of agents required to achieve a certain level of success rate.

- *Bio-inspired source-seeking with no explicit gradient estimation.* Inspired by behaviors of fish groups seeking darker (shaded) regions in environments with complex lighting variations, we develop distributed source-seeking algorithms for a group of sensing agents with no explicit gradient estimation. We choose a baseline for agent groups and decompose the velocity of each agent into two parts. The first part, which is perpendicular to the baseline, is chosen to be proportional to the measurements, agreeing with observations from fish groups. The second part, which is parallel to the baseline, can be designed to control the relative distances among the agents. This decomposition is leveraged to implement formation-maintaining strategies and source seeking behaviors for the entire group. We prove that the moving direction of a group will converge towards the gradient direction while the formation is maintained. We also prove that the system is Input-to-State Stable (ISS).

- *A switching strategy in cooperative exploration.* Biological inspirations lead us to develop a switching strategy for a group of robotic sensing agents searching for a local minimum of an unknown noisy scalar field. Starting with individual exploration, the agents switch to cooperative exploration only when they are not able to converge to a local minimum at a satisfying rate. The switching back to individual exploration is triggered by a significantly improved signal-to-noise ratio (SNR) during cooperative exploration. In addition to theoretical and simulation studies, we develop a multi-agent test-bed and implement the switching strategy in a lab environment. We have observed consistency of theoretical predictions and experimental results, which are robust to unknown noises and communication delays. The switching strategy strikes a balance between exploration complexity and exploration performance in terms of

convergence rate and exploration cost, which may enable more flexibility in autonomy compared to fixed strategies. Other than source seeking problem, the switching strategy can also be applied to other exploration tasks for multi-agent systems such as target tracking as long as a cost function related to convergence rate is defined.

- *Cooperative exploration in 3D spaces.* We develop strategies for a group of mobile sensing agents to cooperatively explore level surfaces of an unknown 3D scalar field. The formation formed by the agents is controlled to track curves on a level surface in the field under steering control laws. We prove that the formation center can move to a desired level surface and can follow a curve with known frame and curvatures. In particular, we present results on tracking lines of curvature on a desired level surface, revealing the 3D geometry of the scalar field. Taubin's algorithm is modified and applied to detect and estimate principal curvatures and principal directions for lines of curvature. We prove the sufficient and necessary conditions that ensure reliable estimates using Taubin's algorithm. We also theoretically justify the minimum number of agents that can be utilized to accomplish the exploration tasks.

8.2 Future Research

One unique feature for MSN is the tight coupling between the motion and sensing dynamics, which does not apply to fixed wireless sensor networks. The motion dynamics will affect the performance of the sensing (filtering) algorithms, and the control for the motion dynamics will use the results from the sensing algorithms. In the future research, we will establish a general motion and sensing co-design procedure for MSN operating in environments with large motion disturbances and information uncertainties. The design of the motion patterns, control strategies, and sensing algorithms draws inspirations from behaviors of biological systems. To place the co-design procedure on firm theoretical ground, we will formulate and justify a set of general design principles. One example is the balance between energy and information in MSN, which has been developed in our work [122].

Under the co-design procedure and principle, a number of possible future research directions can be developed. For example, the analysis of exploring non-smooth fields instead of smooth fields, the control and sensing co-design for mobile sensing agents seeking for a global extremum instead of local extremum, and controlling asynchronous multi-agent systems. The detailed future research directions of this thesis is summarized as follows.

We proposed a discrete-time model for the sensing agents moving in a field. In the current model, the mobile sensing agents move discretely, and we assume that each agent takes one measurement at each time step. One future research direction is to extend the results to modeling agents that move and take measurements continuously in a field. Another future research direction is to relax the Gaussian noise assumption we made in the analysis of the behaviors of the agents in the field and develop theoretical results that applies to more general contexts. In addition, we will connect and apply the proposed explorability analysis to real-world applications so that the difficulty and feasibility of exploring a field can be evaluated.

In the source-seeking problem, we introduced a gradient-free design for multiple sensing agents moving along gradient directions in a field to locate a source. Under the co-design framework, we first propose to generalize the bio-inspired strategy to the exploration of more complex fields that contains nontrivial sets of singularities, as well as three-dimensional scalar fields. The individual agents in a group will still be controlled to follow the speed-up slow-down fashion to locate a source while maintaining relative distances to other agents in a group. However, the theoretical analysis such as the convergence proof and the ISS proof become more involved. The next future research direction is to explore time-varying fields, in which the temporal gradient of the fields needs to be incorporated. The temporal gradient is often connected with the spatial gradient through partial differential equations (PDEs). In addition, we will investigate the source-seeking problem when multiple sources are presented in a field, or develop strategies for the agents to seek for a global extremum in a field instead of local extremum.

The switching strategy allows the switching between individual exploration and cooperative exploration, which introduces flexibility in engineering design. However, the current design assumes that all the agents in a group are homogenous and have the same communication rate. In addition, a central controller is used to collect information from all the agents and synchronize movements of all the agents. We will investigate the problem of distributed control of agents that might have different communication rate. In addition, we will develop control and sensing strategies when the communication range of the agents are limited. Following similar ideas in the source-seeking problem, the implementation of the switching strategy in the source-seeking problem when a moving source is presented or multiple sources are presented is also a possible future research direction.

Finally, we proposed a control and sensing co-design for mobile sensing agents to detect and track a line of curvature in 3D space. The field under exploration is assumed to be smooth. In the future research, we will extend the results in smooth 3D fields to non-smooth 3D fields. We will also investigate the detection and tracking other curves in level surfaces (i.e. geodesic curves) other than lines of curvature. To verify designed control strategies, we will set up 3D multi-agent systems and conduct experiments other than simulations using UAVs.

CHAPTER IX

PUBLICATIONS

Journal Articles

[1] Wencen Wu and Fumin Zhang, "Cooperative Exploration of Level Surfaces of Three Dimensional Scalar Fields," *Automatica*, the IFAC Journal, 47(9), 2044-2051, 2011.

[2] Wencen Wu and Fumin Zhang, "Robust Cooperative Exploration with a Switching Strategy," *IEEE Transactions on Robotics*, 28(4), 828-839, 2012.

[3] Wencen Wu and Fumin Zhang, "A Switching Strategy for Target Tracking by Mobile Sensing Agents," *Journal of Communications*, 8(1), 47-54, 2013.

Book Chapters

[4] Dongsik Chang, Xiaolin Liang, Wencen Wu, Catherine R. Edwards, and Fumin Zhang, "Real-time Modeling of Ocean Current for Navigating Underwater Glider Sensing Networks," ser. *Studies in Computational Intelligence*, Springer, 2012, ch. *Cooperative Robots and Sensor Networks*. accepted on Dec. 13, 2012.

Peer Reviewed Conference Papers

[5] Wencen Wu and Fumin Zhang, "Curvature Based Cooperative Exploration of Three Dimensional Scalar Fields," in *Proc. 2010 American Control Conference (ACC2010)*, pp. 2909-2915, 2010.

[6] Wencen Wu and Fumin Zhang, "A Switching Strategy for Robust Cooperative Exploration," in *Proc. 49th IEEE Conference on Decision and Control (CDC2010)*, pp. 5493-5498, 2010.

[7] Wencen Wu and Fumin Zhang, "Experimental Validation of Source Seeking with a Switching Strategy," in *Proc. 2011 IEEE Conference on Robotics and Automation (ICRA2011)*, pp. 3835-3840, 2011.

[8] Wencen Wu and Fumin Zhang, "Explorability of Noisy Scalar Fields," in *Proc. 50th IEEE Conference on Decision and Control (CDC2011)*, pp. 6439-6444, 2011.

[9] Xiaolin Liang, Wencen Wu, Dongsik Chang, and Fumin Zhang, "Real-time Modeling of Tidal Current for Navigating Underwater Glider Sensing Networks," *Procedia Computer Science*, 10: 1121-1126, 2012.

[10] Wencen Wu, Iain D. Couzin, and Fumin Zhang, "Bio-inspired Source Seeking with no Explicit Gradient Estimation," in *Proc. 3rd IFAC Workshop on Distributed Estimation and Control in Networked System (NecSys'12)*, 240-245, 2012. **(Best Student Paper Award Finalist)**

[11] Wencen Wu and Fumin Zhang, "Coherent Steps of Mobile Sensing Agents in Gaussian Scalar Fields," in *Proc. 51th IEEE Conference on Decision and Control (CDC2012)*, pp. 2814-2819, 2012.

[12] Dongsik Chang, Wencen Wu, Donald R. Webster, Marc J. Weissburg, and Fumin Zhang, "A Bio-inspired Pluming Tracking Algorithm for Mobile Sensing Swarms in Turbulent Flow," *IEEE Conference on Robotics and Automation (ICRA2013)*, accepted on Jan. 7, 2013.

[13] Wencen Wu, Fumin Zhang, and Yorai Wardi, "Energy-Information Tradeoffs in Motion and Sensing for Target Localization," *European Control Conference (ECC2013)*, accepted on Feb. 27, 2013.

REFERENCES

[1] ABRAMOWITZ, M. and STEGUN, I. A., eds., *Handbook of mathematical ffunction with formulas, graphs, and mathematical tables*, ch. 7, p. 297. Dover, 1965.

[2] AGMON, N., KRAUS, S., and KAMINKA, G. A., "Multi-robot perimeter patrol in adversarial settings," in *Proc. 2008 IEEE Int. Conf. Robotics and Automation*, pp. 2339–2345, 2008.

[3] ALEXANDER, K., *An introduction to Lie groups and Lie algebras*. Cambridge University Press, 2008.

[4] AZUMA, S., SAKAR, M., and PAPPAS, G., "Stochastic source seeking by mobile robots," *IEEE Transactions on Automatic Control*, no. 99, 2012. Early Access.

[5] BACHMAYER, R. and LEONARD, N. E., "Vehicle networks for gradient descent in a sampled environment," in *Proc. of 41st IEEE Conf. on Decision and Control*, pp. 113–117, IEEE, 2002.

[6] BELLINGHAM, J. G. and RAJAN, K., "Robotics in remote and hostile environments," *Science*, vol. 318, no. 5853, pp. 1098–1102, 2007.

[7] BERDAHL, A., TORNEY, C., IOANNOU, C., FARIA, J., and COUZIN, I., "Collective sensing of complex environments by animal groups," *In prep.*, 2012.

[8] BERMAN, S., HALASZ, A., KUMAR, V., and PRATT, S., "Bio-inspired group behaviors for the deployment of a swarm of robots to multiple destinations," in *Proc. 2007 IEEE International Conferencen on Robotics and Automation*, pp. 2318–2323, 2007.

[9] BERMAN, S., LINDSEY, Q., SAKAR, M. S., KUMAR, V., and PRATT, S. C., "Experimental study and modeling of group retrieval in ants as an approach to collective transport in swarm robotic systems," *Proceedings of the IEEE*, vol. 99, no. 9, pp. 1470–1481, 2011.

[10] BERTOZZI, A. L., KEMP, M., and MARTHALER, D., "Determining environmental boundaries: Asynchronous communication and physical scales," in *Cooperative Control, A Post-Workshop Volume: 2003 Block Island Workshop on Cooperative Control* (KUMAR, V., LEONARD, N., and MORSE, A., eds.), pp. 35–42, Springer, 2005.

[11] BISHOP, A. N., FIDAN, B., ANDERSON, B. D., DO?AN?AY, K., and PATHIRANA, P. N., "Optimality analysis of sensor-target localization geometries," *Automatica*, vol. 46, no. 3, pp. 479–492, 2010.

[12] BISHOP, R. L., "There is more than one way to frame a curve," *The American Mathematical Monthly*, vol. 82, no. 3, pp. 246–251, 1975.

[13] BIYIK, E. and ARCAK., M., "Gradient climbing in formation via extremum seeking and passivity-based coordination rules," in *Proc. of 46th IEEE Conf. on Decision and Control*, pp. 3133–3138, 2007.

[14] BOLZERN, P., COLANERI, P., and NICOLAO, G. D., "Transient and asymptotic analysis of discrete-time H_∞ filters," *European Journal of Control*, vol. 3, pp. 317–324, 1997.

[15] BOLZERN, P. and MARONI, M., "New conditions for the convergence of H_∞ filters and predictors," *IEEE Transactions on Automatic Control*, vol. 44, pp. 1564–1568, 1999.

[16] BRAITENBERG, V., *Vehicles: Experiments in Synthetic Psychology*. The MIT Press, 1984.

[17] BURGARD, W., MOORS, M., STACHNISS, C., and SCHNEIDER, F. E., "Coordinated multi-robot exploration," *IEEE Transactions on Robotics*, vol. 21, no. 3, pp. 376–386, 2005.

[18] BURIAN, E., YOERGER, D., BRADLEY, A., and SINGH, H., "Gradient search with autonomous underwater vehicles using scalar measurements," in *Proceedings of the 1996 Symposium on Autonomous Underwater Vehicle Technology*, pp. 86 – 98, 1996.

[19] CAO, Y., FUKUNAGA, A., and KHANG, A., "Cooperative mobile robotics: Antecedents and directions," *Autonomous Robots*, vol. 4, no. 1, pp. 7–27, 1997.

[20] CAO, Y. and FIERRO, R., "Dynamic boundary tracking using dynamic sensor nets," in *Proc. 45th IEEE Conf. Decision and Control*, pp. 703–708, 2006.

[21] CASBEERA, D. W., KINGSTONA, D. B., BEARDA, R. W., and MCLAINA, T. W., "Cooperative forest fire surveillance using a team of small unmanned air vehicles," *International Journal of Systems Science*, vol. 37, no. 6, pp. 351–360, 2006.

[22] CHOI, J. and HOROWITZ, R., "Learning coverage control of mobile sensing agents in one-dimensional stochastic environments," *IEEE Transactions on Automatic Control*, vol. 55, no. 3, pp. 804–809, 2010.

[23] CHOI, J., OHC, S., and HOROWITZ, R., "Distributed learning and cooperative control for multi-agent systems," *Automatica*, vol. 45, no. 12, pp. 2802–2814, 2009.

[24] CLARK, C. W., "The evolutionary advantages of group foraging," *Theoretical Population Biology*, vol. 30, no. 1, pp. 45–75, 1986.

[25] CLARK, J. and FIERRO, R., "Cooperative hybrid control of robotic sensors for perimeter detection and tracking," in *Proc. of 2005 American Control Conference*, pp. 3500 – 3505, 2005.

[26] CLARK, J. and FIERRO, R., "Mobile robotic sensors for perimeter detection and tracking," *ISA Transactions*, vol. 46, no. 1, pp. 3–13, 2007.

[27] CORTES, J., "Distributed gradient ascent of random fields by robotic sensor networks," in *Proc. 46th IEEE Conf. on Decision and Control*, pp. 3120–3126, 2007.

[28] CORTES, J., MARTINEZ, S., KARATAS, T., and BULLO, F., "Coverage control for mobile sensing networks," *IEEE Transactions on Robotics and Automation*, vol. 20, no. 2, pp. 243–255, 2004.

[29] COUZIN, I. D., KRAUSE, J., FRANKS, N. R., and LEVIN, S. A., "Effective leadership and decision-making in animal groups on the move," *Nature*, vol. 433, pp. 513–516, 2005.

[30] CUI, X., HARDIN, C. T., RAGADE, R. K., and ELMAGHRABY, A. S., "A swarm approach for emission sources localization," in *Proc. 16th IEEE Int. Conf. Tools with Artificial Intelligence ICTAI 2004*, pp. 424–430, 2004.

[31] DIAS, M. B., ZLOT, R., KALRA, N., and STENTZ, A., "Market-based multirobot coordination: A survey and analysis," *Proceedings of the IEEE*, vol. 94, no. 7, pp. 1257–1270, 2006.

[32] DO CARMO, M. P., *Differential Geometry of Curves and Surfaces*. Englewood Cliffs, NJ: Prentice-Hall, 1976.

[33] DOĞANÇAY, K. and HMAM, H., "Optimal angular senso rseparation for AOA localization," *Signal Processing*, vol. 88, no. 5, pp. 1248–1260, 2008.

[34] DUDEK, G., JENKIN, M., MILIOS, E., and WILKES, D., "A taxonomy for multiagent robotics," *Autonomous Robots*, vol. 3, no. 4, pp. 375–397, 1996.

[35] EDWARDS, S., RUTKOWSKI, A. J., QUINN, R. D., and WILLIS, M. A., "Moth-inspired plume tracking strategies in three-dimensions," in *Proc. 2005 IEEE Int. Conf. Robotics and Automation*, pp. 1669–1674, 2005.

[36] ELAYDI, S. and ZHANG, S., "Stability and periodicity of difference equations with finite delay," *Funkcialaj Ekvacioj*, vol. 37, pp. 401–413, 1994.

[37] FARRELL, J. A., PANG, S., and LI, W., "Plume mapping via hidden Markov methods," *IEEE Transactions on Systems, Man, and Cybernetics, Part B: Cybernetics*, vol. 33, no. 6, pp. 850–863, 2003.

[38] FARRELL, J. A., SHUO, P., and LI, W., "Chemical plume tracing via an autonomous underwater vehicle," *IEEE Journal of Oceanic Engineering*, vol. 30, no. 2, pp. 428–442, 2005.

[39] FERRI, G., JAKUBA, M. V., CASELLI, E., MATTOLI, V., MAZZOLAI, B., YOERGER, D. R., and DARIO, P., "Localizing multiple gas/odor sources in an indoor environment using bayesian occupancy grid mapping," in *Proc. IEEE/RSJ Int. Conf. Intelligent Robots and Systems*, pp. 566–571, 2007.

[40] FERRI, G., JAKUBA, M. V., MONDINI, A., MATTOLI, V., MAZZOLAI, B., YOERGER, D. R., and DARIO, P., "Mapping multiple gas/odor sources in an uncontrolled indoor environment using a Bayesian occupancy grid mapping based method," *Robotics and Autonomous Systems*, vol. 59, no. 11, pp. 988–1000, 2011.

[41] FIORELLI, E., LEONARD, N. E., BHATTA, P., PALEY, D. A., BACHMAYER, R., and FRATANTONI, D. M., "Multi-auv control and adaptive sampling in monterey bay," *IEEE Journal of Oceanic Engineering*, vol. 31, no. 4, pp. 935–948, 2006.

[42] GRAHAM, R. and CORTES, J., "Cooperative adaptive sampling via approximate entropy maximization," in *Proc. 48th IEEE Conf. onf Decision and Control*, pp. 7055–7060, 2009.

[43] GR?NBAUM, D., "Schooling as a strategy for taxis in a noisy environment," *Evolutionary Ecology*, vol. 12, pp. 503–522, 1998.

[44] GU, K., KHARITONOV, V. L., and CHEN, J., *Stability of Time-Delay Systems*. Boston: Birkh*ä*user, 2003.

[45] GUZZONI, D., CHEYER, A., JULIA, L., and KONOLIGE, K., "Many robots make short work: Report of the sri international mobile robot team," *AI Magazine*, vol. 18, no. 1, pp. 55–64, 1997.

[46] HALE, J. K. and LUNEL, S. M. V., *Introduction to Functional Differential Equations*, ch. Stability Theory, p. 151. Springer-Verlag, 1993.

[47] HAQUE, M., RAHMANI, A., EGERSTEDT, M., and YEZZI, A., "Biologically motivated shape optimization of foraging fronts," in *Proc. American Control Conf. (ACC)*, pp. 4143–4148, 2011.

[48] HAQUE, M. A. and EGERSTEDT, M., "Coalition formation in multi-agent systems based on bottlenose dolphin alliances," in *Proc. ACC '09. American Control Conf*, pp. 3280–3285, 2009.

[49] HAYES, A. T., MARTINOLI, A., and GOODMAN, R. M., "Distributed odor source localization," *IEEE Sensors*, vol. 2, pp. 260 – 271, 2002.

[50] HIGHAM, N. J. and KIM, H., "Numerical analysis of a quadratic matrix equation," *IMA Journal of Numerical Analysis*, vol. 20, pp. 499–519, 2000.

[51] HSIEH, C. H., JIN, Z., MARTHALER, D., NGUYEN, B. Q., TUNG, D. J., BERTOZZI, A. L., and MURRAY, R. M., "Experimental validation of an algorithm for cooperative boundary tracking," in *Proc. of 2005 American Control Conference*, pp. 1078–1083, 2005.

[52] ISHIDA, H., KAGAWA, Y., NAKAMOTO, T., and MORIIZUMI, T., "Odor-source localization in the clean room by an autonomous mobile sensing system," *Sensors and Actuators, B: Chemical*, vol. 32, no. 2, pp. 115–121, 1996.

[53] JANG, S., SONG, B., and HONG, S.-K., "Dynamic boundary tracking in active sensor networks," in *Proc. Int. Conf. Control, Automation and Systems ICCAS '07*, pp. 2368–2373, 2007.

[54] JATMIKO, W., IKEMOTO, Y., MATSUNO, T., FUKUDA, T., and SEKIYAMA, K., "Distributed odor source localization in dynamic environment," in *Proc. IEEE Sensors*, 2005.

[55] JAZWINSKI, A. H., *Stochastic Processes And Filtering Theory*, ch. Stochastic Differential Equations, p. 112. Academic Press, 1970.

[56] JIN, Z. and BERTOZZI, A. L., "Environmental boundary tracking and estimation using multiple autonomous vehicles," in *Proc. of 46th IEEE Conf. on Decision and Control*, pp. 4918–4923, 2007.

[57] JOSHI, A., ASHLEY, T., HUANG, Y., and BERTOZZI, A. L., "Experimental validation of cooperative environmental boundary tracking with on-board sensors," in *Proc. of 2009 American Control Conference*, (St. Louis, MO), pp. 2630–2635, 2009.

[58] JUSTH, E. W. and KRISHNAPRASAD, P. S., "Natural frames and interacting particles in three dimensions," in *Proc. of 44th IEEE Conf. on Decision and Control and the European Control Conference 2005*, pp. 2841–2846, IEEE, 2005.

[59] KAY, S. M., *Fundamentals of Statistical Signal Processing, Volume I: Estimation Theory*. Prentice Hall, 1993.

[60] KAZADI, S., GOODMAN, R., TSIKATA, D., and LIN, H., "An autonomous water vapor plume tracking robot using passive resistive polymer sensors," *Autonomous Robots*, vol. 9, no. 2, pp. 175–188, 2000.

[61] KELLER, T., POWELL, I., and WEISSBURG, M., "Role of olfactory appendages in chemically mediated orientation of blue crabs," *Marine Ecology Progress Series*, vol. 261, pp. 217–231, 2003.

[62] KEMP, M., BERTOZZI, A. L., and MARTHALER, D., "Multi-UUV perimeter surveillance," in *Proc. of the 2004 IEEE/OES Workshop on Autonomous Underwater Vehicles*, pp. 102–107, 2004.

[63] KHALIL, H., *Nonlinear Systems, 3rd Ed.* New Jersey: Prentice Hall, 2001.

[64] KINGSTON, D., BEARD, R. W., and HOLT, R. S., "Decentralized perimeter surveillance using a team of uavs," *IEEE Transactions on Robotics*, vol. 24, no. 6, pp. 1394–1404, 2008.

[65] KOWADLO, G. and RUSSELL, R. A., "Robot odor localization: A taxonomy and survey," *The International Journal of Robotics Research*, vol. 27, no. 8, pp. 869–894, 2008.

[66] KRIEGER, M. J. B., BILLETER, J.-B., and KELLER, L., "Ant-like task allocation and recruitment in cooperative robots," *Nature*, vol. 406, no. 6799, pp. 992–995, 2000.

[67] LABELLA, T. H., DORIGO, M., and DENEUBOURG, J.-L., *Distributed autonomous robotic systems*, ch. Self-Organised Task Allocation in a Group of Robots, pp. 389–398. Springer, 2007.

[68] LEMMENS, N., DE JONG, S., TUYLS, K., and NOW, A., *Adaptive agents and multi-agent systems III. Adaption and multi-agent learning.*, ch. Bee Behaviour in Multi-agent Systems, pp. 145–156. Springer, 2008.

[69] LEONARD, N. E., PALEY, D. A., LEKIEN, F., SEPULCHRE, R., FRATANTONI, D. M., and DAVIS, R. E., "Collective motion, sensor networks, and ocean sampling," *Proceedings of the IEEE*, vol. 95, no. 1, pp. 48–74, 2007.

[70] LEONARD, N. E., PALEY, D. A., DAVIS, R. E., FRATANTONI, D. M., LEKIEN, F., and ZHANG, F., "Coordinated control of an underwater glider fleet in an adaptive ocean sampling field experiment in monterey bay," *Journal of Field Robotics*, vol. 27, no. 6, pp. 718–740, 2010.

[71] LI, W., FARRELL, J. A., PANG, S., and ARRIETA, R. M., "Moth-inspired chemical plume tracing on an autonomous underwater vehicle," *IEEE Transactions on Robotics*, vol. 22, no. 2, pp. 292–307, 2006.

[72] LILIENTHAL, A. and DUCKETT, T., "Building gas concentration gridmaps with a mobile robot," *Robotics and Autonomous Systems*, vol. 48, no. 1, pp. 3–16, 2004.

[73] LILIENTHAL, A. and DUCKETT, T., "Experimental analysis of smelling braitenberg vehicles," *Advanced Robotics*, vol. 8, no. 8, pp. 817–834, 2004.

[74] LIU, Y. and PASSINO, K., "Stable social foraging swarms in a noisy environment," *IEEE Transactions on Automatic Control*, vol. 49, no. 1, pp. 30–40, 2004.

[75] LYTRIDIS, C., VIRK, G., REBOUR, Y., and KADAR, E., "Odor-based navigational strategies for mobile agents," *Adaptive Behavior*, vol. 9, no. 3-4, pp. 171–187, 2001.

[76] MARTHALER, D. and BERTOZZI, A. L., *Recent Developments in Cooperative Control and Optimization*, ch. Tracking environmental level sets with autonomous vehicles. Kluwer Academic Publishers, 2003.

[77] MARTINS, A., ALMEIDA, J., and SILVA, E., "Coordinated maneuver for gradient search using multiple AUVs," in *Proc. of OCEANS*, vol. 1, pp. 347 – 352, 2003.

[78] MARTŁNEZ, S. and BULLO, F., "Optimal sensor placement and motion coordination for target tracking," *Automatica*, vol. 42, no. 4, pp. 661–668, 2006.

[79] MATVEEV, A. S., TEIMOORI, H., and SAVKIN, A. V., "Sensor-based tracking of environmental level sets by a unicycle-like mobile robot," in *Proc. IEEE Int Robotics and Automation (ICRA) Conf*, pp. 2984–2988, 2010.

[80] MATVEEV, A., TEIMOORI, H., and SAVKIN., A. V., "Navigation of a non-holonomic vehicle for gradient climbing and source seeking without gradient estimation," in *Proc. of 2010 American Control Conference*, pp. 219 – 223, 2010.

[81] MILLMAN, R. S. and PARKER, G. D., *Elements of differential geometry*. Englewood Cliffs, NJ: Prentice-Hall, 1977.

[82] MOORE, B. J. and DE WIT, C. C., "Source seeking via collaborative measurements by a circular formation of agents," in *Proc. of 2010 American Control Conference*, pp. 6417–6422, 2010.

[83] MOURIKIS, A. I. and ROUMELIOTIS, S. I., "Performance analysis of multirobot cooperative localization," *IEEE Transactions on Robotics*, vol. 22, no. 4, pp. 666–681, 2006.

[84] MURRAY, R. M., "Recent research in cooperative control of multivehicle systems," *Journal of Dynamic Systems, Measurement, and Control*, vol. 129, no. 5, pp. 571–584, 2007.

[85] NAGPAL, K. M. and KHARGONEKAR, P. P., "Filtering and smoothing in a H_∞ setting," *IEEE Transactions on Automatic Control*, vol. 36, pp. 152–166, 1991.

[86] NARDONE, S. and AIDALA, V. J., "Observability criteria for bearings-only target motion analysis," *IEEE Transactions on Aerospace and Electronic Systems*, vol. 17, no. 2, pp. 162–166, 1981.

[87] OGREN, P., FIORELLI, E., and LEONARD, N. E., "Cooperative control of mobile sensor networks: Adaptive gradient climbing in a distributed environment," *IEEE Transactions on Automatic Control*, vol. 49, no. 8, pp. 1292–1302, 2004.

[88] PALEY, D. A., ZHANG, F., and LEONARD, N. E., "Cooperative control for ocean sampling: The glider coordinated control system," *IEEE Transactions on Control Systems Technology*, vol. 16, no. 4, pp. 735–744, 2008.

[89] PANG, S. and FARRELL, J. A., "Chemical plume source localization," *IEEE Transactions on Systems, Man, and Cybernetics, Part B: Cybernetics*, vol. 36, no. 5, pp. 1068–1080, 2006.

[90] PARKE, L. E., "Current state of the art in distributed autonomous mobile robotics," in *Proc. 5th Int. Symp. Distributed Autonomous Robotic Systems*, pp. 3–12, 2000.

[91] PYK, P., BADIA, S. B. I., BERNARDET, U., KNSEL, P., CARLSSON, M., GU, J., CHANIE, E., HANSSON, B. S., PEARCE, T. C., and VERSCHURE, P. F. M. J., "An artificial moth: Chemical source localization using a robot based neuronal model of moth optomotor anemotactic search," *Autonomous Robots*, vol. 20, no. 3, pp. 197–213, 2006.

[92] REKLEITIS, I. M., DUDEK, G., and MILIOS, E. E., "Multi-robot cooperative localization: a study of trade-offs between efficiency and accuracy," in *Proc. IEEE/RSJ Int Intelligent Robots and Systems Conf*, vol. 3, pp. 2690–2695, 2002.

[93] ROBINETT, R. D. and WILSON, D. G., "Collective plume tracing: A minimal information approach to collective control," in *Proc. of 2007 American Control Conference*, pp. 4884–4891, 2007.

[94] RUSSELL, R. A., "Locating underground chemical sources by tracking chemical gradients in 3 dimensions," in *Proc. IEEE/RSJ Int. Conf. Intelligent Robots and Systems*, vol. 1, pp. 325–330, 2004.

[95] RUSSELL, R. A., "Robotic location of underground chemical sources," *Robotica*, vol. 22, pp. 109–115, 2004.

[96] RUSSELLA, R., BAB-HADIASHAR, A., SHEPHERD, R. L., and WALLACE, G. G., "Acomparison of reactive robot chemotaxisalgorithms," *Robotics and Autonomous Systems*, vol. 45, no. 2, pp. 83–97, 2003.

[97] SAVVIDES, A., FANG, J., and LYMBEROPOULOS, D., "Using mobile sensing nodes for dynamic boundary estimation," in *WAMES workshop in conjuction with MobiSy*, pp. 30–33, 2004.

[98] SHAMMA, J., ed., *Cooperative Control of Distributed Multi-Agent Systems*. Wiley, 2006.

[99] SIMIĆ, S. N. and SASTRY, S., "Distributed environmental monitoring using random sensor networks," *INFORMATION PROCESSING IN SENSOR NETWORKS*, vol. 2634, no. 551, pp. 582–592, 2003.

[100] SIMON, D., *Optimal State Estimation*. Hoboken, New Jersey: Wiley-Interscience, 2006.

[101] SONG, T. L., "Observability of target tracking with bearings-only measurements," *IEEE Transactions on Aerospace and Electronic Systems*, vol. 32, no. 4, pp. 1468–1472, 1996.

[102] STANKOVIC, M. and STIPANOVIC, D., "Extremum seeking under stochastic noise and applications to mobile sensors," *Automatica*, vol. 46, pp. 1243–1251, 2010.

[103] STANKOVIC, M. S. and STIPANOVIC, D. M., "Discrete time extremum seeking by autonomous vehicles in a stochastic environment," in *Proc. of 48th IEEE Conf. on Decision and Control*, pp. 4541–4546, 2009.

[104] STANKOVIC, M. S. and STIPANOVIC, D. M., "Stochastic extremum seeking with applications to mobile sensor networks," in *Proc. of 2009 American Control Conference*, pp. 5622–5627, 2009.

[105] SUSCA, S., MARTÍNEZ, S., and BULLO, F., "Monitoring environmental boundaries with a robotic sensor network," *IEEE Transactions on Control Systems Technology*, vol. 16, no. 2, pp. 288–296, 2008.

[106] TAUBIN, G., "Estimating the tensor of curvature of a surface from a polyhedral approximation," in *Proc. of the 5th. Conf. Computer Vision*, pp. 902–907, 1995.

[107] TAYLOR, C. J. and KRIEGMAN, D. J., "Exploration strategies for mobile robots," in *Proc. Conf. IEEE Int Robotics and Automation*, pp. 248–253, 1993.

[108] THEODOR, Y., SHAKED, U., and SOUZA, C., "A game theory approach to robust discrete-time H_∞ estimation," *IEEE Transactions on Signal Processing*, vol. 42, no. 6, pp. 1486–1495, 1994.

[109] TORNEY, C., NEUFELD, Z., and COUZIN, L., "Context-dependent interaction leads to emergent search behavior in social aggregates," *Proc. of the National Academy of Sciences*, vol. 106, no. 52, pp. 22055–22060, 2009.

[110] WASSIM M. HADDAD, V. C., *Nonlinear Dynamical Systems and Control A Lyapunov-Based Approach*. Princton Univrsity Prss, 2008.

[111] WEISSBURG, M. J. and ZIMMER-FAUST, R. K., "Odor plumes and how blue crabs use them in finding prey," *The Journal of Experimental Biology*, vol. 197, pp. 349–375, 1994.

[112] WEISSBURG, M. J. and DUSENBERY, D. B., "Behavioral observations and computer simulations of blue crab movement to a chemical source in a controlled turbulent flow," *Experimental Biology*, vol. 205, pp. 3387–3398, 2002.

[113] WU, W. and ZHANG, F., "Curvature based cooperative exploration in three dimensional scalar fields," in *Proc. of 2010 American Control Conference*, pp. 2909–2915, 2010.

[114] WU, W. and ZHANG, F., "A switching strategy for robust cooperative exploration," in *Proc. of 2010 IEEE Conf. on Decision and Control*, pp. 5493–5498, 2010.

[115] WU, W., COUZIN, I. D., and ZHANG, F., "Bio-inspired source seeking with no explicit gradient estimation," in *Proc. of IFAC Workshop on Distributed Estimation and Control in Networked System*, 2012.

[116] WU, W. and ZHANG, F., "Cooperative exploration of level surfaces of three dimentional scalar fields," *Automatica*, vol. 47(9), pp. 2044–2051, 2011.

[117] WU, W. and ZHANG, F., "Experimental validation of source seeking with a switching strategy," in *Proc. 2011 IEEE Conference on Robotics and Automation*, pp. 3835–3840, 2011.

[118] WU, W. and ZHANG, F., "Explorability of noisy scalar fields," in *Proc. 2011 IEEE Conference on Decision and Control*, pp. 6439–6444, 2011.

[119] WU, W. and ZHANG, F., "Coherent steps of mobile sensing agents in gaussian scalar fields," in *Proc. 2012 IEEE Conference on Decision and Control*, pp. 2814–2819, 2012.

[120] WU, W. and ZHANG, F., "Coherent steps of mobile sensing agents in noisy scalar fields," *IEEE Transactions on Automatic Control*, vol. submitted, 2012.

[121] WU, W. and ZHANG, F., "Robust cooperative exploration with a switching strategy," *IEEE Transactions on Robotics*, vol. 28, no. 4, pp. 828–839, 2012.

[122] WU, W., ZHANG, F., and WARDI, Y., "Energy-information tradeoffs in motion and sensing for target localization," in *in Proc. of European Control Conference*, 2013.

[123] YAESH, I. and SHAKED, U., "A transfer function approach to the problem of discrete-time systems: H_∞ optimal linear control and filtering," *IEEE Transactions on Automatic Control*, vol. 36, pp. 1264–1271, 1991.

[124] YAESH, I. and THEODOR, Y., "H_∞ optimal estimation: a turtorial," in *Proc. of 31st IEEE Conf. on Decision and Control*, (Tucson, Arizona), pp. 2278–2286, 1992.

[125] YAMAUCHI, B., "A frontier-based approach for autonomous exploration," in *Proc. Symp. IEEE Int Computational Intelligence in Robotics and Automation CIRA'97.*, pp. 146–151, 1997.

[126] YAMAUCHI, B., "Frontier-based exploration using multiple robots," in *Proc. of the second international conference on Autonomous agents*, pp. 47–53, 1998.

[127] ZARZHITSKY, D., SPEARS, D. F., and SPEARS, W. M., "Swarms for chemical plume tracing," in *Proc. IEEE Swarm Intelligence Symp. SIS 2005*, pp. 249–256, 2005.

[128] ZHANG, F., FIORELLI, E., and LEONARD, N. E., "Exploring scalar fields using multiple sensor platforms: Tracking level curves," in *Proc. of 46th IEEE Conf. on Decision and Control*, (New Orleans, LA), pp. 3579–3584, 2007.

[129] ZHANG, F., FRATANTONI, D. M., PALEY, D., LUND, J., and LEONARD, N. E., "Control of coordinated patterns for ocean sampling," *International Journal of Control*, vol. 80, pp. 1186–1199, 2007.

[130] ZHANG, F., GOLDGEIER, M., and KRISHNAPRASAD, P. S., "Control of small formations using shape coordinates," in *Proc. 2003 International Conf. of Robotics and Automation*, (Taipei, Taiwan), pp. 2510–2515, IEEE, 2003.

[131] ZHANG, F. and LEONARD, N. E., "Generating contour plots using multiple sensor platforms," in *Proc. IEEE Swarm Intelligence Symp. SIS 2005*, pp. 309–316, 2005.

[132] ZHANG, F. and LEONARD, N. E., "Cooperative control and filtering for cooperative exploration," *IEEE Transactions on Automatic Control*, vol. 55, no. 3, pp. 650–663, 2010.

[133] ZHANG, F., "Geometric cooperative control of particle formations," *IEEE Transactions on Automatic Control*, vol. 55, no. 3, pp. 800–803, 2010.

[134] ZHANG, G., FRICKE, G. K., and GARG, D. P., "Spill detection and perimeter surveillance via distributed swarming agents," *IEEE/ASME Transactions on Mechatronics*, no. 99, pp. 1–9, 2011. Early Access.

[135] ZHAO, S., CHEN, B. M., and LEE, T. H., "Optimal placement of bearing-only sensors for target localization," in *Proc. of 2012 American Control Conference*, pp. 5108–5113, 2012.

[136] ZHONG, M. and CASSANDRAS, C. G., "Distributed coverage control and data collection with mobile sensor networks," *IEEE Transactions on Automatic Control*, vol. 56, no. 10, pp. 2445–2455, 2011.

[137] ZLOT, R., STENTZ, A., DIAS, M. B., and THAYER, S., "Multi-robot exploration controlled by a market economy," in *Proc. IEEE Int. Conf. Robotics and Automation ICRA '02*, vol. 3, pp. 3016–3023, 2002.

VITA

Wencen Wu received her B.S. and M.S. degrees in Electronic, Information and Electrical Engineering from Shanghai Jiao Tong University, in 2006 and 2009, respectively, and her M.S. degree in Electrical and Computer Engineering from Georgia Institute of Technology, in 2010. She is currently a Ph.D candidate in Electrical and Computer Engineering at Georgia Institute of Technology, expecting to graduate in August, 2013. Her research interests focus on dynamics and control, with applications in mobile sensor networks, autonomous systems, and robotics. She has integrated data and insights from biology with models and provable strategies from control theory, and conducted innovative multidisciplinary investigation of mobile sensing networks in complex environments.